

Electrical Machines and Drives

Oliver Wallscheid



Content

- 1 An initial overview of electrical machines and drives
- 2 Fundamental electromagnetic principles and magnetic materials
- 3 DC machines
- 4 Transformers
- 5 Rotating field theory
- 6 Induction machines
- 7 Synchronous machines

Table of contents

- 1 An initial overview of electrical machines and drives

An initial overview of electrical machines and drives

Oliver Wallscheid



What is an electrical machine?

Electrical machine

An electrical machine is a device that converts electrical energy into mechanical energy or vice versa.

- ▶ Electrical energy is routed via machine's external wiring connected to the terminal box.
- ▶ Mechanical energy is transferred via the shaft (if it is a rotatory machine).
- ▶ Historic timetable of the electrical machine development: [KIT article \(by M. Doppelbauer\)](#)

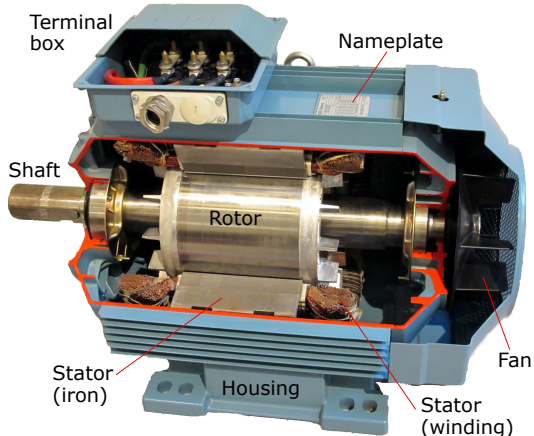
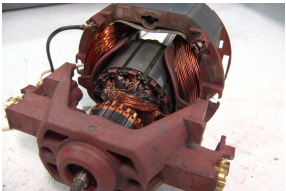


Fig. 1.1: Example of an electrical machine (source: derived from [Wikimedia Commons](#), public domain)

Some exemplary electrical machines



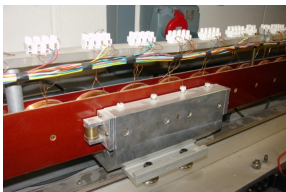
(a) DC machine (source: [Wikimedia Commons](#),
Marrci, [CC BY-SA 3.0](#))



(b) Induction machine (source: [Wikimedia Commons](#),
Zureks, [CC BY-SA 4.0](#))

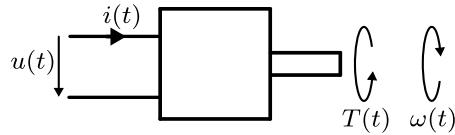


(c) Permanent magnet machine (source: [Wikimedia Commons](#), Andrez, [CC BY-SA 4.0](#))



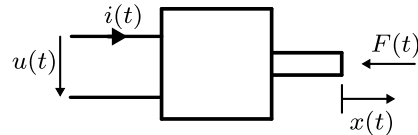
(d) Linear permanent magnet machine (source: [Wikimedia Commons](#), Zureks, [CC BY-SA 4.0](#))

The machine as an electrical-mechanical converter



Load convention
(arrows pointing in
the same direction)

(a) Rotational converter



Load convention
(arrows pointing in
the same direction)

(b) Translational converter

Fig. 1.3: Electrically and mechanically free body diagrams of motors as energy converters with variable notation: time t , voltage u , current i , force F , displacement x , torque T and rational speed ω (adapted from J. Böcker, *Elektrische Antriebstechnik*, Paderborn University, 2020)

Some basic mechanical terms (recap)

	Translational converter	Rotational converter
Kinematic quantities		
Displacement / angle	x	ε
Velocity	$v = \dot{x}$	$\omega = \dot{\varepsilon}$
Acceleration	$a = \ddot{v} = \ddot{x}$	$\alpha = \dot{\omega} = \ddot{\varepsilon}$
Jerk	$j = \dot{a} = \ddot{v} = \dddot{x}$	$\rho = \dot{\alpha} = \ddot{\omega} = \ddot{\varepsilon}$
Dynamical quantities		
Force / torque	F	T
Mass / inertia	m	J
Mechanical power	$P_{\text{me}} = Fv$	$P_{\text{me}} = T\omega$
Work	$W[t_0, t] = \int_{t_0}^t P_{\text{me}}(\tau) d\tau$	$W[t_0, t] = \int_{t_0}^t P_{\text{me}}(\tau) d\tau$
Momentum / rotational momentum	$p = mv$	$L = \omega J$
Kinetic energy	$E_{\text{kin}} = \frac{1}{2}mv^2$	$E_{\text{kin}} = \frac{1}{2}J\omega^2$

Tab. 1.1: Basic mechanical terms for translational and rotational converters

Work vs. energy (recap)

Work

Work is the integral of the power over a time integral (or force over distance) and is a measure of the energy transfer.

Energy

Energy is the capacity to do work, that is, a quantity depending on the state of a system at a given point of time.

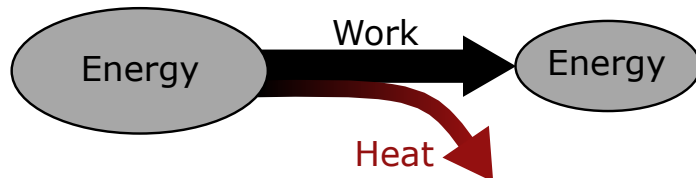


Fig. 1.4: Illustration addressing the work vs. energy terminology (simplified Sankey diagram)

Power balance of an electrical machine

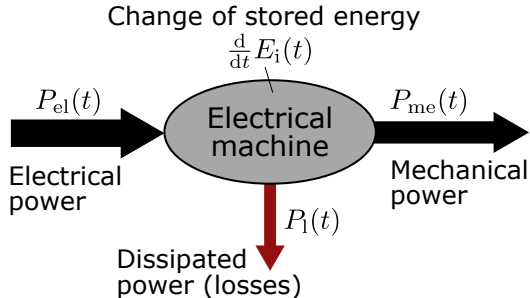


Fig. 1.5: Power balance of an electrical machine (illustrated in motoric operation)

The power balance

$$P_{el}(t) = P_{me}(t) + P_l(t) + \frac{d}{dt}E_i(t) \quad (1.1)$$

must hold for any point in time as energy is conserved, that is, not created or destroyed.

Four quadrants of machine operation

For the steady state ($\dot{E}_i(t) = 0$), we define the **machine efficiency** as the ratio of the converted energy to the input energy:

$$\eta_{\text{mot}} = \frac{P_{\text{me}}}{P_{\text{el}}} = 1 - \frac{P_l}{P_{\text{el}}}, \quad (1.2)$$

$$\eta_{\text{gen}} = \frac{P_{\text{el}}}{P_{\text{me}}} = 1 - \frac{P_l}{P_{\text{me}}}. \quad (1.3)$$

Hence, we need to consider in which **quadrant** the machine operates as this will influence the power flow direction.

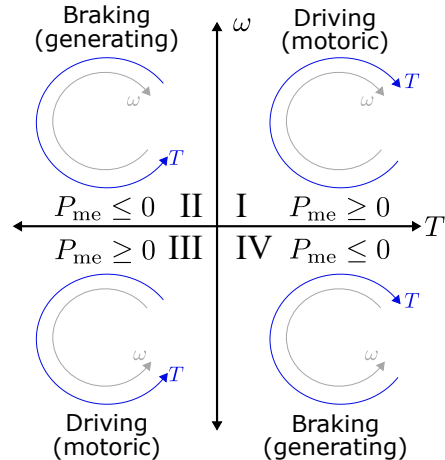


Fig. 1.6: Machine quadrants (derived from Wikimedia Commons, K. Pitter, CC BY-SA 3.0)

What is an electrical drive ?

Electrical drive

An electrical drive is a system that controls the torque, speed or position of an electrical machine connected to some mechanical process.

- ▶ Integrates the 'stupid' electrical machine into an 'intelligent' controlled system.
- ▶ The energy source and mechanical process ('load') are not part of the drive system.

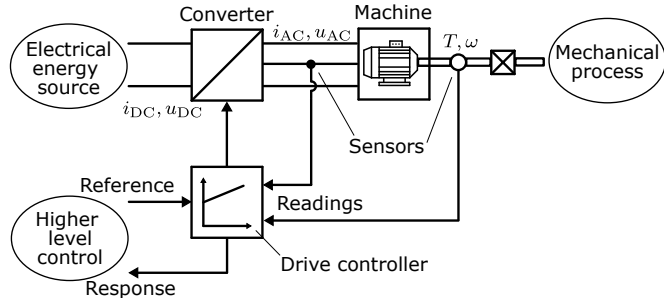


Fig. 1.7: Block diagram of an electrical drive (adapted from J. Böcker, *Elektrische Antriebstechnik*, Paderborn University, 2020)

Examples of electrical machine and drive applications (1)



(a) Electric cars (source: [Wikimedia Commons](#), M. Movchin and F. Mueller, CC BY-SA 3.0)



(b) Wind turbine generators (source: [pxhere.com](#), public domain)



(c) Factory robots (source: [Wikimedia Commons](#), A. Reinhold, CC BY-SA 4.0)



(d) Electric tools (source: [flickr.com](#), M. Verch, CC BY 2.0)

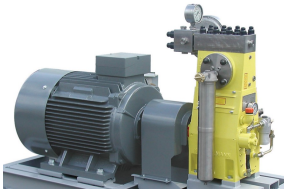
Examples of electrical machine and drive applications (2)



(e) High-speed trains (source: [Wikimedia Commons](#), P. Elektro, CC BY-SA 3.0)



(f) Electric aircraft (source: [Wikimedia Commons](#), M. Weinold, CC BY-SA 4.0)



(g) Pumps (source: [Wikimedia Commons](#), Hammelmann, CC BY-SA 3.0)



(h) Cranes (source: [Wikimedia Commons](#), Belfast Dissenter, CC BY-SA 4.0)

A broad range of nominal power ratings



Fig. 1.9: Power range overview (inspired from A. Binder, *Elektrische Maschinen und Antriebe (lecture slides)*, Darmstadt University, 2022 with additional figure sources: [A. Wolf](#), [Asurnipal](#), [M. Williams](#), [R. Spekking](#), [Foxcorner](#), [A. Tredz](#) and [J. Halicki](#) under varying CC licenses)

Why is knowledge about electric machines and drives important?

Electric machines and drives are an essential pillar of the modern society

Without electric machines and drives, our todays society would not be possible. Starting from providing electricity via electrical generators to powering electric vehicles, tools and entire factory production lines, electric machines and drives are everywhere, that is, they enable our today's living standard.

Energy efficiency and sustainability is key

Electric machines and drives utilize approx. 50 % of the global electricity with about 8 billion electric motors in use in the EU (source: [European Commission](#) and [International Energy Agency](#)). Therefore, improving their efficiency is an essential factor to reduce the global energy consumption and the associated CO₂ emissions.

Learning objectives

- ▶ Understand the generation of magnetic fields, force formation and voltage induction in electrical machines.
- ▶ Differentiate the main types of electrical machines and drives:
 - ▶ DC machines.
 - ▶ Induction machines.
 - ▶ Synchronous machines.
 - ▶ And their plentiful variants ...
- ▶ Understand their basic design and operation principles.
- ▶ Analyze the operation of electrical machines and drives:
 - ▶ in steady state and
 - ▶ in transient conditions.
- ▶ Have fun learning about electrical machines and drives.

Necessary prior knowledge for this course

You should have a basic understanding of the following topics:

- ▶ Linear differential equations (modeling, solution techniques)
- ▶ Linear algebra basics (e.g., vector and matrix operations)
- ▶ Vector analysis (differentiation and integration of vector fields)
- ▶ Basic signal theory knowledge (e.g., Fourier series, Laplace transform)
- ▶ Basic knowledge of electrical circuit theory
- ▶ Basic knowledge of mechanics

What we will not cover, that is, you do not need to know (covered in separate courses):

- ▶ Control engineering (design drive controllers)
- ▶ Power electronics (design switchable actuators)

Recommended reading

- ▶ A. Binder, Elektrische Maschinen und Antriebe (in German), Vol. 2, Springer, 2017
- ▶ D. Schröder and R. Kennel, Elektrische Antriebe: Grundlagen (in German), Vol. 7, Springer Vieweg, 2021
- ▶ A. Huges and B. Drury, Electric Motors and Drives: Fundamentals, Types and Applications, Vol. 5, Newnes, 2019
- ▶ S. Chapman, Electric Machinery Fundamentals, Vol. 5, McGraw-Hill, 2011
- ▶ I. Boldea and S. Nasar, Electric Drives, Vol. 3, CRC Press, 2022

Table of contents

- 2 Fundamental electromagnetic principles and magnetic materials

Fundamental electromagnetic principles and magnetic materials

Oliver Wallscheid



Ampère's circuital law: magnetic field strength

Relates the circulation of a magnetic field around a closed loop to the electric current passing through the loop:

Integral form: $\oint_{\partial S} \mathbf{H} \cdot d\mathbf{s} = I_f, \quad (2.1)$

Differential form: $\nabla \times \mathbf{H} = \mathbf{J}_f. \quad (2.2)$

Here, \mathbf{H} is the magnetic field strength, \mathbf{J}_f is the free current density, and I_f is the free current enclosed by the loop ∂S .

- ▶ Free current: current that is not bound to a material (i.e., without polarization and magnetization currents).
- ▶ SI-units: $[H] = \frac{\text{A}}{\text{m}}$, $[J] = \frac{\text{A}}{\text{m}^2}$

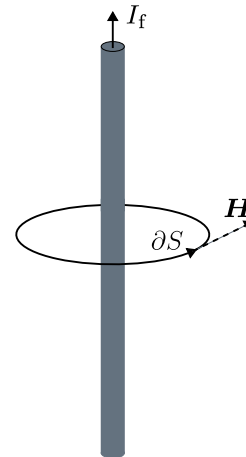


Fig. 2.1: Illustration of the magnetic field strength \mathbf{H} around a simple conductor

Ampère's circuital law: free current example

What is the free current I_f enclosed by the loop ∂S ?

- ▶ The current I_1 flows in the direction of the loop ∂S (according to right-hand rule).
- ▶ The current I_1 must be counted N times due to the N turns of wire around the loop ∂S .
- ▶ The current I_2 flows in the opposite direction of the loop ∂S (according to right-hand rule).
- ▶ Result:

$$I_f = N \cdot I_1 - I_2.$$

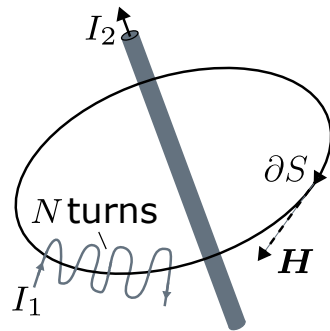


Fig. 2.2: Arrangement with two electrical conductors

Ampère's circuital law: simple solenoid example

Ampere's law for magnetic flux density B in vacuum:

Integral form: $\oint_{\partial S} \mathbf{B} \cdot d\mathbf{s} = \mu_0 I, \quad (2.3)$

Differential form: $\nabla \times \mathbf{B} = \mu_0 \mathbf{J}. \quad (2.4)$

Here, μ_0 is the permeability of free space, \mathbf{J} is the total current density and I is the total current enclosed by the loop ∂S .

- ▶ SI-unit: $[B] = T = \frac{Vs}{m^2} = \frac{N}{Am}$
- ▶ Example contour ∂S on the right covering N turns and length l (flux density within solenoid):

$$\oint_{\partial S} \mathbf{B} \cdot d\mathbf{s} = N\mu_0 I \Leftrightarrow B = \frac{N\mu_0 I}{l}$$

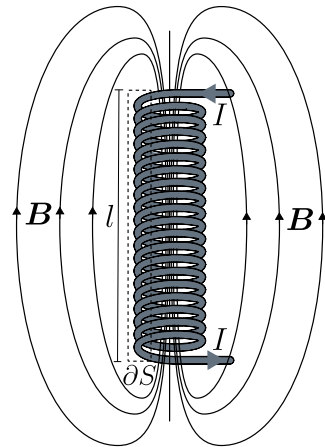


Fig. 2.3: Magnetic flux density evaluated at the contour ∂S (adapted from: [Wikimedia Commons](#), Goodphy, CC BY-SA 4.0)

Shortcomings of the Ampère's circuital law

Applying Ampère's circuital law to a capacitor with a changing electric field \mathbf{E} leads to a contradiction:

- ▶ Applying (2.2) to S_1 yields:

$$\oint_{\partial S_1} \mathbf{H} \cdot d\mathbf{s} = I.$$

- ▶ In the case of S_2 we receive:

$$\oint_{\partial S_2} \mathbf{H} \cdot d\mathbf{s} = 0.$$

- ▶ However, both surfaces share the same bounding contour ∂S .
- ▶ Issue: The magnetic field strength \mathbf{H} is not able to describe the displacement current.

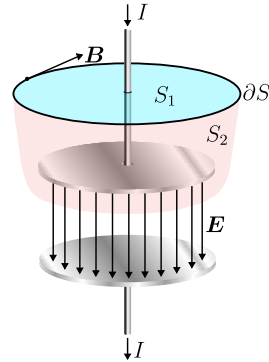


Fig. 2.4: Surfaces S_1 and S_2 share the same bounding contour ∂S . However, S_1 is pierced by conduction current, while S_2 is pierced by displacement current (adapted from: Wikimedia Commons, public domain).

The Ampère – Maxwell equation

The charge of capacitor is:

$$Q = \oint_{S_2} \mathbf{D} \cdot d\mathbf{S}.$$

If the electric field ($\mathbf{D} = \epsilon_0 \epsilon_r \mathbf{E}$) changes, a displacement current results:

$$I_d = \frac{d}{dt} \oint_{S_2} \mathbf{D} \cdot d\mathbf{S}$$

- ▶ Is not a classical electric current (moving charges) but a term to describe the changing electric field.
- ▶ Above, ϵ_0 is the vacuum permittivity and ϵ_r is the relative permittivity of a material.

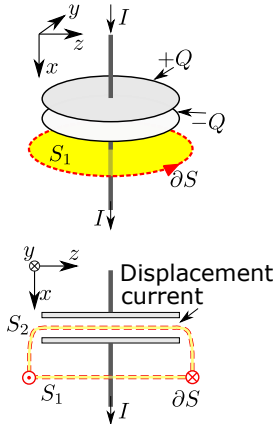


Fig. 2.5: Illustration for calculating the displacement current (adapted from: [Wikimedia Commons](#), public domain).

The Ampère – Maxwell equation (cont.)

Adding the displacement current to (2.2) we receive the Ampère – Maxwell equation:

Integral form: $\int_{\partial S} \mathbf{H} \cdot d\mathbf{s} = \iint_S \left(\mathbf{J}_f + \frac{d}{dt} \mathbf{D} \right) \cdot d\mathbf{S},$ (2.5)

Differential form: $\nabla \times \mathbf{H} = \mathbf{J}_f + \frac{\partial \mathbf{D}}{\partial t}.$ (2.6)

Above, \mathbf{D} is the electric displacement field.

- ▶ SI-unit: $[D] = \frac{C}{m^2}$
- ▶ SI-unit: $[E] = \frac{V}{m}$
- ▶ $\epsilon_0 \approx 8.854 \cdot 10^{-12} \frac{F}{m}$

Magnetic flux and flux linkage

The magnetic flux ϕ is the surface integral of the normal component of \mathbf{B} over that surface:

$$\phi = \iint_S \mathbf{B} \cdot d\mathbf{S}. \quad (2.7)$$

As there are no magnetic monopoles, the magnetic flux through a closed surface (which is covering a volume without holes) is always zero:

$$\oint_S \mathbf{B} \cdot d\mathbf{S} = 0. \quad (2.8)$$

The flux linkage ψ is the product of the magnetic flux ϕ and the number of turns N of a coil:

$$\psi = N\phi. \quad (2.9)$$

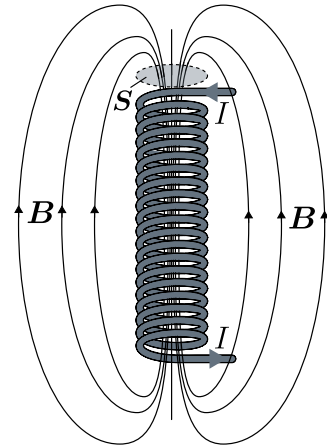


Fig. 2.6: Magnetic flux ϕ evaluated at the surface S (adapted from: [Wikimedia Commons](#), Goodphy, CC BY-SA 4.0)

Magnetic leakage flux

- ▶ In the scenarios with multiple coils, the magnetic flux generated by one coil will influence also the other coils.
- ▶ Exception: two coils are perfectly perpendicular to each other.
- ▶ However, the magnetic flux typically does not fully couple with the other coils
- ▶ The difference is the leakage flux ϕ_σ .

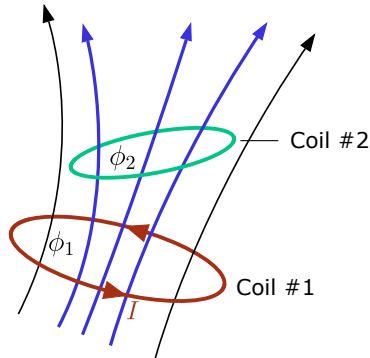


Fig. 2.7: The magnetic flux ϕ_1 generated by the current I does only partly couple with the second coil, while the difference $\phi_1 - \phi_2$ is the leakage flux (adapted from: [Wikimedia Commons](#), M. Wacenovsky, public domain)

Inductance

The inductance L describes the ratio between the magnetic flux linkage $\psi(t)$ to the current $i(t)$:

$$\psi(t) = Li(t). \quad (2.10)$$

Example: From the solenoid in Fig. 2.6 we know that the magnetic flux linkage ψ is:

$$\psi = N \iint_S \mathbf{B} \cdot d\mathbf{S} = \frac{1}{l} N^2 \mu_0 I \pi r^2$$

with r being the radius of the solenoid. Hence, the inductance L is:

$$L = \frac{\psi}{I} = \frac{N^2 \mu_0 \pi r^2}{l}.$$

- ▶ SI-unit: $[L] = \text{H} = \frac{\text{Vs}}{\text{A}}$
- ▶ The inductance is an important parameter describing inductive systems.

Self and mutual inductance

Based on the inductive coupling between the two coils from Fig. 2.8, we can define the magnetic flux matrix:

$$\phi = \begin{bmatrix} \phi_{11} & \phi_{12} \\ \phi_{21} & \phi_{22} \end{bmatrix}. \quad (2.11)$$

- ▶ ϕ_{11} : magnetic flux component of coil 1 due to its own current i_1
- ▶ ϕ_{12} : magnetic flux component of coil 1 due to the current i_2 in coil 2
- ▶ ϕ_{21} : magnetic flux component of coil 2 due to the current i_1 in coil 1
- ▶ ϕ_{22} : magnetic flux component of coil 2 due to its own current i_2

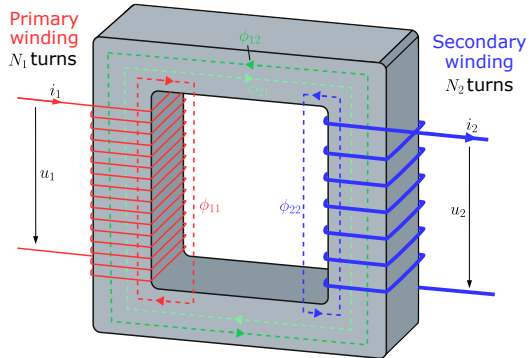


Fig. 2.8: Two coils coupled via a common core
(adapted from: [Wikimedia Commons](#), Bill C.,
CC BY-SA 3.0)

Self and mutual inductance (cont.)

Utilizing the permeance definition (“magnetic conductance”)

$$\Lambda = \frac{\phi}{Ni}, \quad (2.12)$$

we can represent (2.11) as:

$$\phi_{11} = \Lambda_{11}N_1i_1, \quad \phi_{12} = \Lambda_{12}N_2i_2, \quad \phi_{21} = \Lambda_{21}N_1i_1, \quad \phi_{22} = \Lambda_{22}N_2i_2. \quad (2.13)$$

The resulting flux linkage per coil is then:

$$\begin{aligned} \psi_1 &= N_1 (\phi_{11} + \phi_{21} + \phi_{12}), & \psi_2 &= N_2 (\phi_{22} + \phi_{12} + \phi_{21}), \\ &= \underbrace{(\Lambda_{11}N_1^2 + \Lambda_{21}N_1^2)}_{L_1} i_1 + \underbrace{\Lambda_{12}N_1N_2}_{M_{12}} i_2, & &= \underbrace{(\Lambda_{22}N_2^2 + \Lambda_{12}N_1^2)}_{L_2} i_2 + \underbrace{\Lambda_{21}N_1N_2}_{M_{21}} i_1. \end{aligned} \quad (2.14)$$

Above, L_1 and L_2 are the self-inductances, M_{12} and M_{21} are the mutual inductances.

Self and mutual inductance (cont.)

Hence, we can define the flux linkages of both coils using the following inductance matrix:

$$\boldsymbol{\psi} = \begin{bmatrix} \psi_1 \\ \psi_2 \end{bmatrix} = \begin{bmatrix} L_1 & M_{12} \\ M_{21} & L_2 \end{bmatrix} \begin{bmatrix} i_1 \\ i_2 \end{bmatrix} = \mathbf{L}\mathbf{i}. \quad (2.15)$$

Due to the symmetry of the inductive coupling, the mutual inductances are identical:

$$M_{12} = M_{21} = M. \quad (2.16)$$

Based on (2.14), we can also split the self-inductance L_i of the i -th coil into the sum of the leakage inductance $L_{i,\sigma}$ and the magnetizing inductance $L_{i,m}$:

$$L_i = L_{i,\sigma} + L_{i,m} = \Lambda_{ii}N_i^2 + \Lambda_{ji}N_i^2 \quad \text{with } i \neq j. \quad (2.17)$$

Finally, we can define the coupling coefficient k as:

$$k = \frac{M}{\sqrt{L_1 L_2}}, \quad 0 \leq k \leq 1, \quad (2.18)$$

which indicates how strong or weak the inductive coupling between the coils is.

Boosting the magnet field with ferromagnetic materials

While \mathbf{H} depends on the currents applied to an object, \mathbf{B} depends on the material properties of the object. In free space (vacuum), the relation is linear and represented by the magnetic constant μ_0 :

$$\mathbf{B} = \mu_0 \mathbf{H} \quad \text{with} \quad \mu_0 \approx 4\pi \cdot 10^{-7} \frac{\text{N}}{\text{A}^2}. \quad (2.19)$$

To boost \mathbf{B} for a given \mathbf{H} , ferromagnetic materials are typically used. These materials have a high relative magnetic permeability μ_r :

$$\mathbf{B} = \mu \mathbf{H} = \mu_0 \mu_r \mathbf{H}. \quad (2.20)$$

Note that μ_r is a dimensionless quantity and that (2.20) assumes linear and isotropic material behavior.

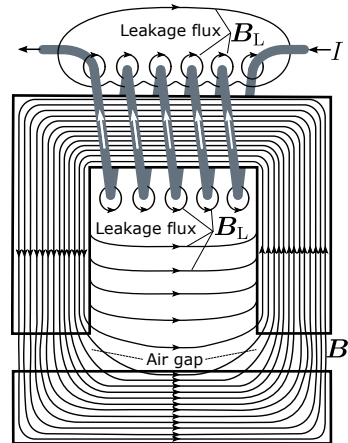


Fig. 2.9: Simplified magnetic field lines of an iron yoke with a coil (adapted from: [Wikimedia Commons](#), public domain)

Relative permeability and magnetic saturation

Material	μ_r (range)
Air / copper / aluminum	(\approx)1
Iron (99.8 % pure)	5000
Electrical steel	2000 - 35000
Ferrite	200 - 20000

Tab. 2.1: Typical relative permeabilities of materials

Linear magnetic behavior ($\mu_r = \text{const.}$) is only a local approximation. When considering larger H ranges, the (differential) permeability becomes nonlinear:

$$\mu_r(H) = \frac{dB}{dH}. \quad (2.21)$$

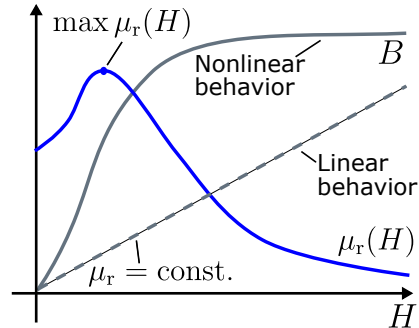


Fig. 2.10: Illustrative magnetization curves for ferromagnets (and ferrimagnets) and corresponding permeabilities (adapted from: [Wikimedia Commons](#), public domain)

Magnetic domains (1)

- ▶ Magnetic domains are regions within a material where the magnetic moments of atoms are aligned (“mini magnets”).
- ▶ The magnetization within each domain points in a uniform direction, but the magnetization of different domains may point in different directions.



Fig. 2.11: Animation of moving domain walls (source: [Wikimedia Commons](#), Zureks, CC BY-SA 3.0)

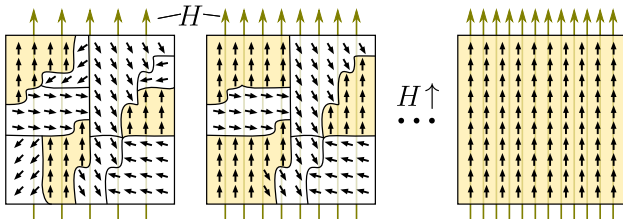


Fig. 2.12: Change of magnetic domains due to an external magnetic field (adapted from: [Wikimedia Commons](#), M. Run, CC BY-SA 4.0)

Magnetic domains (2)

- ▶ A large region of material with a constant magnetization throughout creates a large magnetic field (diagram a) below). This requires a lot of magnetostatic energy stored in the field.
- ▶ To reduce this energy, the sample can “split” into two domains, with the magnetization in opposite directions in each domain which reduces the overall field (diagram b) below).
- ▶ To reduce the field energy further, each of these domains can split also, resulting in smaller parallel domains with magnetization in alternating directions, with smaller amounts of field outside the material (diagram c) below).

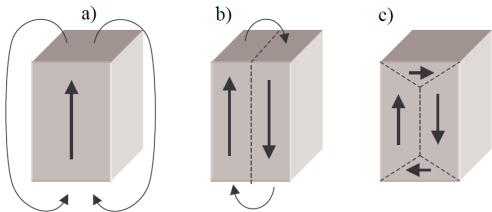


Fig. 2.13: Simplified representation of the formation of magnetic domains on the basis of energy minimization (source: [Wikimedia Commons](#), public domain)

Hysteresis

- ▶ Material defects lead to small, random jumps in magnetization called Barkhausen jumps.
- ▶ Domain walls move irregularly.
- ▶ Process also depends on the history of the magnetization process (dynamic system).

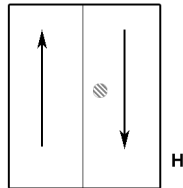


Fig. 2.14: Animation of the Barkhausen jump (source: Wikimedia Commons, public domain)

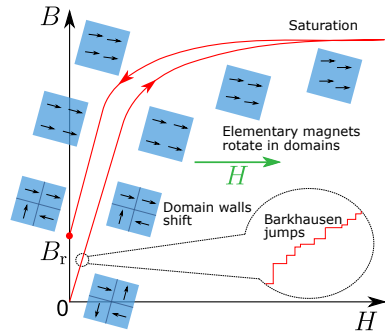


Fig. 2.15: Simplified hysteresis curve in first quadrant with magnetic domains illustration
(adapted from: [Wikimedia Commons](#), Fralama, CC BY-SA 3.0)

Hysteresis curve and losses

- ▶ With an external and varying field H , a closed hysteresis curve is obtained.
- ▶ Traversing through the curve requires to move the domain walls and rotate the elementary magnets within the domains.
- ▶ This process requires work and leads to heat dissipation (losses).
- ▶ The area enclosed by the hysteresis curve is identical to the relative remagnetization work (per volume, that is, $[w_h] = \frac{J}{m^3}$):

$$w_h = \oint \mathbf{H} \cdot d\mathbf{B}. \quad (2.22)$$

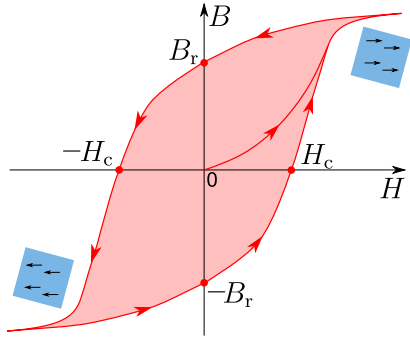


Fig. 2.16: Exemplary hysteresis curve with B_r being the remanence field density and H_c the coercivity field strength

How can we model the hysteresis losses?

- ① **Data look-up table:** Measure the hysteresis curve and its losses directly on a test bench (cf. [MagNet project data hub](#)).
- ② **Loss-fitted models:** Use empirical models to fit the hysteresis losses (e.g., Steinmetz model):

$$P_h = k_h f^a \max\{B\}^b.$$

- ③ **Curve-fitted models:** Use empirical models to describe the hysteresis curve and derive the losses (e.g., ODE as in the Jiles-Atherton model):

$$\frac{dB}{dH} = f(B, H).$$

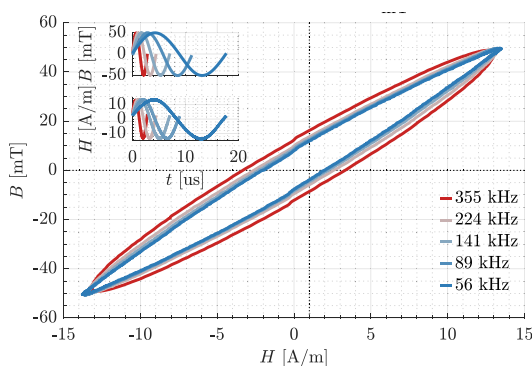


Fig. 2.17: Measured B - H loops for sinusoidal excitation at different frequencies (source: [IEEE TPEL](#), Serrano et al., CC BY 4.0)

Alternative to boost the magnet field: permanent magnets (PMs)

- ▶ Create own persistent magnetic fields.
- ▶ Consist of hard ferromagnetic (or ferrimagnetic) materials.
- ▶ Nearly constant magnetization offset B_{PM} in the usual operating range:

$$\mathbf{B} = \mu_0 \mu_r \mathbf{H} \approx \mu_0 \mathbf{H} + \mathbf{B}_{PM}. \quad (2.23)$$



Fig. 2.18: PMs on a rotor (source: flickr.com, AIDG, CC BY-NC-SA 2.0)

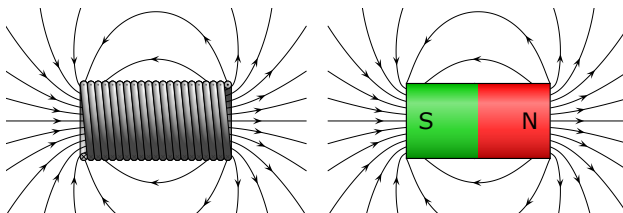


Fig. 2.19: Permanent magnets as alternatives to current-based excitation (source: Wikimedia Commons, M. Run, CC BY-SA 3.0)

Hysteresis curve of permanent magnets

- ▶ PM's magnetization is nearly completely saturated and constant in common operation area.
- ▶ The greater the coercivity H_c , the greater the resistance of the PM to demagnetization by external fields.
- ▶ Beyond the so-called knee point, PMs are (partially) demagnetized.
- ▶ Important figure of merit is the so-called energy product:

$$(BH)_{\max} = \max \{-BH\}. \quad (2.24)$$

- ▶ The higher $(BH)_{\max}$ the less PM material is needed for an application.

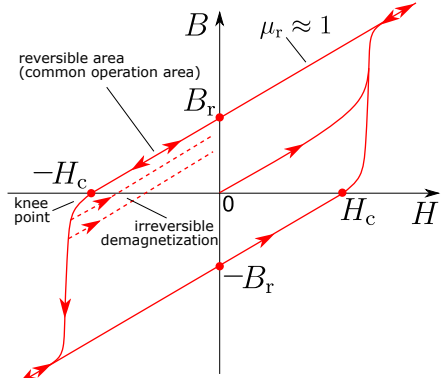


Fig. 2.20: Exemplary hysteresis curve of a permanent magnet

Hysteresis curve of permanent magnets (temperature dependence)

- ▶ Besides pressure and vibrations, PMs are also sensitive to temperature.
- ▶ The coercivity H_c and the remanence B_r decrease with increasing temperature.
- ▶ Hence, with higher temperatures, a PM gets more susceptible to demagnetization.

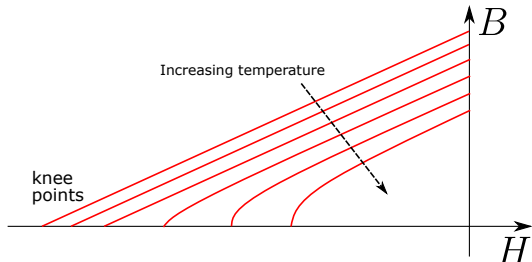


Fig. 2.21: Qualitative representation of the temperature dependence of permanent magnets

Energy product overview of permanent magnets

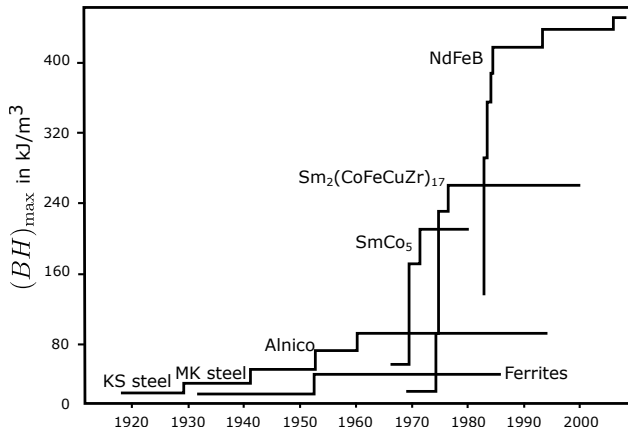


Fig. 2.22: Historic development of PM materials and their energy product (adapted from: [Wikimedia Commons](#), Kopiersperre, CC BY-SA 4.0)

Manufacturing process of NdFeB permanent magnets

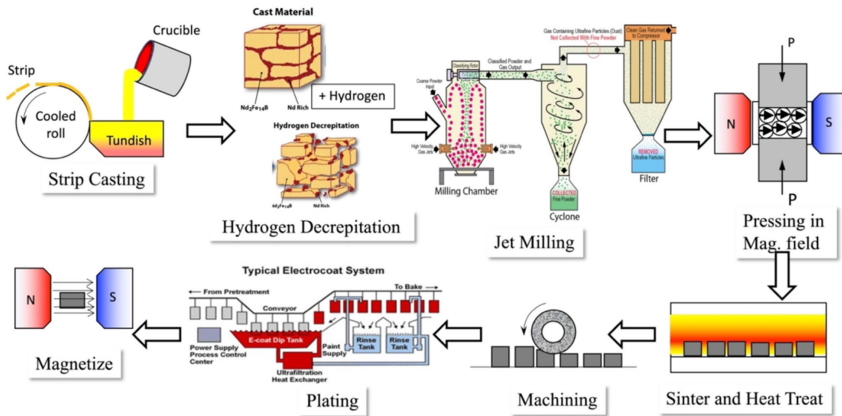


Fig. 2.23: Basic process steps for the NdFeB-based magnets (source: Springer JOM, J. Cui et al., CC BY 4.0)

Electromagnetic induction (Maxwell – Faraday equation)

A changing magnetic field induces an electric field according to the Maxwell – Faraday equation:

Integral form: $\oint_{\partial S} \mathbf{E} \cdot d\mathbf{s} = -\frac{d}{dt} \iint_S \mathbf{B} \cdot d\mathbf{S},$ (2.25)

Differential form: $\nabla \times \mathbf{E} = -\frac{\partial \mathbf{B}}{\partial t}.$ (2.26)

Here, \mathbf{E} is the electric field strength and S is the surface enclosed by the loop $\partial S.$

- ▶ **Lenz's law:** The induced electric field opposes the change in magnetic field (negative sign above).

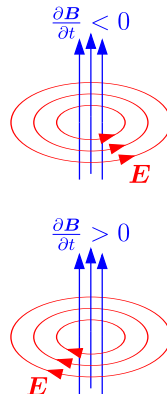


Fig. 2.24: Representation of the magnetic and electric field relation (adapted from: [Wikimedia Commons](#), Qniemiec, CC BY-SA 3.0)

Electromotive force (EMF) and electromagnetic induction

If the integration path ∂S is identical to a conductor loop, the changing magnetic field induces a voltage u_i (electromotive force, EMF) according to Faraday's law:

$$u_i = \oint_{\partial S} \mathbf{E} \cdot d\mathbf{s} = -\frac{d}{dt} \iint_S \mathbf{B} \cdot d\mathbf{S}. \quad (2.27)$$

- ▶ Despite its name, the term EMF does not describe a force in the physical sense (as u_i is obviously a voltage).
- ▶ The term remains a historical artifact from the early days of electrical engineering, but is still frequently used in today's literature.

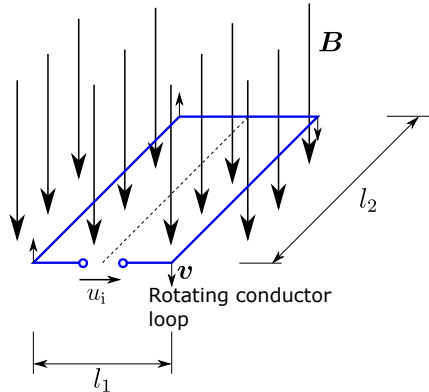


Fig. 2.25: Induced voltage / EMF in a rotating conductor loop (adapted from: [Wikimedia Commons](#), M. Lenz, CC0 1.0)

Intermediate wrap up: electromagnetic principles and magnetic materials

$$u \frac{\oint_{\partial S} \mathbf{E} \cdot d\mathbf{s} = -\frac{d}{dt} \iint_S \mathbf{B} \cdot d\mathbf{S}}{\text{Induction law}} \mathbf{B}$$
$$i \frac{\text{Ampere's law (simple version)}}{\oint_{\partial S} \mathbf{H} \cdot d\mathbf{s} = i} \mathbf{H}$$

Material property
 $\mathbf{B} = \mu_0 \mu_r \mathbf{H}$

Fig. 2.26: Illustration of the connections between the phenomena discussed previously (derived from: [Wikimedia Commons](#), M. Lenz, CC0 1.0)

Lorentz force

The force \mathbf{F} acting on a particle of electric charge q with instantaneous velocity \mathbf{v} , due to an external electric field \mathbf{E} and magnetic field \mathbf{B} , is given by

$$\mathbf{F} = q(\mathbf{E} + \mathbf{v} \times \mathbf{B}). \quad (2.28)$$

- ▶ The term $q\mathbf{E}$ is called the electric force.
- ▶ The term $q(\mathbf{v} \times \mathbf{B})$ is called the magnetic force.
- ▶ In Cartesian coordinates, the Lorentz force is given by:

$$\begin{aligned} F_x &= q(E_x + v_y B_z - v_z B_y), \\ F_y &= q(E_y + v_z B_x - v_x B_z), \\ F_z &= q(E_z + v_x B_y - v_y B_x). \end{aligned} \quad (2.29)$$

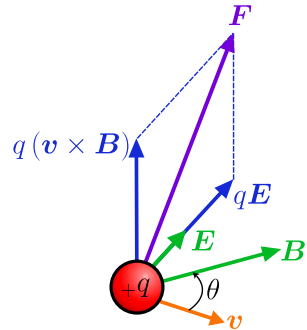


Fig. 2.27: Lorentz force \mathbf{F} on a particle (of charge q) in motion (instantaneous velocity \mathbf{v}) with given \mathbf{E} and \mathbf{B} fields (adapted from: [Wikimedia Commons](#), Maschen, CC0)

Hand rule of the magnetic Lorentz force

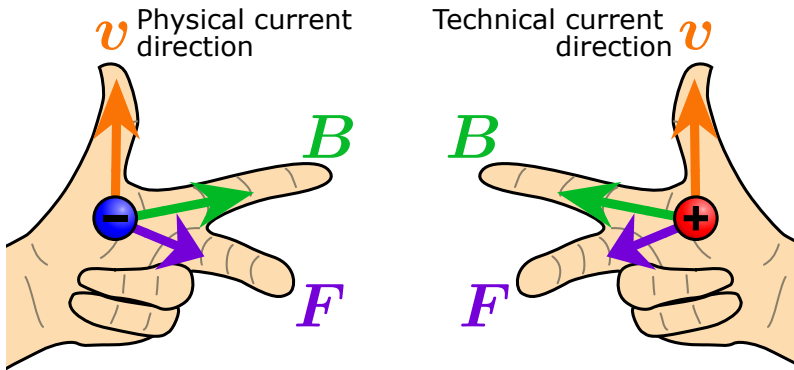


Fig. 2.28: Right and left hand rule for the magnetic Lorentz force $q(\mathbf{v} \times \mathbf{B})$ (adapted from: Wikimedia Commons, M. Run, CC BY-SA 3.0)

Lorentz force density for a continuous charge distribution

For a continuous charge distribution in motion, the Lorentz force density (force per unit volume) becomes:

$$\mathbf{f} = \rho \mathbf{E} + \mathbf{J} \times \mathbf{B}. \quad (2.30)$$

- ▶ ρ is the charge density (charge per unit volume).
- ▶ $\mathbf{J} = \rho \mathbf{v}$ is the current density.

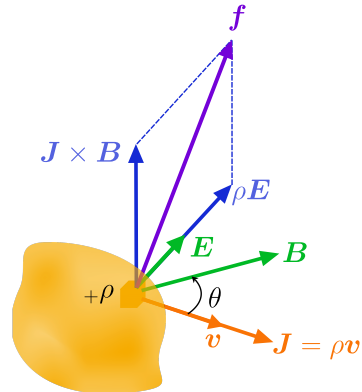


Fig. 2.29: Lorentz force density \mathbf{f} on a continuous charge distribution (charge density ρ) in motion (adapted from: [Wikimedia Commons](#), Maschen, CC0)

Magnetic networks

- ▶ **Motivation:** Model magnetic systems with a simplified lumped-parameter approach and apply analysis techniques analogous to electric networks.
- ▶ **Assumption:** magnetic field is homogenous within a lumped element (cf. Fig. 2.30).
- ▶ The magnetic flux per element is:

$$\phi_k = A_k B_k. \quad (2.31)$$

- ▶ The magnetic voltage (magnetomotive force – MMF) per element is:

$$\theta_k = l_k H_k. \quad (2.32)$$

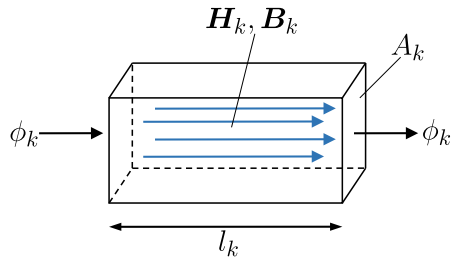


Fig. 2.30: Magnetic element with homogenous magnetic field (adapted from J. Böcker, [Mechatronics and Electrical Drives](#), CC BY-NC-ND)

Magnetic networks (cont.)

- The magnetic reluctance per element is:

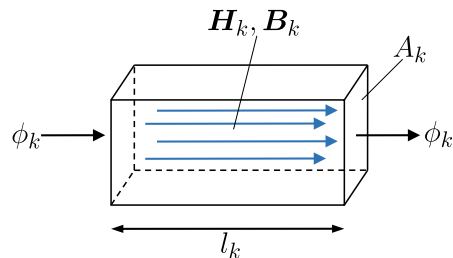
$$R_k = \frac{\theta_k}{\phi_k} = \frac{l_k}{\mu_0 \mu_{rk} A_k}. \quad (2.33)$$

- The magnetic conductivity (or permeance) per element is:

$$\Lambda_k = \frac{1}{R_k} = \frac{\mu_0 \mu_{rk} A_k}{l_k}. \quad (2.34)$$

- As the magnetic field is free of sources ($\nabla \cdot \mathbf{B} = 0$), it follows (node rule – analogous to Kirchhoff's first law):

$$\sum_k \phi_k = 0. \quad (2.35)$$



Magnetic networks (cont.)

Considering magnetostatic situations where the displacement current can be neglected, Ampère's law reads:

$$\oint_{\partial S} \mathbf{H} \cdot d\mathbf{s} = I_f = NI = \sum_k \theta_k = \sum_k l_k H_k. \quad (2.36)$$

So far, the equation has not the structure of the second Kirchhoff's law (loop rule). However, we can force this desired format by placing the term with the electric currents on the left-hand side of the equation:

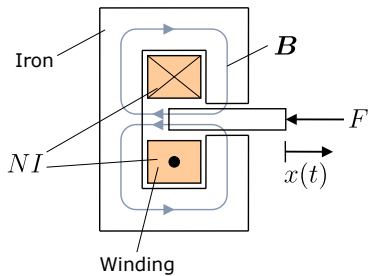
$$\sum_k \theta_k - \theta_0 = 0 \quad \text{with} \quad \theta_0 = NI \quad (\text{MMF term}). \quad (2.37)$$

Comparison: electric and magnetic network quantities

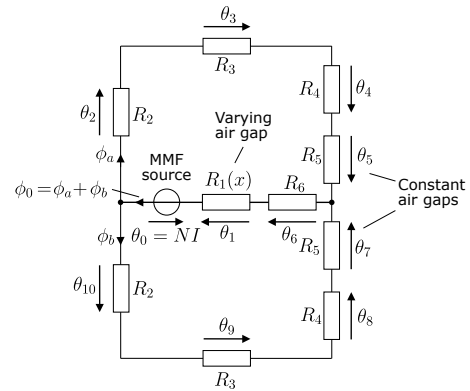
Electric network	Magnetic network				
Voltage	$u = \int \mathbf{E} \cdot d\mathbf{s}$	V	Magnetomotive force	$\theta = \int \mathbf{H} \cdot d\mathbf{s}$	A
Electric field	\mathbf{E}	$\frac{\text{V}}{\text{m}}$	Magnetic field	\mathbf{H}	$\frac{\text{A}}{\text{m}}$
Current	i	A	Magnetic flux	ϕ	Vs
Resistance	R	Ω	Reluctance	R	$\frac{1}{\text{H}}$
Conductance	G	S	Permeance	Λ	H
Conductivity	σ	$\frac{S}{\text{m}}$	Permeability	μ	$\frac{\text{H}}{\text{m}}$
Ohm's law	$u = Ri$		Hopkinson's law	$\theta = R\phi$	
Kirchoff's first law	$\sum i_k = 0$		Equivalent first law	$\sum \phi_k = 0$	
Kirchoff's second law	$\sum u_k = 0$		Equivalent second law	$\sum \theta_k - \theta_0 = 0$	

Tab. 2.2: Electric and magnetic network quantities and their analogies

Magnetic network example: simple magnetic actuator



(a) Simple magnetic actuator



(b) Magnetic network representation of the actuator

Fig. 2.31: Example for a simple magnetic actuator and its magnetic network representation (adapted from J. Böcker, [Mechatronics and Electrical Drives, CC BY-NC-ND](#))

Eddy currents

- ▶ A changing magnetic field induces a voltage.
- ▶ In bulky conductive materials (e.g., electromagnetic steel) this voltage drives currents called eddy currents.
- ▶ Eddy currents lead to energy losses and heat dissipation.
- ▶ To reduce eddy currents, laminated cores are used as they decrease the effective current path width and, therefore, increase the effective resistance per sheet.

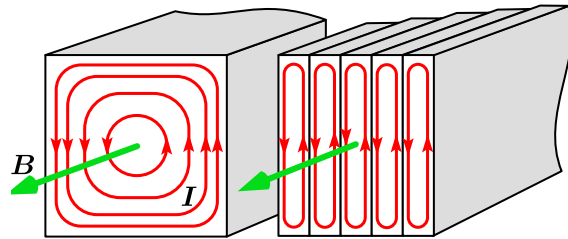


Fig. 2.32: Eddy current formations in solid and laminated steel cores (source: [Wikimedia Commons](#), Chetvorno, CC0)

Eddy currents: single sheet example

Assumption

Sheet's thickness d is much smaller than the sheet's width w and the magnetic flux density \mathbf{B} is homogenous in the normal direction of S and introduces a sinusoidal excitation $\mathbf{B}(x, y, t) = \hat{\mathbf{B}} \sin(\omega t)$.

From (2.26) integrating over S , we get

$$2wE(x, t) = -\frac{\partial B}{\partial t} 2xw$$

with $2w$ being the effective contour length of ∂S and $2xw$ being the effective surface area.

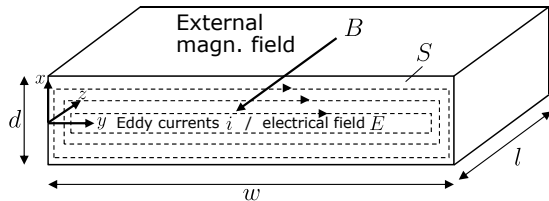


Fig. 2.33: Single sheet and induced eddy currents

Eddy currents: single sheet example (cont.)

With Ohm's law and the material conductivity σ , we get the current density J :

$$J(x, t) = \sigma E(x, t) = -x\sigma \frac{\partial B}{\partial t}.$$

Inserting the assumed magnetic flux density distribution it follows:

$$J(x, t) = -x\sigma\omega\hat{B}\cos(\omega t).$$

The relative power loss (per volume) density $p(x, t)$ results in:

$$p(x, t) = \frac{1}{\sigma} J^2(x, t) = x^2\sigma\omega^2\hat{B}^2\cos^2(\omega t).$$

The average power loss per volume (considering the x -direction) is:

$$p(t) = \frac{1}{d} \int_{-d/2}^{d/2} p(x, t) dx = \frac{1}{12}\sigma\omega^2 d^2 \hat{B}^2 \cos^2(\omega t).$$

Eddy currents: single sheet example (cont.)

The average power loss per volume and time is then:

$$p = \frac{1}{T} \int_0^T p(t) dt = \frac{1}{24} \sigma (\omega d \hat{B})^2.$$

Although this is a simplified model, it shows the significance of

- ▶ the sheet's thickness d ,
- ▶ and excitation conditions ω and \hat{B} .

This finding motivated empirical fitting approaches, like Bertotti's model for the eddy currents:

$$p_e \approx k_e f^2 \hat{B}^2.$$

Power loss types in electrical machines

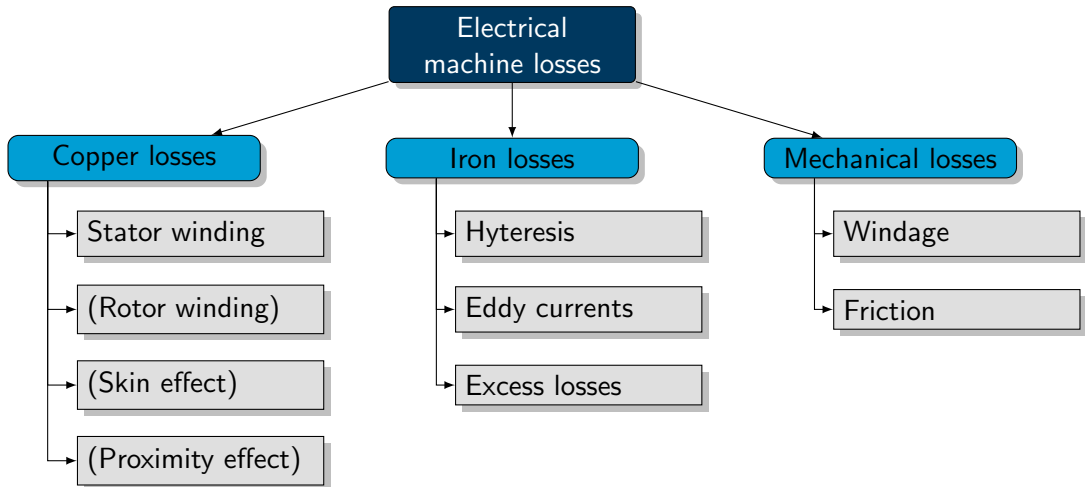


Fig. 2.34: Overview of power loss types in electrical machines

Table of contents

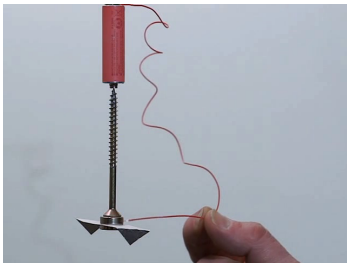
3 DC machines

DC machines

Oliver Wallscheid



Homopolar / unipolar machines



(a) Video of an operating homopolar machine (source: [Wikimedia Commons](#), Smial, Free Art License)

(b) Electric current, magnetic field and Lorentz force (adapted: [Wikimedia Commons](#), M. Run, CC BY-SA)

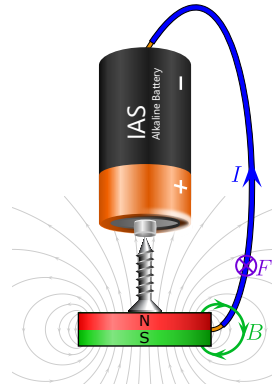


Fig. 3.1: Working principle of homopolar machines demonstrated with a simple permanent magnet, battery and screw design

Homopolar / unipolar machines (cont.)

- ▶ Homopolar machines are the simplest form of electric machines.
- ▶ They are also true DC machines, as the current and flux paths are unidirectional.
- ▶ The general design prevents connecting multiple rotor turns in series to increase the voltage, that is, only a relatively low voltage is induced.
- ▶ Consequently, homopolar machines require high currents (in the order of kA or even MA) to reach a useful power range which limited their application.

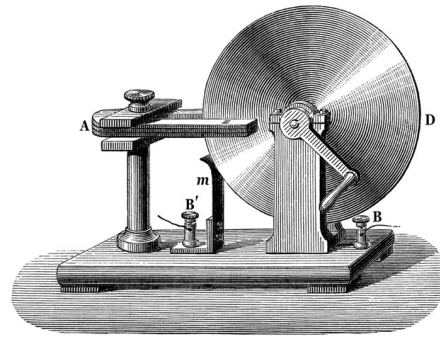


Fig. 3.2: The Faraday disk: another homopolar machine (source: [Wikimedia Commons](#), public domain)

Working principle of usual DC machines

Let's consider Fig. 3.3 and assume that the flux density B is constant in the air gap and that the conductor loop has the axial length l_z . According to the Lorentz force we have

$$F = I_a B l_z. \quad (3.1)$$

The torque T on the conductor loop is given by

$$T = 2F \frac{d}{2} \cos(\varepsilon) = I_a B l_z d \cos(\varepsilon). \quad (3.2)$$

If the loop spins with an angular velocity ω , mechanical power $P_{\text{me}} = T\omega$ is transferred.

Question: What is happening if the coil is outside the magnetic field?

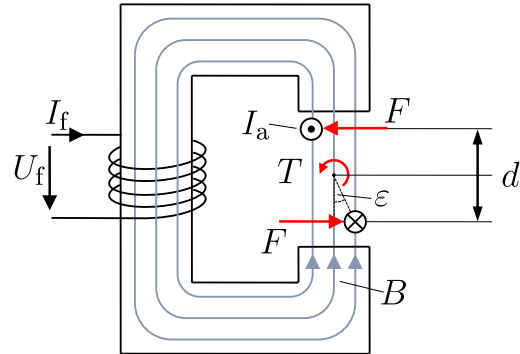


Fig. 3.3: Torque on a conductor loop (adapted from J. Böcker, *Elektrische Antriebstechnik*, Paderborn University, 2020)

DC-machine cross section

- ▶ To ensure a quasi-continuous torque, the current through the conductor loop(s) in the rotor must have a constant direction.
- ▶ This is achieved by using a commutator (brushes).
- ▶ Compared to homopolar machines, DC machines require a mechanical rectification of the current.

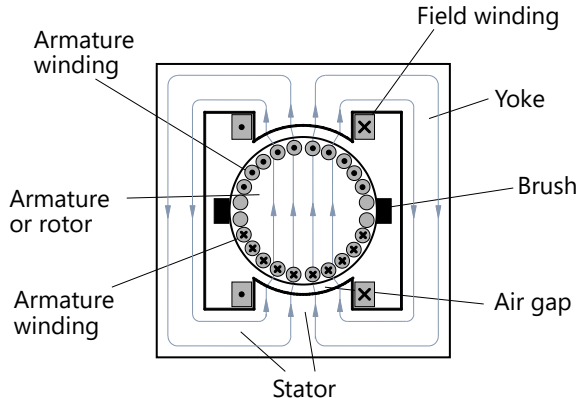


Fig. 3.4: Simplified DC machine cross section (adapted from J. Böcker, *Elektrische Antriebstechnik*, Paderborn University, 2020)

Commutation

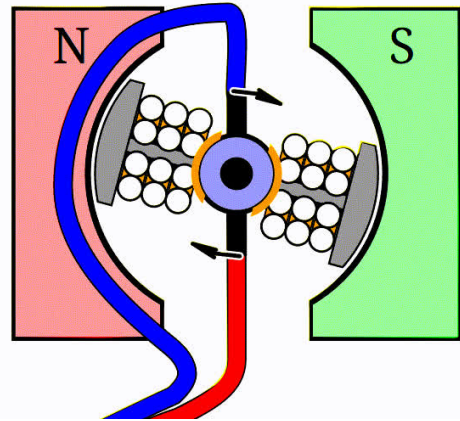
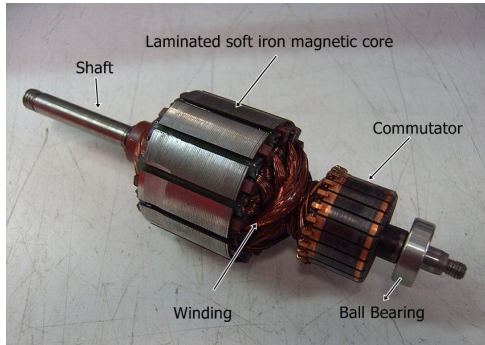


Fig. 3.5: Animation of the commutation process
(source: [Wikimedia Commons](#), M. Frey, CC BY-SA 3.0)

Armature and commutator



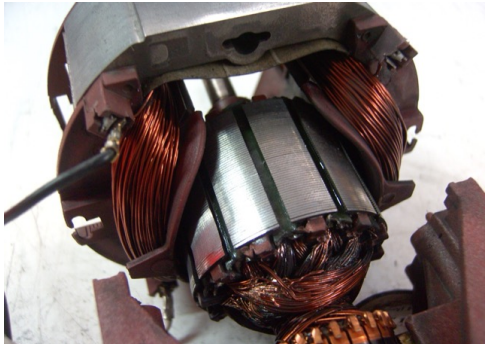
(a) Commutator with brushes and springs (source: [Wikimedia Commons](#), Marrrci, CC BY-SA 3.0)



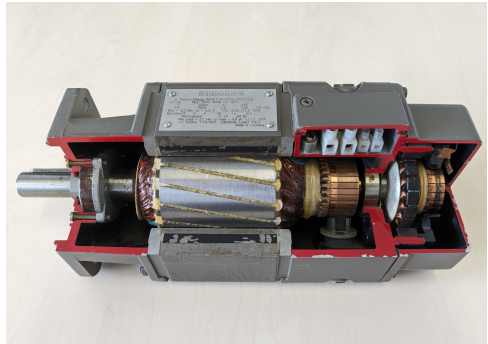
(b) DC machine armature with commutator (source: [Wikimedia Commons](#), public domain)

Fig. 3.6: Examples of commutators and armatures

Armature and commutator (cont.)



(c) Armature inside stator (source: [Wikimedia Commons](#), Marrrci, CC BY-SA 3.0)



(d) DC machine with permanent magnet excitation and tacho speed sensor

Fig. 3.6: Examples of commutators and armatures (cont.)

Basic structure of the armature

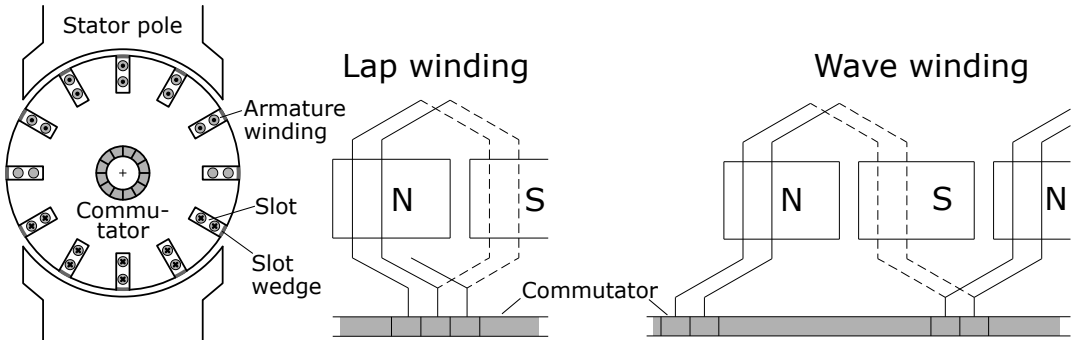


Fig. 3.7: Cross section of a drum-type armature including principle winding schemes (adapted from W. Novender, *Elektrische Maschinen*, Technische Hochschule Mittelhessen, 2023)

Types of winding conductors

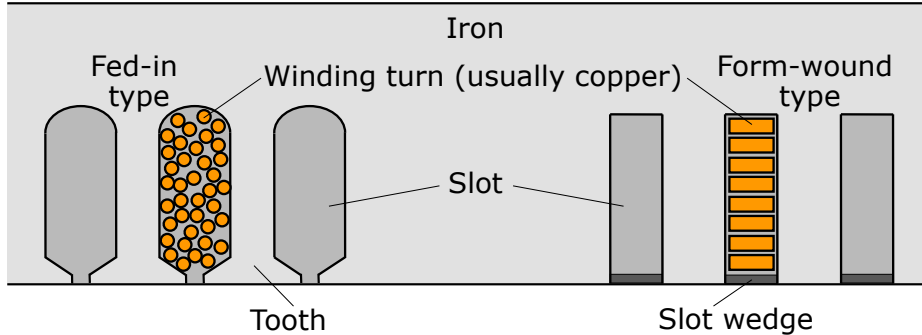


Fig. 3.8: Types of winding conductors – unwound representation along the circumference (adapted from J. Böcker, *Controlled Three-Phase Drives*, Paderborn University, 2021)

Commutation process with an armature lap winding

Armature movement →

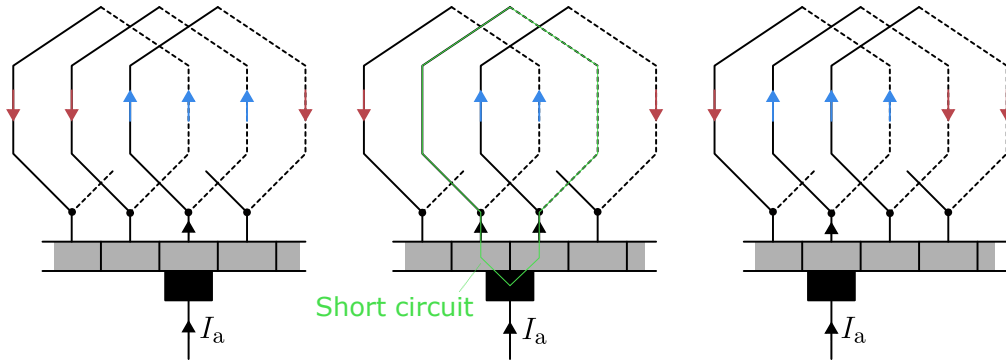


Fig. 3.9: Three still images of the commutation process with a simplified winding representation (from left to right): when the brush touches two commutator segments, the according conductor loop is short-circuited and the current is reduced to zero. The brush then moves to the next commutator segment and the current starts flowing again but in the opposite direction (adapted from W. Novender, *Elektrische Maschinen*, Technische Hochschule Mittelhessen, 2023).

DC machines with multiple pole pairs

- ▶ To reduce the effective length per armature conductor loop, the winding can form multiple pole pairs p .
- ▶ This will reduce the inductance per loop which is beneficial for the commutation process.
- ▶ The stator excitation must meet the same number of pole pairs.
- ▶ Given some inner stator diameter d_s , the resulting pole pitch is:

$$\tau_p = \frac{\pi d_s}{2p}, \quad \rho_p = \frac{\pi}{p}. \quad (3.3)$$

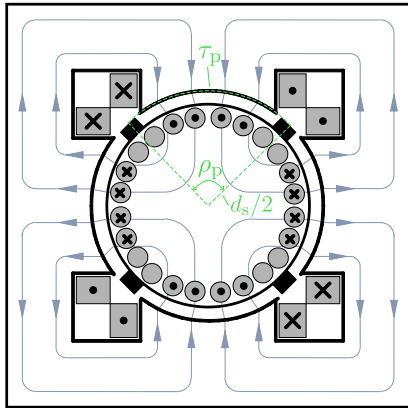


Fig. 3.10: Simplified DC machine cross section with $p = 2$ pole pairs (adapted from J. Böcker, *Elektrische Antriebstechnik*, Paderborn University, 2020)

Armature winding characteristics

For describing the armature winding layout, the following parameters are introduced:

- Q : number of slots, N_c : number of conductor turns per coil,
 K : number of commutator elements, $u = K/Q$: slot to commutator ratio,
 $z_a = 2KN_c$: total number of armature conductors.

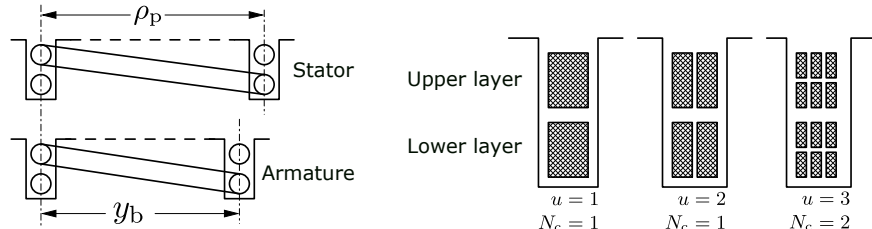


Fig. 3.11: Coil width and slot design characteristics (adapted from W. Novender, *Elektrische Maschinen*, Technische Hochschule Mittelhessen, 2023)

Double layer winding

- ▶ The forward conductor of one coil and the return conductor of another coil are placed in the same slot. This is the common winding scheme (although not limited to it).
- ▶ Enables chording of the winding ($\rho_p \neq y_b$), another degree of freedom for the machine design (cf. Fig. 3.11).

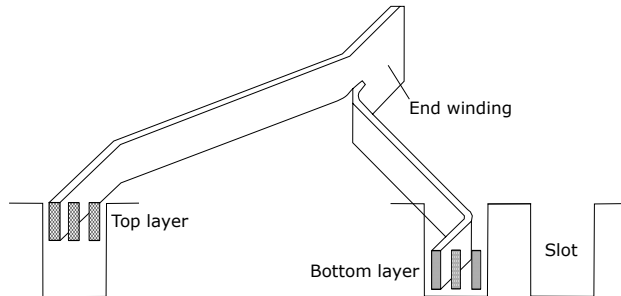


Fig. 3.12: Double layer winding with $u = 3$ with a solid conductor element (which can be pre-manufactured for cost reasons – inspired from A. Binder, *Elektrische Maschinen und Antriebe*, Vol. 2, Springer, 2017)

Lap winding characteristics

- ▶ Back pitch y_b : coil span from the back end
- ▶ Front pitch y_f : coil span from the front end
- ▶ Resultant pitch y_r : distance between two consecutive coils
- ▶ Commutator pitch y_c : distance between two consecutive commutator segments

Progressive winding

Fig. 3.13 shows a progressive winding layout with $y_b > y_f$, i.e., the coils do not cross themselves.

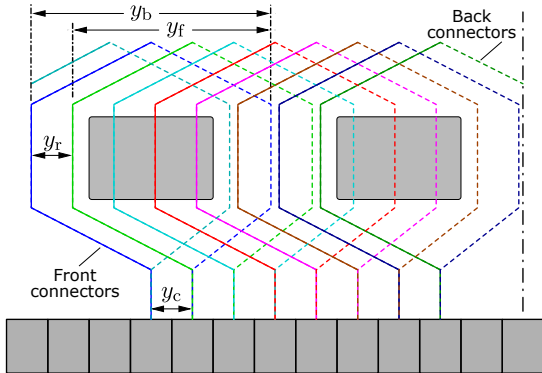


Fig. 3.13: Distance definitions of the armature lap winding (adapted from W. Novender, *Elektrische Maschinen*, Technische Hochschule Mittelhessen, 2023)

Lap winding characteristics (cont.)

Retrogressive winding

Fig. 3.14 shows a Retrogressive winding layout with $y_b < y_f$, i.e., each coil crosses itself.

- ▶ Retrogressive windings require more conductor material due to the crossing of the coils and, therefore, are less common.
- ▶ Technical feasibility requires $y_b - y_f = \pm y_c$, i.e., the lap winding progresses or retrogresses by one commutator element.

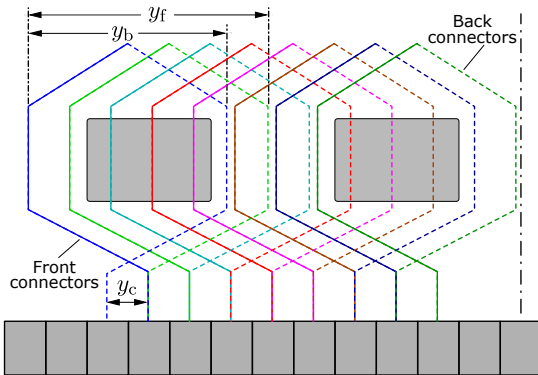


Fig. 3.14: Lap winding with a retrogressive scheme
(adapted from W. Novender, *Elektrische Maschinen*, Technische Hochschule Mittelhessen, 2023)

Lap winding: final remarks and single pole pair example

- ▶ Armature turns per pole:

$$N_p = \frac{KN_c}{2p}$$

- ▶ Current per armature conductor: $I_c = \frac{I_a}{2p}$

Parallel connection of poles

For $p > 1$ the lap winding parallels the armature coils for each pole enabling a higher current (but limited voltage) rating.

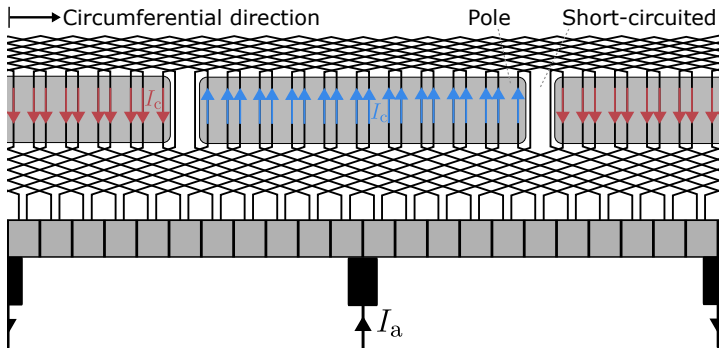


Fig. 3.15: Lap winding with commutator unrolled along the circumferential coordinate

Wave winding characteristics

- Commutator pitch (wave winding):
 $y_c = y_f + y_b$, i.e., each coil spans (nearly) the entire pole pitch.

Progressive winding

Fig. 3.16 shows a progressive winding layout since each new wave winding coil starts one commutator element to the right.

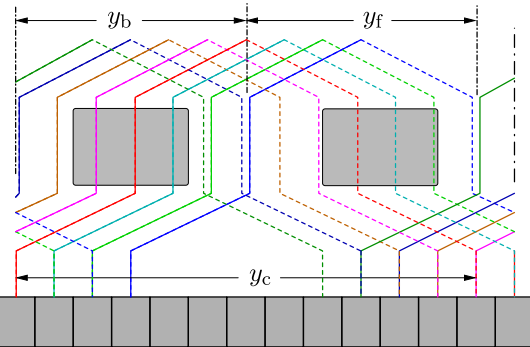


Fig. 3.16: Distance definitions of the armature wave winding (adapted from W. Novender, *Elektrische Maschinen*, Technische Hochschule Mittelhessen, 2023)

Wave winding: final remarks and single pole pair example

- ▶ Armature turns per pole:
 $N_p = \frac{KN_c}{2}$
- ▶ Current per armature conductor: $I_c = \frac{I_a}{2}$

Series connection of poles

For $p > 1$ the wave winding connects the armature coils for all poles in series enabling a higher voltage (but limited current) rating.

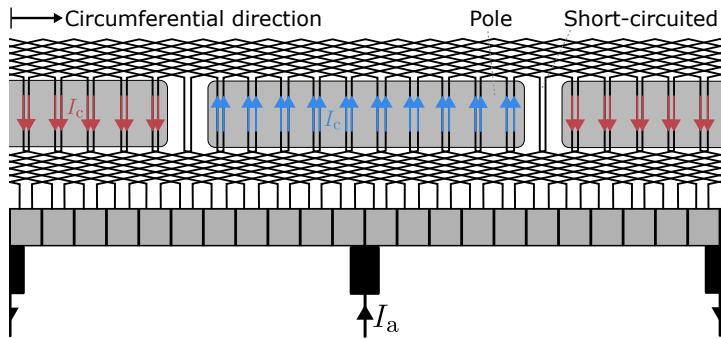


Fig. 3.17: Wave winding with commutator unrolled along the circumferential coordinate

Lap and wave winding comparison

Introducing the parameter

$$a = \text{number of parallel armature conductors} \quad (3.4)$$

we can wrap up the following summary:

$$\text{Current per conductor: } I_c = \frac{I_a}{2a}, \quad \text{Armature turns per pole: } N_p = \frac{KN_c}{2a}. \quad (3.5)$$

Comparison

- ▶ Lap winding: $a = p$ (parallel connection of poles)
- ▶ Wave winding: $a = 1$ (series connection of poles)

Commutation process

During the commutation time Δt_c the brush bridges two commutator segments and the short-circuited conductor coil current i_c is changing signs. Here, two major scenarios can be distinguished:

- The commutation is such fast that high local current densities are prevented.
- The commutation is slow and high local current densities lead to sparking effects.

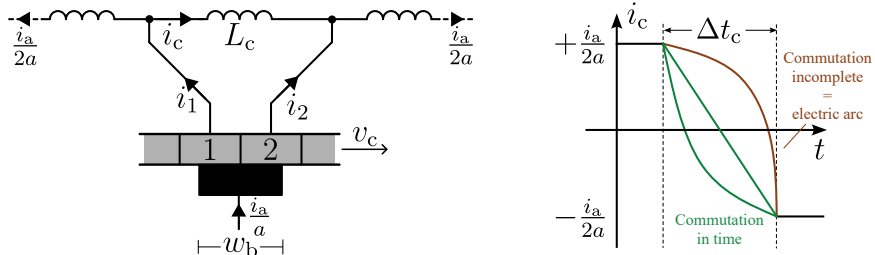


Fig. 3.18: Left: simplified equivalent circuit diagram of the short-circuited coil during commutation.
Right: qualitative trajectories of the conductor current i_c

Commutation process (cont.)

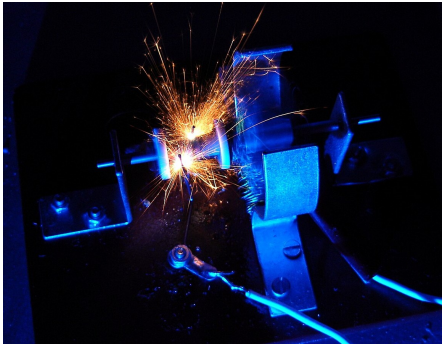


Fig. 3.19: Commutator sparking of a simple DC machine (source: [Wikimedia Commons](#), M. Frey, CC BY-SA 4.0)

Assuming that the brush width w_b is much bigger than one commutator segment (which is usual practice), the commutation time Δt_c is given by

$$\Delta t_c \approx \frac{w_b}{v_c}. \quad (3.6)$$

Here, v_c is the brush velocity

$$v_c = \omega \frac{d_a}{2} \quad (3.7)$$

with the armature angular velocity ω and the armature diameter d_a . Due to the changing current in the coil, the so-called reactane voltage u_r is induced:

$$u_r = L_c \frac{di_c}{dt} \approx L_c \frac{i_a}{a\Delta t_c} = L_c i_a \frac{\omega d_a}{aw_b^2}. \quad (3.8)$$

Air gap field

Assumption: The air gap field distribution is homogenous

and without any leakage (cf. Fig. 3.20).

Consequently, we model the magnetic machine behavior with the simplified network shown in Fig. 3.21.

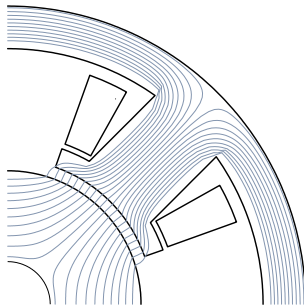


Fig. 3.20: Idealized field lines (adapted from W. Novender,
Elektrische Maschinen, Technische Hochschule Mittelhessen, 2023)

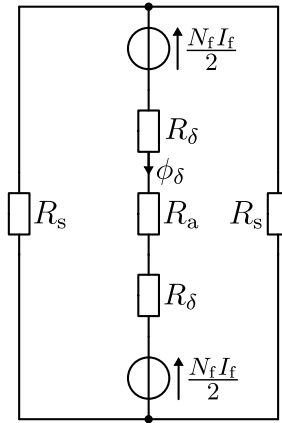


Fig. 3.21: Simplified magnetic network of a DC machine

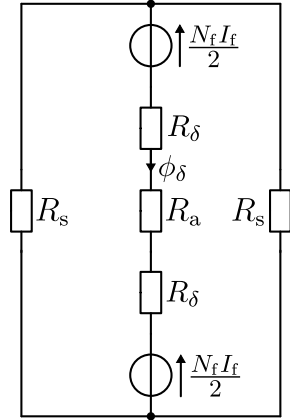
Air gap field (cont.)

We introduce the following magnetic reluctances

$$\begin{aligned} R_s &= \frac{l_s}{\mu_{r,fe}\mu_0 A_s} \quad (\text{stator reluctance}), \\ R_a &= \frac{l_a}{\mu_{r,fe}\mu_0 A_a} \quad (\text{armature reluctance}), \\ R_\delta &= \frac{\delta}{\mu_0 A_\delta} \quad (\text{air gap reluctance}). \end{aligned} \quad (3.9)$$

Above l_i and A_i are the respective lengths and cross-sectional areas of the field paths while δ is the air gap width. Furthermore, we have

$$\mu_{r,\delta} = 1, \quad \mu_{r,fe} \gg 1.$$



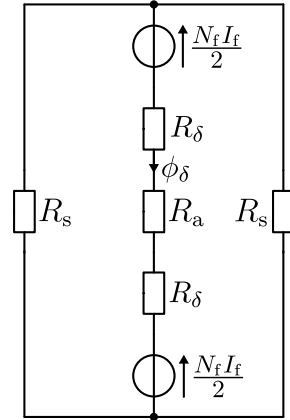
Air gap field (cont.)

With N_f field winding turns and the field current I_f , the air gap flux is given by:

$$\begin{aligned}\phi_\delta &= \frac{N_f I_f}{2R_\delta + R_a + \frac{1}{2}R_s} \\ &= \mu_0 N_f I_f \left(2\frac{\delta}{A_\delta} + \frac{l_a}{\mu_{r,\text{Fe}} A_a} + \frac{1}{2} \frac{l_s}{\mu_{r,\text{Fe}} A_s} \right)^{-1}. \quad (3.10)\end{aligned}$$

While the relative permeability of the iron paths is depending on the magnetic flux ($\mu_{r,\text{Fe}} = \mu_{r,\text{Fe}}(\phi)$) due to saturation (cf. Fig. 2.10) rendering (3.10) a nonlinear equation, we will assume that the air gap reluctance is dominating

$$R_\delta \gg \{R_a, R_s\}. \quad (3.11)$$



Air gap field (cont.)

Based on (3.10) together with (3.11) we can simplify the effective air gap flux to

$$\phi_\delta = \frac{N_f I_f}{2R_\delta} = \frac{N_F I_f}{2 \frac{\delta}{\mu_0 A_\delta}} = \frac{\mu_0 N_f A_\delta}{2\delta} I_f. \quad (3.12)$$

Here, δ is the air gap width and A_δ the effective cross-sectional area of the air gap which is

$$A_\delta = \alpha p \tau_p l_z. \quad (3.13)$$

Above, the following assumptions and definitions are made:

- ▶ l_z is the axial length of the machine.
- ▶ The air gap width is very small such that the pole pitch τ_p can be used as a good approximation for the air gap circumference.
- ▶ α is the pole coverage, that is, the ratio of the active pole surfaces to the pole pitch (cf. Fig. 3.22 on next slide) representing the average field density in the air gap.

Air gap field (cont.)

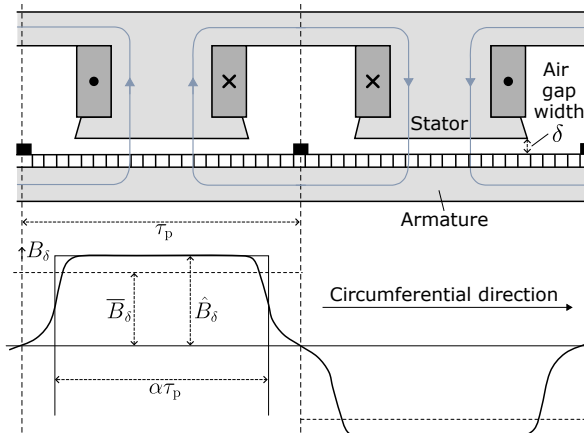


Fig. 3.22: Principle magnetic field paths through stator and rotor as well as the (idealized) normal component of the magnetic field density B_δ in the air gap (inspired from A. Binder, *Elektrische Maschinen und Antriebe*, Vol. 2, Springer, 2017)

Torque

From (3.12) we can calculate the air gap flux density \hat{B}_δ per pole pair as

$$\hat{B}_\delta = \frac{\phi_\delta}{A_\delta} = \frac{\mu_0 N_f}{2\delta p} I_f. \quad (3.14)$$

Assuming that the magnetic field only flows through each armature conductor in a perpendicular direction (cf. Fig. 3.23), the absolute Lorentz force per armature conductor is resulting in

$$F_c = \hat{B}_\delta l_z I_c = \frac{\mu_0 N_f l_z}{4\delta p a} I_f I_a. \quad (3.15)$$

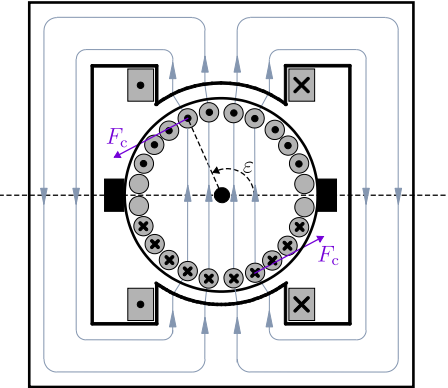


Fig. 3.23: Simplified DC machine cross section with exemplary armature conductor force representation (adapted from J. Böcker, *Elektrische Antriebstechnik*, Paderborn University, 2020)

Torque (cont.)

Assuming that the force direction acting on each armature conductor is perpendicular to the armature shaft, the torque per conductor for an armature diameter d_a is

$$T_c = F_c \frac{d_a}{2} = \frac{\mu_0 N_f l_z d_a}{8\delta p a} I_f I_a. \quad (3.16)$$

The resulting (average) machine torque T for N_a armature conductor loops from which an α share is covered by the poles (cf. Fig. 3.22) is

$$T = 2\alpha N_a T_c = \frac{\mu_0 \alpha N_f N_a l_z d_a}{4\delta p a} I_f I_a. \quad (3.17)$$

With $\tau_p = \pi d_s / (2p) = \pi d_a / (2p)$ assuming a very small air gap width δ (cf. Fig. 3.10) we can also rewrite the torque as

$$T = \frac{\mu_0 \alpha N_f N_a l_z \tau_p}{2\pi \delta a} I_f I_a. \quad (3.18)$$

Effective field inductance and effective flux linkage

To write (3.18) more compact, we introduce the effective field inductance

$$L'_f = \frac{\mu_0 \alpha N_f N_a l_z d_a}{4\delta p a} = \frac{\mu_0 \alpha N_f N_a l_z \tau_p}{2\pi \delta a}. \quad (3.19)$$

Compared to the self-inductance of the field winding

$$L_f = \frac{N_f^2}{2R_\delta} = \frac{\mu_0 p \tau_p l_z N_f^2}{4\delta}, \quad (3.20)$$

we find

$$L'_f = \underbrace{\frac{2p}{a\pi} \frac{N_a}{N_f}}_c L_f = c L_f. \quad (3.21)$$

Finally, we define the effective field flux linkage ψ'_f to rewrite the torque expression

$$\psi'_f = L'_f I_f, \quad T = c L_f I_f I_a = L'_f I_f I_a = \psi'_f I_a. \quad (3.22)$$

Flux linkage of a single armature coil

From Fig. 3.22 we assume the air gap flux density normal component along ε to be:

$$B(\varepsilon) = \begin{cases} \bar{B}_\delta, & 0 \leq \varepsilon < \pi, \\ -\bar{B}_\delta, & \pi \leq \varepsilon < 2\pi. \end{cases} \quad (3.23)$$

The flux linkage of a single armature coil starting at position ε is then

$$\begin{aligned} \phi_c(\varepsilon) &= \iint_S \mathbf{B} \cdot d\mathbf{S} = l_z d_a \int_{\varepsilon}^{\varepsilon+\pi} B(\varepsilon) d\varepsilon \\ &= l_z d_a \bar{B}_\delta \begin{cases} (\pi/2 - \varepsilon), & 0 \leq \varepsilon < \pi \\ (\varepsilon - 3\pi/2), & \pi \leq \varepsilon < 2\pi. \end{cases} \end{aligned} \quad (3.24)$$

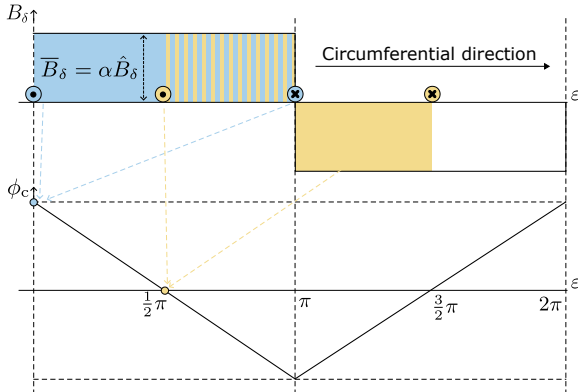


Fig. 3.24: Flux linkage ψ_c of a single armature coil based on the simplified, rectangular air gap flux density $B_\delta(\varepsilon)$ from Fig. 3.22 – light blue and yellow areas represent two exemplary armature coil positions.

Induced voltage

Assuming that the armature is rotating with the (constant) speed n (or angular velocity $\omega = 2\pi n = \dot{\varepsilon}$), the induced voltage per armature conductor loop is

$$u_{i,c} = -\frac{d}{dt}\phi_c = -\frac{d}{d\varepsilon}\phi_c \frac{d}{dt}\varepsilon = -\omega l_z d_a \bar{B}_\delta \begin{cases} -\omega, & 0 \leq \varepsilon < \pi, \\ \omega, & \pi \leq \varepsilon < 2\pi. \end{cases} \quad (3.25)$$

To calculate the total induced voltage u_i , we consider

- ▶ the rectification of the induced voltage by the commutator,
- ▶ N_a total armature conductor loops,
- ▶ $2a$ parallel armature conductors per pole pair (depends on winding scheme, cf. (3.4)),

resulting in:

$$u_i = \frac{N_a}{2a} |u_{i,c}| = \frac{N_a}{2a} \omega l_z d_a \bar{B}_\delta = \omega I_f \frac{\mu_0 \alpha N_f N_a l_z d_a}{4\delta p a} = \omega I_f \frac{\mu_0 \alpha N_f N_a l_z \tau_p}{2\pi \delta a} = \omega I_f L'_f = \omega \psi'_f. \quad (3.26)$$

Equivalent circuit diagram and summary of important equations

Field and armature voltage equations:

$$\begin{aligned} u_f &= R_f i_f + L_f \frac{di_f}{dt} \\ u_a &= R_a i_a + L_a \frac{di_a}{dt} + u_i \end{aligned} \quad (3.27)$$

Induced voltage:

$$u_i = \omega \psi'_f = \omega i_f L'_f$$

Torque:

$$T = L'_f i_f i_a = \psi'_f i_a$$

Note: we represent the machine currents with small letters to indicate that they are time-dependent (e.g., if the external voltage supplied is varying).

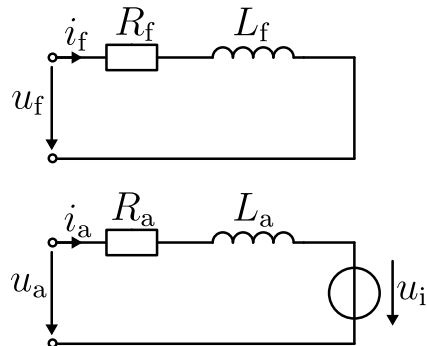


Fig. 3.25: Equivalent circuit diagram of the DC machine

Power balance and efficiency

Based on (3.25) (note the load convention), the electrical power of the DC machine is:

$$P_{\text{el}} = u_a i_a + u_f i_f. \quad (3.28)$$

This power is separated into the mechanical power P_{me} , the dissipated power losses P_l , and the change of the stored magnetic energy $\frac{d}{dt}E_{\text{mag}}$:

$$P_{\text{el}} = P_{\text{me}} + P_l + \frac{d}{dt}E_{\text{mag}}. \quad (3.29)$$

The power losses are (assuming dominant ohmic losses):

$$P_l = R_f i_f^2 + R_a i_a^2. \quad (3.30)$$

The mechanical power is:

$$P_{\text{me}} = T\omega = \psi_f' i_a \omega. \quad (3.31)$$

The magnetically stored energy is

$$E_{\text{mag}} = \frac{1}{2}L_f i_f^2 + \frac{1}{2}L_a i_a^2. \quad (3.32)$$

Power balance and efficiency (cont.)

In steady state, the DC machine efficiency η is defined as

$$\eta_{\text{mot}} = \frac{P_{\text{me}}}{P_{\text{el}}} = \frac{T\omega}{u_a i_a + u_f i_f} = \frac{L'_f i_f i_a \omega}{R_a i_a^2 + \omega L'_f i_f i_a + R_f i_f^2}, \quad (3.33)$$

$$\eta_{\text{gen}} = \frac{P_{\text{el}}}{P_{\text{me}}} = \frac{u_a i_a + u_f i_f}{T\omega} = \frac{R_a i_a^2 + \omega L'_f i_f i_a + R_f i_f^2}{L'_f i_f i_a \omega}.$$

It can be noted that

- ▶ The machine parameters R_a , R_f , and L'_f are influencing the efficiency.
- ▶ The efficiency is a function of the load torque T and the speed ω , that is, depending on the operating point.
- ▶ If i_f and i_a are independently controllable, the efficiency can be optimized as a certain torque can be produced with infinitely many combinations of i_f and i_a .

Intermediate remarks on the DC machine model

During the derivation of the DC machine model, we made several assumptions:

- ▶ The air gap magnetic field is homogenous and without any leakage.
- ▶ The air gap reluctance is dominating the magnetic circuit (neglecting the iron path reluctances including potential magnetic saturation).
- ▶ The magnetic field lines follow distinct paths through the armature winding.
- ▶ There is no mutual inductance between the stator and rotor (ideal orthogonal windings).
- ▶ The magnetic field in the air gap and in the armature is governed by the field winding current only (that is, we have neglected the armature current impact on the field).

Model accuracy

We represent the DC machine by a time-invariant, lumped-parameter model which is based on several substantial simplifications. While this model is likely sufficient for many applications, systematic deviations between the observed behavior of real machines and the model predictions are to be expected.

Armature reaction

- So far, we have neglected the impact of the armature current on the magnetic field.
- If $i_a \neq 0$, the magnetic field lines in the air gap are distorted leading to a so-called armature reaction (cf. Fig. 3.26).

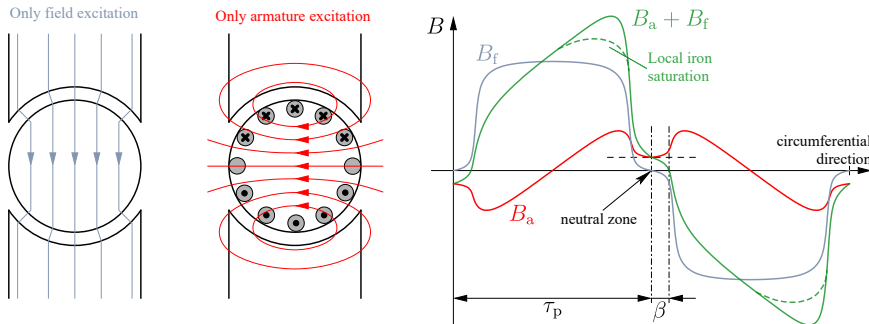
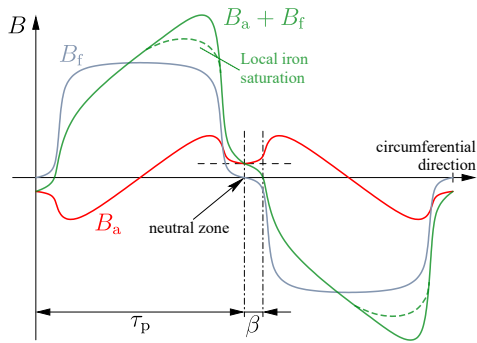


Fig. 3.26: Superposition of the field and armature magnetic excitation and the resulting air gap field normal components (adapted from W. Novender, *Elektrische Maschinen*, Technische Hochschule Mittelhessen, 2023)

Armature reaction (cont.)

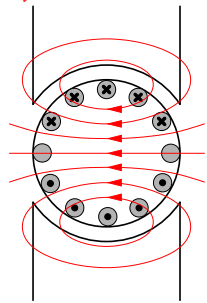
Issues related to the armature reaction:

- ▶ The neutral zone (field-free commutation area) is shifted by β degrees in the circumferential direction, that is, exacerbate the commutation process (increased risk of sparking).
- ▶ High local field densities can lead to magnetic saturation which will increase the iron path reluctance and consequently decrease the machine's torque capability. Also, the iron losses will increase.
- ▶ The imbalanced magnetic field leads to an imbalanced Lorentz force distribution on the armature conductors which can cause mechanical distortions.



Counter measures: compensation winding and interpoles

Only armature-related distortion



Only interpoles and compensation winding

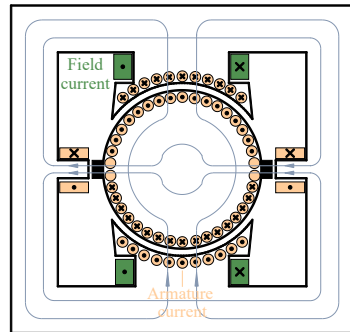
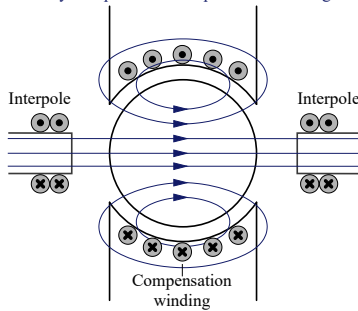


Fig. 3.27: Armature reaction counter measures utilizing compensation winding and interpoles: both are excited by the armature current with an opposite orientation to account for the load-dependent impact of the armature reaction (adapted from W. Novender, *Elektrische Maschinen*, Technische Hochschule Mittelhessen, 2023 and J. Böcker, *Elektrische Antriebstechnik*, Paderborn University, 2020)

Counter measures: compensation winding and interpoles (cont.)

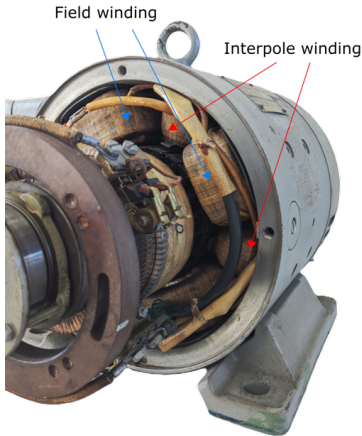


Fig. 3.28: Example of a DC machine with interpole winding (one may identify that the interpole winding is connected to the brushes and, therefore, excited by the armature current)

Counter measures: compensation winding and interpoles (cont.)

Compensation winding design: In order to compensate for the armature reaction within the air gap, the compensation winding MMF θ_{cw} must meet the armature MMF θ_a :

$$|\theta_{\text{cw}}| = \frac{z_{\text{cw}}}{2a_{\text{cw}}p} I_a \stackrel{!}{=} \alpha \frac{z_a}{2a_{\text{ap}}} I_a = |\theta_a|. \quad (3.34)$$

Above, the following parameters are used:

- ▶ a_{cw}/a_a : number of parallel conductors of the compensation and armature windings,
- ▶ z_{cw}/z_a : number of conductors of the compensation and armature windings.

In (3.34) α is only related to θ_a as we assume the armature area to be bigger (or at least the same size) as the field pole (cf. Fig. 3.27). From (3.34) we can calculate the required compensation winding conductors

$$z_{\text{cw}} = \alpha z_a \frac{a_{\text{cw}}}{a_a} = 2pQ_{\text{cw}}N_{\text{cw}} \quad (3.35)$$

which can be met by choosing Q_{cw} slots and N_{cw} turns per pole.

Counter measures: compensation winding and interpoles (cont.)

Interpole winding design: As discussed in (3.8), the reactane voltage $u_r \approx L_c i_a \omega d_a / (aw_b^2)$ is self-induced within the short-circuited coil during commutation. To counteract this, the interpole winding is designed such that the neutral zone is (over-)compensated leading to an induced voltage u_{ip} which is opposite to u_r :

$$|u_{ip}| \stackrel{!}{=} |u_r|. \quad (3.36)$$

Assuming a rotational angular velocity ω and some (homogenous) $B_{ip} \neq 0$ flux density in the interpole area, the induced voltage u_{ip} is

$$u_{ip} = N_c \omega d_a l_z B_{ip}. \quad (3.37)$$

Here, N_c is the number of armature conductor turns per coil assuming that exactly one coil is placed in the interpole area.

Counter measures: compensation winding and interpoles (cont.)

From (3.36) and (3.37) we can calculate the required interpole flux density B_{ip} :

$$B_{ip} = \frac{u_r}{N_c \omega d_a l_z} = \frac{L_c i_a}{2 N_c l_z a w_b}. \quad (3.38)$$

Applying the compensation winding design approach (3.34) results in:

$$\oint_{\partial S} \mathbf{H} \cdot d\mathbf{s} = \theta_{ip} + \theta_{cw} - \theta_a = \theta_{ip} - \theta_a(1-\alpha). \quad (3.39)$$

The MMFs per pole are:

$$\theta_{ip} = N_{ip} i_a, \quad \theta_a = N_a i_a. \quad (3.40)$$

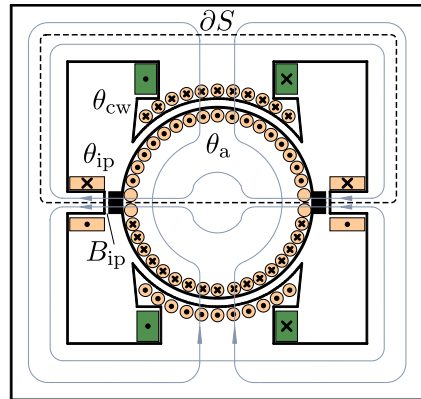


Fig. 3.29: Integration contour ∂S and related MMF components for the interpole winding design (adapted from J. Böcker, *Elektrische Antriebstechnik*, Paderborn University, 2020)

Counter measures: compensation winding and interpoles (cont.)

Assuming that the air gap reluctance is dominating the magnetic circuit, we receive

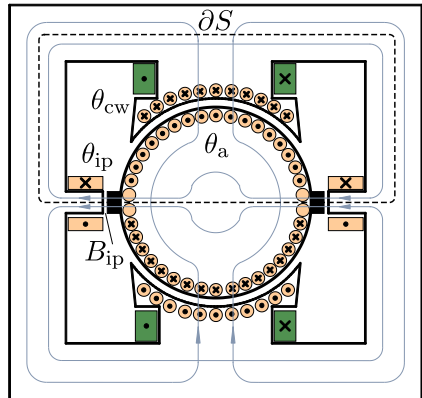
$$\oint_{\partial S} \mathbf{H} \cdot d\mathbf{s} = 2\delta H_{ip} = N_{ip}i_a - N_a i_a(1 - \alpha). \quad (3.41)$$

The flux density in the interpole area is then

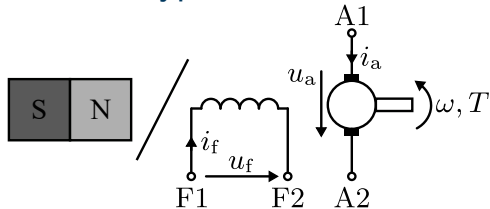
$$B_{ip} = \mu_0 \frac{N_{ip} - N_a(1 - \alpha)}{2\delta} i_a. \quad (3.42)$$

The comparison with (3.38) reveals:

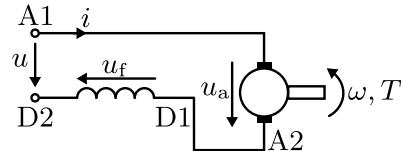
$$\begin{aligned} \mu_0 \frac{N_{ip} - N_a(1 - \alpha)}{2\delta} i_a &\stackrel{!}{=} \frac{L_c}{2N_c l_z a w_b} i_a \\ \Leftrightarrow N_{ip} &= N_a(1 - \alpha) + \frac{L_c \delta}{\mu_0 N_c l_z a w_b}. \end{aligned} \quad (3.43)$$



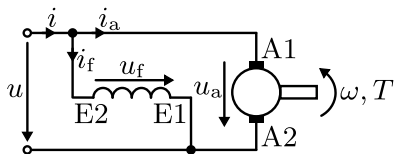
Connection types of DC machines



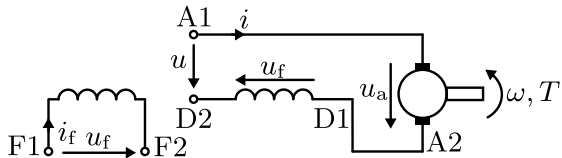
(a) Separately excited (or perm. magnet) DC machine



(b) Series DC machine



(c) Shunt DC machine



(d) Compound DC machine

Fig. 3.29: Connection types of DC machines incl. terminal block designations (note: the not shown interpole winding has the terminal block designation B1-B2 and the compensation winding C1-C2)

Steady-state behavior: separately excited DC machine

Assuming a fixed excitation ψ'_f (e.g., by a permanent magnet or constant field current), the separately excited DC machine's voltage demand for a certain speed is:

$$U_a = R_a I_a + \omega \psi'_f. \quad (3.44)$$

On the other hand, the speed-torque characteristic for a fixed armature voltage supply U_a is

$$T = (U_a - \omega \psi'_f) \frac{\psi'_f}{R_a} = U_a \frac{\psi'_f}{R_a} - \omega \frac{\psi'^2_f}{R_a}. \quad (3.45)$$

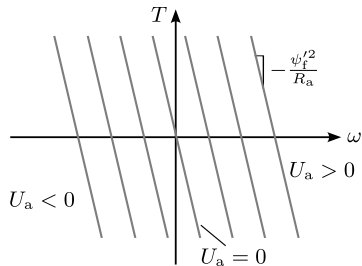
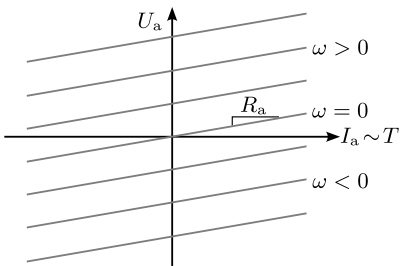


Fig. 3.30: Steady-state characteristics curves (adapted from J. Böcker, *Elektrische Antriebstechnik*, Paderborn University, 2020)

Steady-state behavior: separately excited DC machine (cont.)

For $U_a = \text{const.} > 0$, the starting torque (i.e., the torque at zero speed) and the corresponding armature current are:

$$\begin{aligned} T(\omega = 0) &= T_0 = U_a \frac{\psi'_f}{R_a}, \\ I_a(\omega = 0) &= I_{a,0} = \frac{U_a}{R_a}. \end{aligned} \quad (3.46)$$

On the other hand for $T = 0$, the no-load speed ω_0 is:

$$\omega_0 = \frac{U_a}{\psi'_f}. \quad (3.47)$$

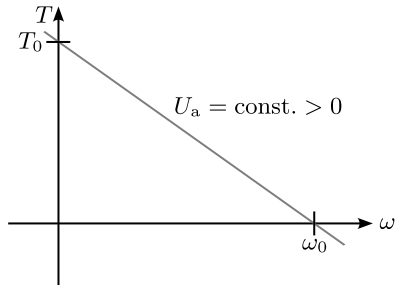


Fig. 3.31: Starting torque and no-load speed of a separately excited DC machine (adapted from J. Böcker, *Elektrische Antriebstechnik*, Paderborn University, 2020)

Steady-state behavior: separately excited DC machine (cont.)

As the start up of a DC machine with a fixed armature voltage U_a can lead to very high armature currents, which potentially cause damage, dropping resistors can be used to limit the armature current. While this approach was historically very common (e.g., in rail vehicles), its additional power losses and the necessity to carry bulky resistors are obvious drawbacks.

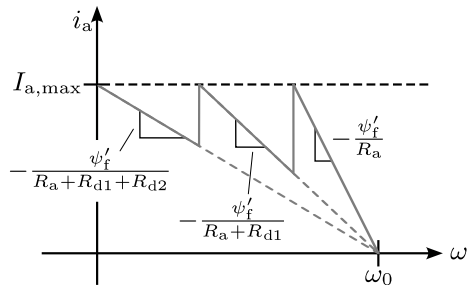
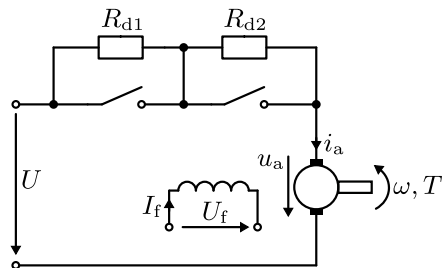


Fig. 3.32: Operation with dropping resistor during start up to limit the armature voltage (adapted from J. Böcker, *Elektrische Antriebstechnik*, Paderborn University, 2020)

Operation constraints: separately excited DC machine

Now we consider U_a being controllable (e.g., via buck converter), that is, we can also change I_a . Nevertheless, the machine is still limited by the voltage and current constraint:

$$U_{\max} \leq U_a = \frac{R_a}{\psi'_f} T + \omega \psi'_f, \quad I_{\max} \leq I_a. \quad (3.48)$$

For sake of simplicity we only consider the first quadrant (cf. Fig. 1.6), that is, positive torque and speed mode. From (3.48) $T \leq \psi'_f I_{\max}$ follows. Also, the maximum speed is limited:

$$\omega \leq \frac{U_{\max}}{\psi'_f} - \frac{R_a}{\psi'^2_f} T. \quad (3.49)$$

Hence, for a constant excitation ψ'_f , the torque must be reduced starting at ω_1 while ω_0 represents the no-load speed where no torque can be generated anymore:

$$\omega_1 = \frac{U_{\max}}{\psi'_f} - \frac{R_a}{\psi'_f} I_{\max}, \quad \omega_0 = \frac{U_{\max}}{\psi'_f}. \quad (3.50)$$

Operation constraints: separately excited DC machine (cont.)

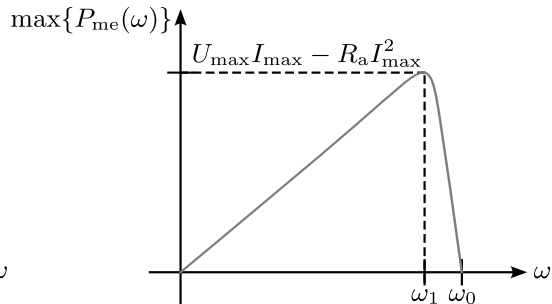
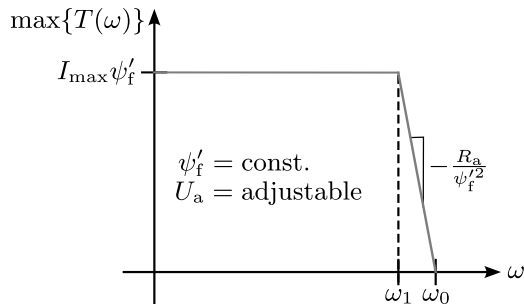


Fig. 3.33: Maximum achievable torque and mechanical power for the separately excited DC machine with a fixed excitation ψ'_f but controllable armature voltage U_a and current I_a

Field weakening of the separately excited DC machine

In the previous scenario, the no-load speed ω_0 is limited by the maximum armature voltage U_{\max} . However, if the field winding current I_f is also controllable, the no-load speed can be increased by decreasing the excitation ψ'_f (so-called field weakening). Consider an armature operation both at the voltage and current constraint:

$$U_{\max} = R_a I_{\max} + \omega \psi'_f = R_a I_{\max} + \omega L'_f i_f. \quad (3.51)$$

For $\omega > \omega_1$ the field weakening is applied by reducing i_f to stay exactly at the armature voltage constraint:

$$i_f = \frac{1}{\omega} \frac{U_{\max} - R_a I_{\max}}{L'_f}. \quad (3.52)$$

Hence, we need to reduce the excitation with $1/\omega$ resulting in the torque and mechanical power

$$T = \frac{1}{\omega} (U_{\max} I_{\max} - R_a I_{\max}^2), \quad P_{\text{me}} = U_{\max} I_{\max} - R_a I_{\max}^2. \quad (3.53)$$

Field weakening of the separately excited DC machine (cont.)

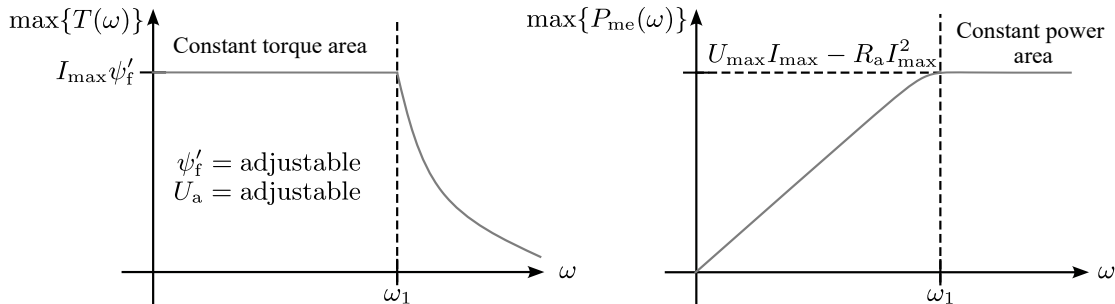


Fig. 3.34: Maximum achievable torque and mechanical power for the separately excited DC machine with a variable excitation ψ'_f as well as controllable armature voltage U_a and current I_a

Steady-state behavior: shunt DC machine

The shunt DC machine is characterized by:

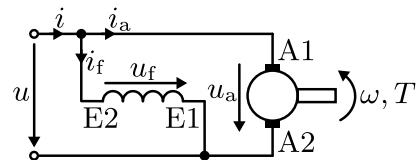
$$U = U_a = U_f, \quad I = I_a + I_f. \quad (3.54)$$

The steady-state currents are:

$$\begin{aligned} I_f &= \frac{U_f}{R_f}, \\ I_a &= \frac{U_a - \omega L'_f I_f}{R_a} = \frac{1 - L'_f / R_f \omega}{R_a} U, \\ I &= I_a + I_f = \left(\frac{1}{R_a} + \frac{1}{R_f} - \frac{L'_f \omega}{R_a R_f} \right) U. \end{aligned} \quad (3.55)$$

The resulting steady-state torque is:

$$T = L'_f I_f I_a = L'_f \frac{1 - L'_f / R_f \omega}{R_a R_f} U^2. \quad (3.56)$$



Steady-state behavior: series DC machine

The series DC machine is characterized by:

$$U = U_a + U_f, \quad I = I_a = I_f. \quad (3.57)$$

We can rewrite the terminal voltage as

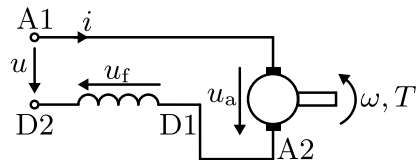
$$U = (R_a + R_f) I + \omega L'_f I = R'(\omega) I \quad (3.58)$$

with the effective speed-dependent resistance

$$R'(\omega) = R_a + R_f + \omega L'_f. \quad (3.59)$$

The steady-state torque is then

$$T = L'_f I^2 = L'_f \left(\frac{U}{R'(\omega)} \right)^2. \quad (3.60)$$



Steady-state behavior: series DC machine (cont.)

If the series DC machine is operated at the negative mechanical speed

$$\omega_r = -\frac{R_a + R_f}{L'_f}, \quad (3.61)$$

the current and the torque get (theoretically) infinite. This is due to the fact that the back EMF is exactly compensating the resistive voltage drop. Moreover, from (3.60) we can observe that

$$T \rightarrow 0 \Rightarrow \omega \rightarrow \infty \quad (3.62)$$

holds for any DC voltage $U \neq 0$. This is due to inherent, load-dependent flux weakening effect of the series DC machine.

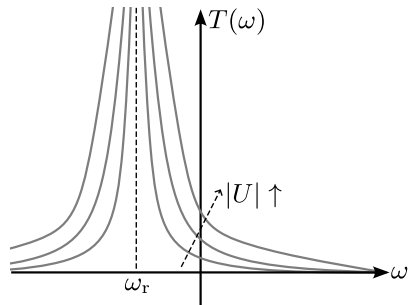


Fig. 3.35: Steady-state torque-speed characteristics for different DC voltage levels

Universal machine: series DC machine with sinusoidal excitation

From (3.60) it becomes clear that $T \sim I^2$ holds and, hence, the torque is independent of the sign of the current. Hence, the series DC machine can be also operated with an AC voltage supply (so-called universal machine).

Consider the sinusoidal excitation

$$\begin{aligned} u(t) &= \hat{u} \cos(\omega_{\text{el}} t + \varphi_u) = \operatorname{Re} \left\{ \hat{u} e^{j(\omega_{\text{el}} t + \varphi_u)} \right\} \\ &= \operatorname{Re} \left\{ \underline{U} e^{j\omega_{\text{el}} t} \right\}, \end{aligned}$$

which is represented by the complex phasor

$$\underline{U} = U e^{j\phi_u} = \frac{1}{\sqrt{2}} \hat{u} e^{j\varphi_u}. \quad (3.63)$$

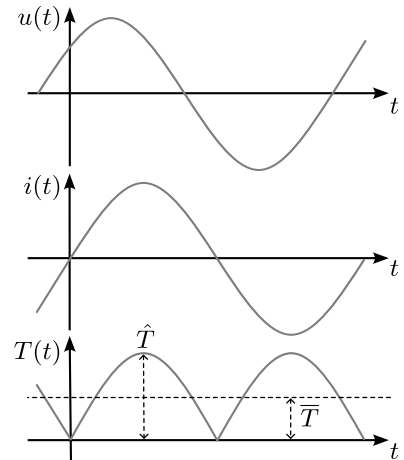


Fig. 3.36: Qualitative voltage, current and torque signals for a universal motor

Universal machine: series DC machine with sinusoidal excitation (cont.)

From (3.27) and (3.57) we can derive the complex voltage and current relations:

$$\underline{U} = R'(\omega)\underline{I} + j\omega_{el}L\underline{I} \quad (3.64)$$

with $L = L_f + L_a$. The current phasor is

$$\underline{I} = \frac{\underline{U}}{R'(\omega) + j\omega_{el}L} \quad (3.65)$$

resulting in the instantaneous current (setting $\varphi_u = 0$)

$$i(t) = \operatorname{Re} \left\{ \sqrt{2} \underline{I} e^{j\omega_{el}t} \right\} = \sqrt{2} \operatorname{Re} \left\{ \frac{U (R'(\omega) - j\omega_{el}L)}{R'(\omega)^2 + \omega_{el}^2 L^2} e^{j\omega_{el}t} \right\} \quad (3.66)$$

$$= \sqrt{2} \frac{U}{\sqrt{R'(\omega)^2 + \omega_{el}^2 L^2}} \cos \left(\omega_{el}(t - \frac{L}{R'(\omega)}) \right). \quad (3.67)$$

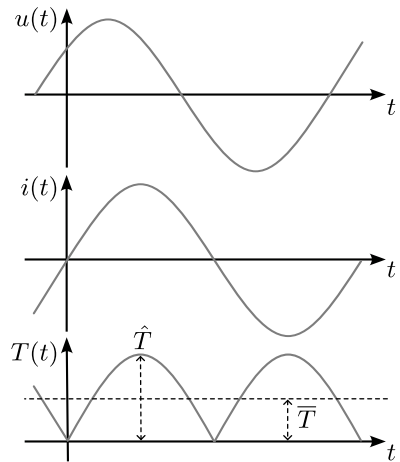
Universal machine: series DC machine with sinusoidal excitation (cont.)

The resulting instantaneous torque is

$$\begin{aligned} T(t) &= L'_f i^2(t) \\ &= 2L'_f \frac{U^2}{R'(\omega)^2 + \omega_{\text{el}}^2 L^2} \cos \left(\omega_{\text{el}}(t - \frac{L}{R'(\omega)}) \right)^2 \\ &= L'_f \frac{U^2}{R'(\omega)^2 + \omega_{\text{el}}^2 L^2} \left[1 + \cos \left(2\omega_{\text{el}}(t - \frac{L}{R'(\omega)}) \right) \right]. \end{aligned}$$

The peak and average torque are

$$\begin{aligned} \hat{T} &= 2L'_f \frac{U^2}{R'(\omega)^2 + \omega_{\text{el}}^2 L^2} = L'_f \frac{\hat{u}^2}{R'(\omega)^2 + \omega_{\text{el}}^2 L^2}, \\ \overline{T} &= \frac{\omega_{\text{el}}}{2\pi} \int_0^{\frac{2\pi}{\omega_{\text{el}}}} T(t) dt = \frac{1}{2} \hat{T}. \end{aligned} \quad (3.68)$$



Universal machine: series DC machine with sinusoidal excitation (cont.)

Some remarks on the universal machine:

- ▶ Only if the reactance $\omega_{el}L$ impact on the voltage demand is negligible, the universal machine average torque at AC mode is identical to the series DC machine torque in DC mode applying the same effective voltage.
- ▶ Due to the AC field current, both the armature and stator should be based on a laminated iron core design to reduce iron losses.
- ▶ The peak armature and field currents are $\sqrt{2}$ times higher in the AC case than in DC operation. To prevent magnetic saturation, the iron paths must be designed larger than for an equivalent DC machine (i.e., leading to more volume and weight).

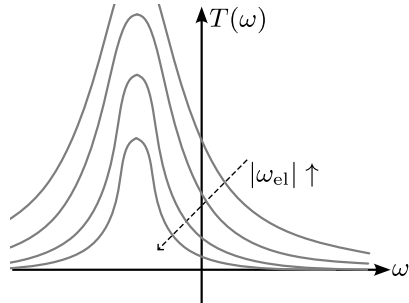


Fig. 3.37: Steady-state torque-speed characteristics for different AC voltage frequencies at a fixed voltage amplitude

Commutation of the universal machine

Assuming that the entire air gap field ϕ_δ is linked by the commutation coil, the time-varying excitation field induces an additional spark voltage u_{sp} within the commutation coil:

$$u_{sp} = -N_c \frac{p}{a} \frac{d\phi_\delta}{dt}. \quad (3.69)$$

Due to the time-varying excitation current, we have $\phi_\delta(t) = \hat{\phi}_\delta \cos(\omega_{el}t)$ and, hence,

$$u_{sp} = N_c \frac{p}{a} \omega_{el} \hat{\phi}_\delta \sin(\omega_{el}t). \quad (3.70)$$

This additional induced spark voltage is shifted by (approx.) 90 degrees to the excitation field. Consequently, the interpole winding current is not in phase and does not compensate u_{sp} .

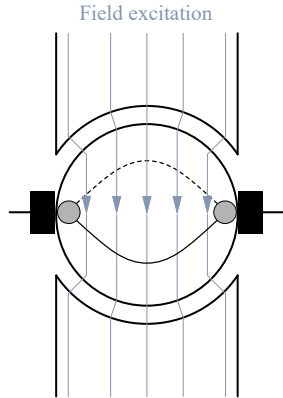


Fig. 3.38: Simplified illustration of the induced voltage within the short-circuited commutation coil by the varying excitation field

Commutation of the universal machine (cont.)

Assuming an ideal inductive behavior of the short-circuited coil, the induced spark voltage (3.70) leads to the current

$$i_{\text{sp}} = -\frac{N_c}{L_c} \frac{p}{a} \hat{\phi}_\delta \cos(\omega_{\text{el}} t). \quad (3.71)$$

This additional current will cause commutator sparking and, hence, the universal machine commutation process is more challenging than for a pure DC machine.

Conclusion on the universal machine

The drawbacks of the universal machine in terms of sizing and commutation sparking (leading to higher wear) are the reasons why this machine type is typically limited to low-cost applications (e.g., household appliances) nowadays.

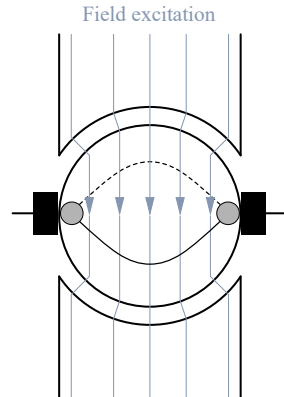


Table of contents

4

Transformers

Transformers

Oliver Wallscheid



Transformer definition

Transformer

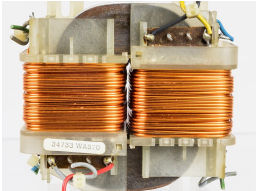
A transformer is a static device that transfers electrical energy between two or more circuits through electromagnetic induction. It converts the AC voltage levels between inputs and outputs.

- ▶ While a transformer is sometimes called a “static machine”, it does not meet the formal definition of an electrical machine (compare first chapter).
- ▶ However, transformers share some working principles with electrical machines and are also often used as components of electrical power systems including drives.



Fig. 4.1: Transformer integrated at a utility pole (source: pxhere.com, public domain)

Examples of transformers



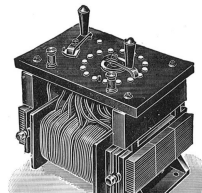
(a) Power supply transformer (source: [Wikimedia Commons](#), R. Spekking, CC BY-SA 4.0)



(b) Single-phase transformer (source: [Wikimedia Commons](#), Georg, CC BY-SA 4.0)



(c) Three-phase transformer (source: [Wikimedia Commons](#), Asurnipal, CC BY-SA 4.0)



(d) Variable tapped transformer (source: [Wikimedia Commons](#), public domain)

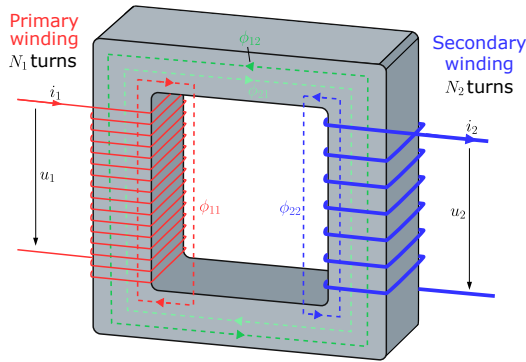
Electromagnetic modeling of the single-phase transformer

Recap from (2.15): for some given current i , the flux linkages ψ in the transformer windings are

$$\psi = \begin{bmatrix} \psi_1 \\ \psi_2 \end{bmatrix} = \begin{bmatrix} L_1 & M \\ M & L_2 \end{bmatrix} \begin{bmatrix} i_1 \\ i_2 \end{bmatrix} = \mathbf{L}i$$

where L_1 and L_2 are the self-inductances of the primary and secondary winding, respectively, and M is the mutual inductance.

Note: The above equation is an algebraic relation, that is, it is valid for any time instant t and applies to both AC and DC excitation of the transformer.



Dynamic modeling of the single-phase transformer

The dynamic transformer behavior can be represented by the ECD in Fig. 4.3, which also considers the internal resistances of the windings. Applying Faraday's law, the resulting differential equations are:

$$u_1(t) = R_1 i_1(t) + \frac{d\psi_1(t)}{dt}, \quad u_2(t) = R_2 i_2(t) + \frac{d\psi_2(t)}{dt}. \quad (4.1)$$

Inserting (2.15) delivers:

$$u_1(t) = R_1 i_1(t) + L_1 \frac{di_1(t)}{dt} + M \frac{di_2(t)}{dt}, \quad u_2(t) = R_2 i_2(t) + L_2 \frac{di_2(t)}{dt} + M \frac{di_1(t)}{dt}. \quad (4.2)$$

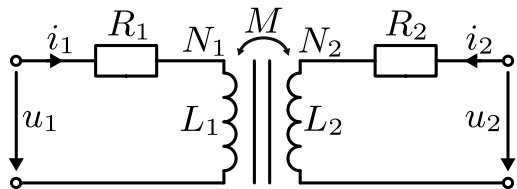


Fig. 4.3: General equivalent circuit diagram (ECD) of a transformer (note: that both ports of the transformer are denoted in the load convention reference frame which is an arbitrary representation decision).

Dynamic modeling of the single-phase transformer (cont.)

The model (4.2) can be represented by the T-type ECD in Fig. 4.4. It may be noted that $L_1 - M$ and $L_2 - M$ can have negative values due to the model representation.

By rearranging (4.2), we can also write the dynamic transformer model in vector-matrix form:

$$\begin{bmatrix} u_1(t) \\ u_2(t) \end{bmatrix} = \mathbf{u}(t) = \begin{bmatrix} R_1 & 0 \\ 0 & R_2 \end{bmatrix} \begin{bmatrix} i_1(t) \\ i_2(t) \end{bmatrix} + \begin{bmatrix} L_1 & M \\ M & L_2 \end{bmatrix} \frac{d}{dt} \begin{bmatrix} i_1(t) \\ i_2(t) \end{bmatrix} = \mathbf{R}\mathbf{i}(t) + \mathbf{L} \frac{d}{dt} \mathbf{i}(t). \quad (4.3)$$

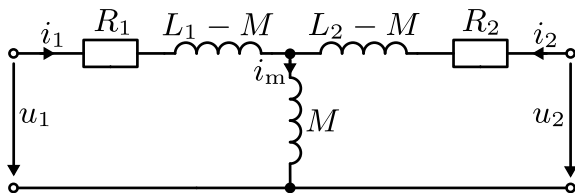


Fig. 4.4: T-type ECD of a transformer (note that the model (4.3) assumes linear time-invariant (LTI) behavior, which among other effects neglects magnetic saturation).

Dynamic modeling of the single-phase transformer (cont.)

Rearranging (4.3) gives the state-space representation of the transformer model

$$\frac{d}{dt} \mathbf{i}(t) = \mathbf{L}^{-1} (\mathbf{u}(t) - \mathbf{R}\mathbf{i}(t)) \quad (4.4)$$

with

$$\mathbf{L}^{-1} = \frac{1}{L_1 L_2 - M^2} \begin{bmatrix} L_2 & -M \\ -M & L_1 \end{bmatrix} = \frac{1}{\sigma} \begin{bmatrix} \frac{1}{L_1} & \frac{-M}{L_1 L_2} \\ \frac{-M}{L_1 L_2} & \frac{1}{L_2} \end{bmatrix}.$$

Above, σ is the leakage coefficient defined as (compare also (2.18))

$$\sigma = \frac{L_1 L_2 - M^2}{L_1 L_2} = 1 - \frac{M^2}{L_1 L_2} = 1 - k^2. \quad (4.5)$$

Finally, the state-space representation of the transformer model (with the currents as states) is

$$\frac{d}{dt} \mathbf{i}(t) = \begin{bmatrix} -\frac{R_1}{\sigma L_1} & \frac{R_2 M}{\sigma L_1 L_2} \\ \frac{R_1 M}{\sigma L_1 L_2} & -\frac{R_2}{\sigma L_2} \end{bmatrix} \mathbf{i}(t) + \begin{bmatrix} \frac{1}{\sigma L_1} & -\frac{M}{\sigma L_1 L_2} \\ -\frac{M}{\sigma L_1 L_2} & \frac{1}{\sigma L_2} \end{bmatrix} \mathbf{u}(t) = \mathbf{A}\mathbf{i}(t) + \mathbf{B}\mathbf{u}(t). \quad (4.6)$$

Steady-state modeling of the single-phase transformer

Assuming that the transformer operates in steady state and that all quantities are sinusoidal, the state-space model (4.6) can be simplified and represented by complex phasors:

$$x(t) = \hat{x} \cos(\omega_{\text{el}} t + \varphi_x) = \operatorname{Re} \left\{ \hat{x} e^{\text{j}(\omega_{\text{el}} t + \varphi_x)} \right\} = \operatorname{Re} \left\{ \underline{X} e^{\text{j}\omega_{\text{el}} t} \right\}.$$

From (4.3) we receive

$$\underline{U} = \begin{bmatrix} \underline{U}_1 \\ \underline{U}_2 \end{bmatrix} = \underline{R} \underline{I} + \text{j} \omega_{\text{el}} \underline{L} \underline{I} = \underline{Z} \underline{I} = \begin{bmatrix} R_1 + \text{j} \omega_{\text{el}} L_1 & \text{j} \omega_{\text{el}} M \\ \text{j} \omega_{\text{el}} M & R_2 + \text{j} \omega_{\text{el}} L_2 \end{bmatrix} \begin{bmatrix} \underline{I}_1 \\ \underline{I}_2 \end{bmatrix}. \quad (4.7)$$

For some given \underline{U} we can calculate the current phasor \underline{I} (i.e., the steady-state current response) by solving:

$$\underline{I} = \underline{Z}^{-1} \underline{U}. \quad (4.8)$$

Alternative scenarios can be also considered, e.g., defining \underline{U}_1 (input voltage) and \underline{I}_2 (load current) as given and solving for \underline{I}_1 and \underline{U}_2 by rearranging (4.7).

Steady-state modeling of the single-phase transformer (cont.)

Assuming that the transformer is not loaded ($I_2 = 0$) and that it is lossless ($R_1 = 0$), (4.7) simplifies to

$$\begin{bmatrix} \underline{U}_1 \\ \underline{U}_2 \end{bmatrix} = \begin{bmatrix} j\omega_{el}L_1 \\ j\omega_{el}M \end{bmatrix} \underline{I}_1. \quad (4.9)$$

The voltage transformation ratio in this case results in

$$\frac{\underline{U}_1}{\underline{U}_2} = \frac{j\omega_{el}L_1 I_1}{j\omega_{el}M I_1} = \frac{L_1}{M}. \quad (4.10)$$

Assuming further that the transformer is leakage-free ($L_{1,\sigma} = 0$), the voltage transformation ratio simplifies to (compare also (2.17))

$$\frac{\underline{U}_1}{\underline{U}_2} = \frac{L_1}{M} = \frac{\Lambda_{21}N_1^2}{\Lambda_{21}N_1N_2} = \frac{N_1}{N_2} = \ddot{u}. \quad (4.11)$$

Hence, this famous result is only valid for the abstract case of a lossless, leakage-free, and, unloaded transformer – i.e., not applicable to real-world transformers

Transformation of the secondary side variables

Sometimes it can be helpful to (mathematically) transform the secondary side variables to ease the mathematical analysis. This can be done by introducing the transformation factor α :

$$u'_2 = \alpha u_2, \quad i'_2 = \frac{1}{\alpha} i_2. \quad (4.12)$$

Here, u'_2 and i'_2 are the transformed secondary side voltage and current, respectively. The primary voltage equation reads

$$\begin{aligned} u_1(t) &= R_1 i_1(t) + L_1 \frac{di_1(t)}{dt} + M \frac{di_2(t)}{dt} = R_1 i_1(t) + L_1 \frac{di_1(t)}{dt} + \alpha M \frac{di'_2(t)}{dt} \\ &= R_1 i_1(t) + L_1 \frac{di_1(t)}{dt} + M' \frac{di'_2(t)}{dt} \end{aligned} \quad (4.13)$$

with the transformed mutual inductance $M' = \alpha M$.

Transformation of the secondary side variables (cont.)

Multiplying the secondary voltage equation with α gives

$$\begin{aligned}\alpha u_2(t) &= \alpha R_2 i_2(t) + \alpha L_2 \frac{di_2(t)}{dt} + \alpha M \frac{di_1(t)}{dt} \\ \Leftrightarrow u'_2(t) &= \alpha^2 R_2 i'_2(t) + \alpha^2 L_2 \frac{di'_2(t)}{dt} + \alpha M \frac{di_1(t)}{dt} \\ \Leftrightarrow u'_2(t) &= R'_2 i'_2(t) + L'_2 \frac{di'_2(t)}{dt} + M' \frac{di_1(t)}{dt}\end{aligned}\quad (4.14)$$

with the transformed resistance $R'_2 = \alpha^2 R_2$ and inductance $L'_2 = \alpha^2 L_2$.

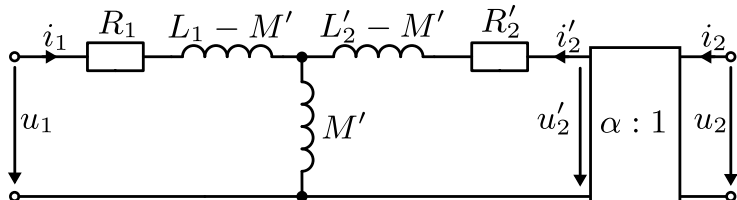


Fig. 4.5: T-type ECD of a transformer with transformed secondary side variables for some arbitrary transformation factor α (note that k and σ are transformation invariant.)

Transformation of the secondary side variables by the turn ratio

With

$$\alpha = \dot{u} = N_1/N_2$$

being the turn ratio as the transformation factor, we receive:

$$M' = (N_1/N_2)M = L_{1,m}, \quad L'_2 = (N_1^2/N_2^2)L_2 \quad (4.15)$$

with $L_{1,m}$ being the primary magnetizing inductance, cf. (2.17). Moreover, we have

$$L_1 - M' = L_{1,\sigma}, \quad L'_2 - M'2 = (N_1^2/N_2^2)L_{2,\sigma} = L'_{2,\sigma} \quad (4.16)$$

with $L_{1,\sigma}$ and $L_{2,\sigma}$ being the leakage inductances of the primary and secondary winding.

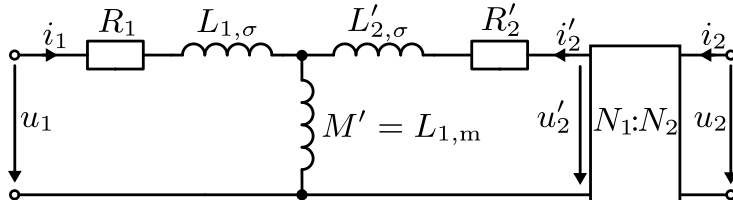


Fig. 4.6: T-type ECD of a transformer with $\alpha = N_1/N_2$ (note that all inductances within this model representation have a direct physical interpretation.)

Transformation towards a single stray inductance

With

$$\alpha = M/L_2$$

as the transformation factor, we receive:

$$L'_2 - M' = \alpha^2 L_2 - \alpha M = L_{2,\sigma} = 0, \quad (4.17)$$

that is, the secondary transformed leakage inductance is vanishing. Moreover, we have

$$L_1 - M' = L'_{1,\sigma} = \sigma L_1, \quad M' = M^2/L_2. \quad (4.18)$$

With the alternative choice $\alpha = L_1/M$, the leakage inductance gets concentrated on the secondary side (not explicitly shown).

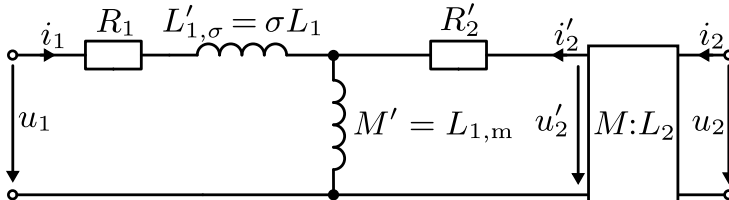


Fig. 4.7: T-type ECD of a transformer with $\alpha = M/L_2$

Typical transformer core types

- ▶ The core of a transformer typically build from laminated steel sheets (cf. Fig. 2.32). Alternatively, sintered ferrite material is also used for high-frequency applications.
- ▶ To improve the coupling between primary and secondary winding, it is beneficial to place the windings around the same leg. Hence, the middle example in Fig. 4.8 will exhibit a larger leakage.

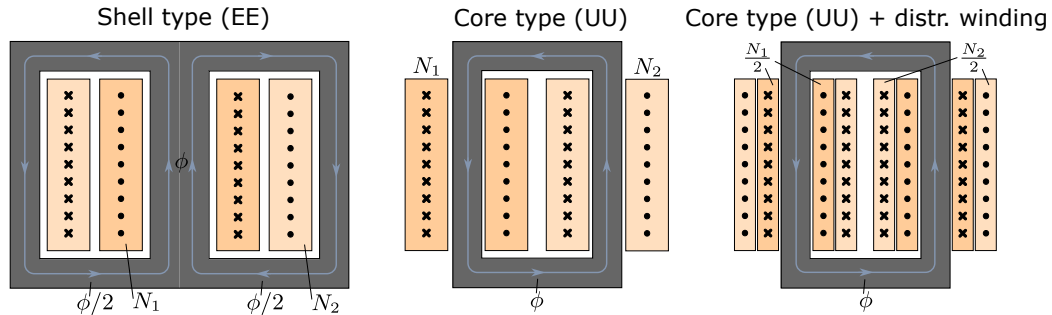


Fig. 4.8: Examples of typical transformer core types

Toroidal core

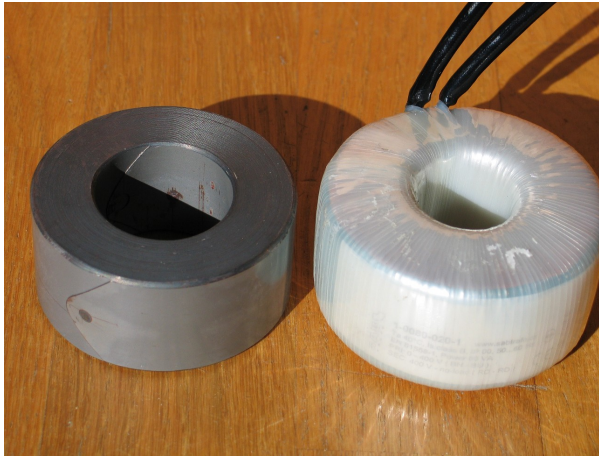


Fig. 4.9: Examples of a toroidal core and a transformer made from it – note the laminated, wound up steel sheets to form the toroid (source: [Wikimedia Commons](#), public domain)

Typical transformer winding schemes

- ▶ The below examples show improving magnetic coupling (lower leakage) from left to right due to the reducing effective distance between the turns of the primary and secondary winding.
- ▶ Beyond these examples, various winding variations (e.g., a combination of the below schemes) are used to optimize the transformer design for specific applications.

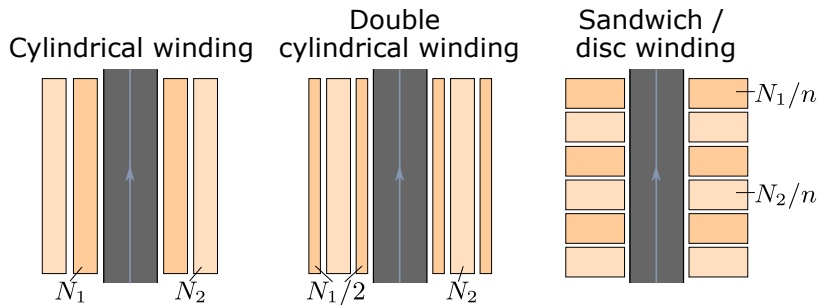


Fig. 4.10: Examples of typical transformer winding schemes

Core loss model (hysteresis and eddy current losses)

To also consider the iron losses inside the transformer core, a first-order model with the additional core loss resistance R_c can be introduced:

$$P_{l,c} \approx R_c I_c^2 \approx \frac{U_1^2}{R_c}. \quad (4.19)$$

Here, we consider a pure sinusoidal operation with I_c and U_1 being root-mean-square (RMS) values. Obviously, this is only a very rough model approximation (compare Fig. 2.16 and Fig. 2.32), but for many transformer designs the core losses can be significant and neglecting them completely would not be justified.

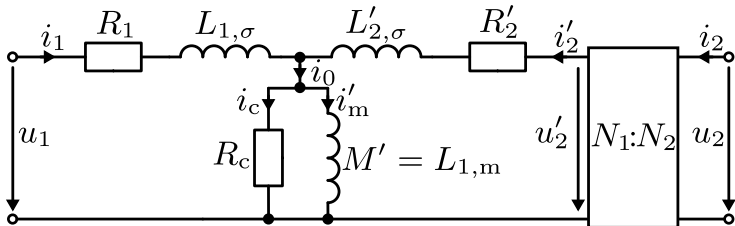


Fig. 4.11: T-type ECD of a transformer with an additional core loss resistance R_c

Transformer model parameterization via measurements – open-circuit test

Applying a sinusoidal test voltage $U_{1,o}$ and several measurement devices during an open-circuit arrangement, we can determine

$$\ddot{u} \approx \frac{U_{1,o}}{U_{2,o}} = \frac{N_1}{N_2}, \quad S_{1,o} = U_{1,o} I_{1,o}, \quad \cos(\varphi_o) = \frac{P_{1,o}}{U_{1,o} I_{1,o}} \quad (4.20)$$

with $P_{1,o}$ being the active input power consumed by the transformer and $\cos(\varphi_o)$ is the power factor. With the assumptions $R_1 \ll R_c$ and $L_{1,\sigma} \ll M'$, we can approximate

$$R_c \approx \frac{U_{1,o}^2}{P_{1,o}}, \quad X_{M'} = \omega_{el} M' \approx \frac{U_{1,o}}{I_{1,o}} \sin(\varphi_o) \quad (4.21)$$

given the angular frequency $\omega_{el} = 2\pi f_{el}$ and the reactance $X_{M'}$ of the mutual inductance.

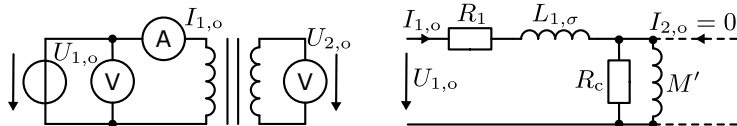


Fig. 4.12: Open-circuit (no-load) test: measuring circuit and its ECD

Transformer model parameterization via measurements – short-circuit test

Short-circuiting the secondary and applying a sinusoidal test voltage $U_{1,s}$, we can determine

$$Z_s = \sqrt{(R_1 + R'_2)^2 + (X_{L_{1,\sigma}} + X_{L'_{2,\sigma}})^2}, \quad \cos(\varphi_s) = \frac{P_{1,s}}{U_{1,s} I_{1,s}} \quad (4.22)$$

with Z_s being the short-circuit impedance while assuming that the impedance across M' and R_c is much larger, i.e., the short-circuit current will not flow via this branch. Hence, we have

$$R_1 + R'_2 = Z_s \cos(\varphi_s), \quad X_{L_{1,\sigma}} + X_{L'_{2,\sigma}} = Z_s \sin(\varphi_s). \quad (4.23)$$

Since we have four remaining unknown component values but only two independent equations, we additionally assume a symmetrical transformer design, leading to

$$R_1 = R'_2 = \frac{1}{2} Z_s \cos(\varphi_s), \quad \omega_{el} L_{1,\sigma} = X_{L_{1,\sigma}} = \omega_{el} L'_{2,\sigma} = X_{L'_{2,\sigma}} = \frac{1}{2} Z_s \sin(\varphi_s). \quad (4.24)$$

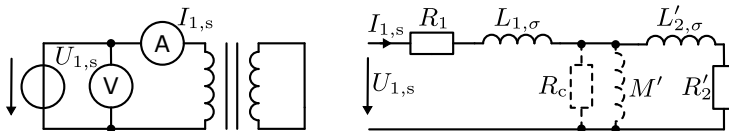


Fig. 4.13: Short-circuit test:
measuring circuit and its ECD

Further short-circuit considerations

Typically the short-circuit test voltage $U_{1,s}$ is limited such that the short-circuit current $I_{1,s}$ is reaching its nominal value $I_{1,n}$:

$$U_{1,s} = u_{1,s} U_{1,n}, \quad I_{1,s} = \frac{U_{1,s}}{Z_s} = I_{1,n}. \quad (4.25)$$

Here, $u_{1,s}$ is the relative short-circuit voltage w.r.t. the nominal voltage $U_{1,n}$. Typical values are $u_{1,s} = 3 \dots 13\%$.

While the short-circuit test is conducted with a reduced primary voltage, the prospective short-circuit (PSC) current during normal operation (typical as a fault result) can be significantly higher:

$$I_{1,psc} = \frac{U_{1,n}}{Z_s} = \frac{U_{1,s}}{Z_s} = \frac{I_{1,n}}{u_{1,s}}. \quad (4.26)$$

Hence, the transformer parameters Z_s and $u_{1,s}$ are crucial for the short-circuit behavior and the protection coordination of the transformer. Lower bounds are typically enforced by standards to prevent catastrophic damages, in particular in the electrical energy sector.

Voltage transformer application: measuring high AC voltages

If the voltage to be measured is too high for direct measurement, a voltage transformer can be used to step down the voltage to a suitable level:

$$u_2(t) = \frac{1}{\ddot{u}} u_1(t).$$

Hence, we choose $\ddot{u} > 1$. Moreover, the voltage sensor on the secondary side comes with a high internal resistance R_i to avoid a significant current and, therefore, power flow. Neglecting the leakage inductance, we can model the voltage transformer as shown in Fig. 4.14 with

$$R'_1 = \ddot{u}^2 R_i, \quad R'_2 = \ddot{u}^2 R_2, \quad M' = L_{1,m}.$$

The primary RL circuit represents a high-pass filter for the voltage signal, i.e., the transformer is only suitable for AC signals with $\omega_{el} > R_1/M'$ (cutoff frequency).

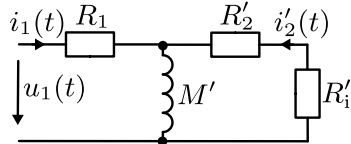
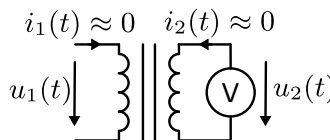


Fig. 4.14: Voltage transformer measuring circuit and its ECD (represented as transformed quantities with $\alpha = N_1/N_2$)

Current transformer application: measuring high AC currents

If the current to be measured is too high for direct measurement, a current transformer can be used to step down the current to a suitable level:

$$i_2(t) = \dot{u} i_1(t).$$

Hence, we choose $\dot{u} < 1$. Moreover, the current sensor on the secondary side comes with a minimal internal resistance R_i to avoid a significant ohmic power losses. Likewise, the transformer should be designed for low R_1 and R_2 (e.g., $N_1 = 1$ on the primary and sufficiently large cable cross-sections).

The secondary RL circuit represents a high-pass filter for the current signal, i.e., the transformer is only suitable for AC signals with $\omega_{\text{el}} > (R'_2 + R'_i)/M'$ (cutoff frequency).

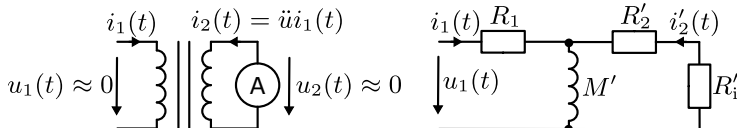


Fig. 4.15: Current transformer measuring circuit and its ECD (represented as transformed quantities with $\alpha = N_1/N_2$)

Connection nomenclature and tapped transformer

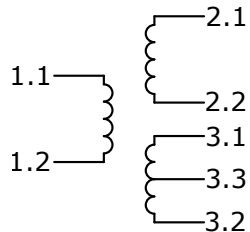


Fig. 4.16: Connection nomenclature of single-phase transformers (the lower secondary side connection represents a tapped winding)

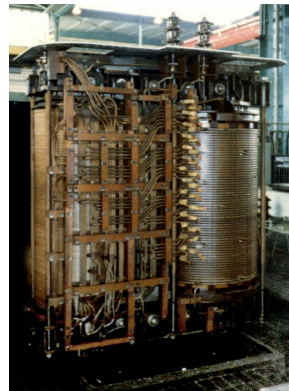


Fig. 4.17: Tapped transformer with multiple taps on the secondary side for a train drive application (source: [Wikimedia Commons](#), Saibo, CC BY-SA 3.0)

Autotransformer

- ▶ Uses a common winding for both primary and secondary side with one or multiple taps.
- ▶ No galvanic isolation between primary and secondary side.
- ▶ The autotransformer can be used to step-up or step-down the voltage.

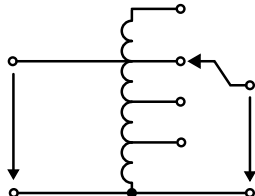


Fig. 4.18: Simplified autotransformer representation



Fig. 4.19: Exemplary autotransformer
(source: [Wikimedia Commons](#),
R. Spekking, CC BY-SA 4.0)

Autotransformer – step-down configuration

Assuming idealized conditions (no leakage, no losses), the apparent power of the standard transformer S and of the autotransformer S_{at} are:

$$S = U_1 I_1 = U_2 I_2, \quad S_{\text{at}} = (U_1 + U_2) I_1 = U_2 (I_2 - I_1). \quad (4.27)$$

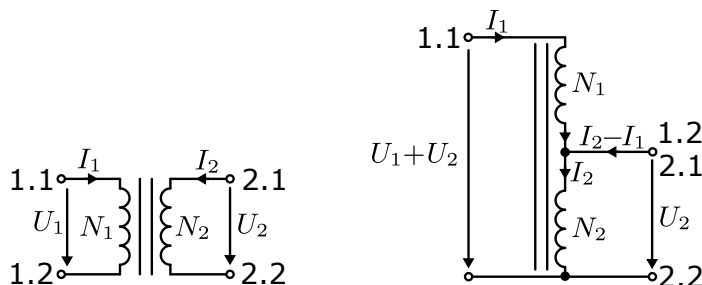


Fig. 4.20: Step-down autotransformer made from a standard two-winding transformer by connecting 1.2 from the primary to 2.1 on the secondary side

Autotransformer – step-down configuration (cont.)

From (4.27) we can express the autotransformer apparent power S_{at} in terms of the standard transformer apparent power S :

$$S_{\text{at}} = (U_1 + U_2)I_1 = S + U_2 I_1 = S + U_1 I_1 \frac{U_2}{U_1} = S(1 + \frac{1}{\ddot{u}}). \quad (4.28)$$

Here, \ddot{u} is the (idealized) voltage transformation ratio of the standard transformer – compare (4.11). Hence, we can express the apparent power of the autotransformer in terms of the standard transformer apparent power:

$$\frac{S_{\text{at}}}{S} = 1 + \frac{1}{\ddot{u}} = 1 + \frac{N_2}{N_1}. \quad (4.29)$$

Since $N_2/N_1 > 0$ the autotransformer can transfer more apparent power than the standard transformer since the autotransformer combines two power transfer mechanisms:

- ▶ the apparent power $U_1 I_1$ is transferred via the magnetic coupling (induction) and
- ▶ the apparent power $U_2 I_1$ is transferred via the electrical conduction between primary and secondary (not available in the galvanically-isolated standard transformer).

Autotransformer – step-up configuration

The apparent power of the step-up autotransformer is

$$S_{\text{at}} = U_1(I_1 - I_2) = (U_1 + U_2)I_2 = S\left(1 + \frac{U_1}{U_2}\right) = S(1 + \ddot{u}) = S\left(1 + \frac{N_1}{N_2}\right). \quad (4.30)$$

Likewise to the step-down autotransformer, the step-up autotransformer can transfer more apparent power than the standard transformer.

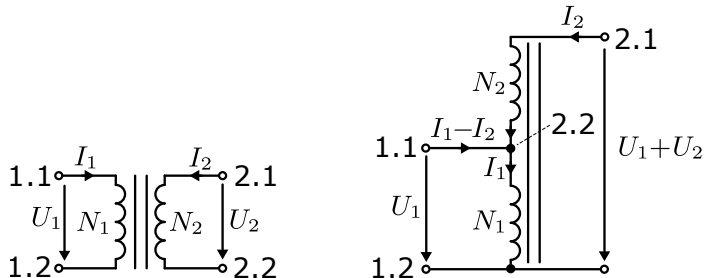


Fig. 4.21: Step-up autotransformer made from a standard two-winding transformer by connecting 1.1 from the primary to 2.2 on the secondary side

Autotransformer remarks

The previous analysis has revealed that the apparent power boost over the standard transformer is significant if

- ▶ $N_2 \gg N_1$ (step-down case) or
- ▶ $N_1 \gg N_2$ (step-up case),

that is, the autotransformer's input and output voltage have only a small difference. In this case, the autotransformer can be more efficient and cost-effective than the standard transformer (at the drawback of the lacking galvanic isolation).



Fig. 4.22: 750 MVA, 380 kV / 230 kV three-phase autotransformer (source: [Wikimedia Commons](#), P. Mertens, CC BY-SA 3.0)

Autotransformer remarks (cont.)

Another challenge of the autotransformer is its short-circuit behavior. From the step-up case we know:

$$S_{\text{at}} = S \left(1 + \frac{N_1}{N_2}\right).$$

Dividing both sides by U_1 delivers

$$I_{1,\text{at}} = I_1 \left(1 + \frac{N_1}{N_2}\right) \quad (4.31)$$

Hence, in case of a short circuit the steady-state current of the autotransformer is $1 + N_1/N_2$ times higher than the standard transformer:

$$I_{1,\text{at,psc}} = I_{1,\text{psc}} \left(1 + \frac{N_1}{N_2}\right). \quad (4.32)$$

The same applies to the step-down case. Therefore, the autotransformer may require additional short-circuit protection measures to prevent damages (e.g., additional choke).

Three-phase transformer

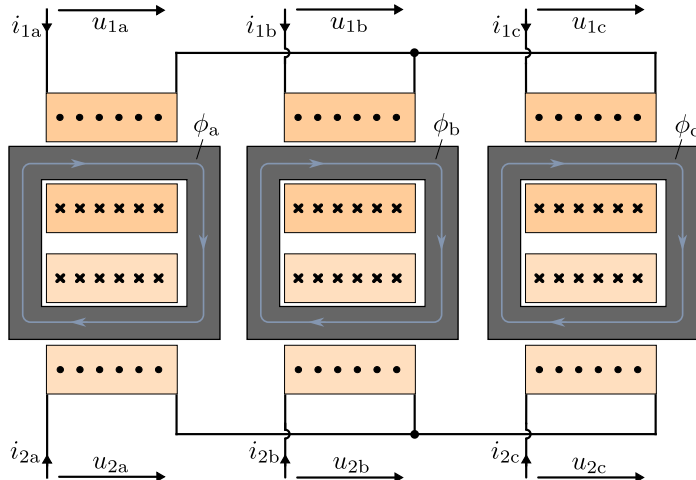


Fig. 4.23: Simple three-phase transformer with three independent single-phase transformers connected in star both on the primary and secondary side

Three-phase transformer with five legs

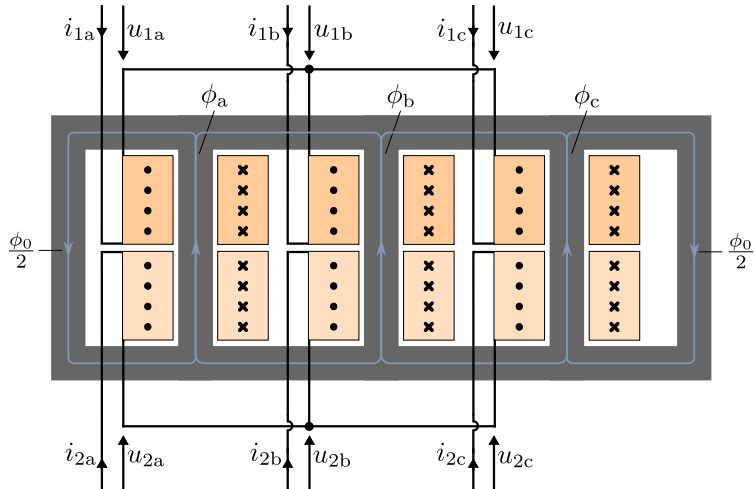


Fig. 4.24: Three-phase five-leg transformer connected in star both on the primary and secondary side

Three-phase transformer with five legs (cont.)

Obviously, the three-phase five-leg design from Fig. 4.24 can save space and material compared to the three independent single-phase transformers from Fig. 4.23. However, there might be a zero flux component

$$\phi_0(t) = \phi_a(t) + \phi_b(t) + \phi_c(t) \quad (4.33)$$

flowing via the winding-free legs. This zero flux component can be avoided if the primary and secondary side are connected both in star configuration

$$i_{1a}(t) + i_{1b}(t) + i_{1c}(t) = 0, \quad i_{2a}(t) + i_{2b}(t) + i_{2c}(t) = 0$$

and if the magnetic reluctances Λ_m of the three main legs are equal (i.e., symmetric design, no saturation):

$$\phi_0 = \phi_a + \phi_b + \phi_c = \Lambda_m N_1 (i_{1a}(t) + i_{1b}(t) + i_{1c}(t)) + \Lambda_m N_2 (i_{2a}(t) + i_{2b}(t) + i_{2c}(t)) = 0.$$

Three-phase transformer with three legs (double star connection)

- ▶ If the flux zero component ϕ_0 can be avoided, a three-leg design as shown in Fig. 4.25 can be used.
- ▶ However, if $\phi_0 \neq 0$ due to an asymmetric design, magnetic saturation or non-ideal symmetrical operation, the zero component will act as a stray field leaving the core.
- ▶ This can lead to increased losses in auxiliary components (e.g., housing) and electromagnetic interference issues.

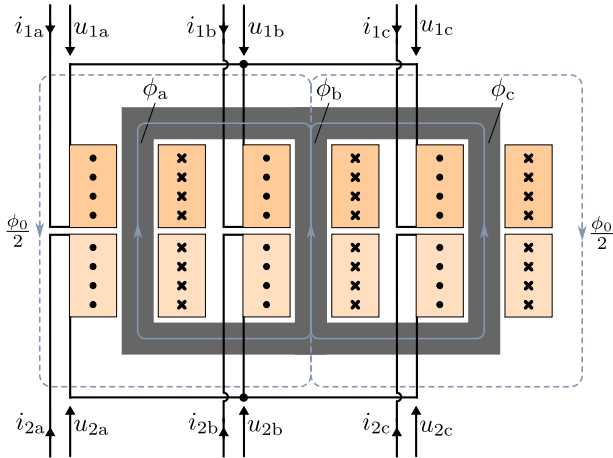


Fig. 4.25: Three-phase three-leg transformer connected in star both on the primary and secondary side

Three-phase transformer with three legs (star-delta connection)

If the primary or secondary side is connected in delta configuration, this side can carry a zero sequence current:

$$i_0 = \frac{1}{3} (i_a(t) + i_b(t) + i_c(t)) \neq 0.$$

This zero sequence current would not be visible in the phase conductors:

$$\begin{aligned} i_{ab} &= i_a - i_b, \\ i_{bc} &= i_b - i_c, \\ i_{ca} &= i_c - i_a. \end{aligned} \tag{4.34}$$

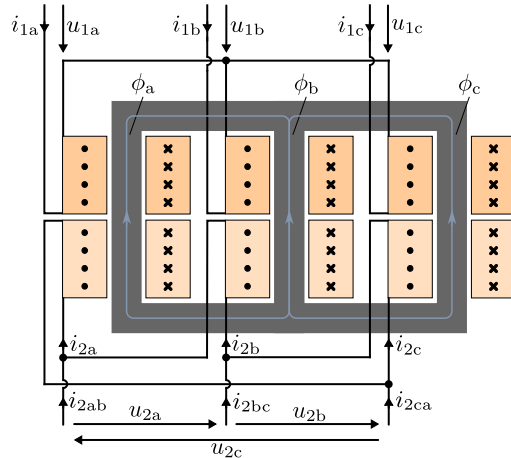


Fig. 4.26: Three-phase three-leg transformer connected in a star-delta configuration (delta on secondary is exemplary)

Zero flux and zero current components in three-phase transformers

Based on (4.34) the winding currents on the delta side becomes

$$i_a = i_0 + \frac{1}{3} (i_{ab} - i_{ca}), \quad i_b = i_0 + \frac{1}{3} (i_{bc} - i_{ab}), \quad i_c = i_0 + \frac{1}{3} (i_{ca} - i_{bc}). \quad (4.35)$$

If the secondary side is connected in delta, the zero sequence current will result from

$$\phi_0 = \phi_a + \phi_b + \phi_c = \phi(i_{1a}, i_{2a}, i_{20}) + \phi(i_{1b}, i_{2b}, i_{20}) + \phi(i_{1c}, i_{2c}, i_{20}) = 0 \quad (4.36)$$

where $\phi(\cdot)$ is the (potentially nonlinear) magnetic flux function (e.g., including saturation).

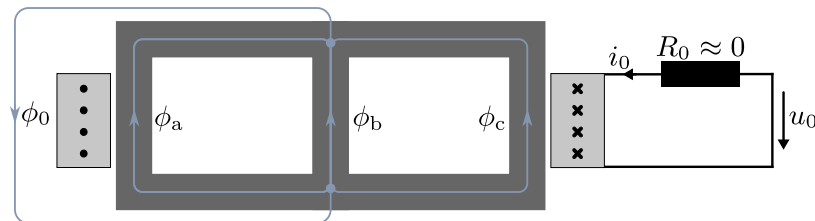


Fig. 4.27: Substitute model to represent the zero flux component

Three-phase transformer connection and winding types

Each side of a three-phase transformer can be connected in:

Y/y: star connection, D/d: delta connection, Z/z: zigzag connection.

The winding nomenclature is as follows:

- ▶ First upper case letter: primary side (high voltage)
- ▶ Second lower case letter: secondary side (low voltage)
- ▶ Number (0...11): phase deviation between the primary and secondary side in °30 steps
- ▶ Optional: N/n for neutral connection of high/low side.

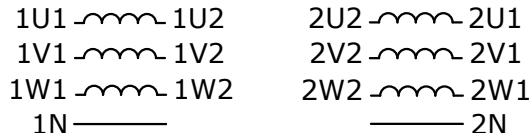


Fig. 4.28: Connection nomenclature of three-phase transformers

Three-phase transformer connection and winding types (example: Yd1)

Transformer connection Yd1 indicates

- ▶ Y: star connection on the primary side,
- ▶ d: delta connection on the secondary side,
- ▶ 1: phase deviation of $1 \cdot 30^\circ = 30^\circ$ between the primary and secondary side.

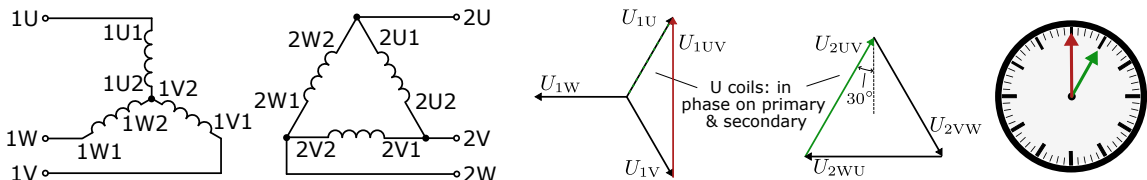


Fig. 4.29: Winding configuration and resulting phasor diagrams for Yd1 connection

Three-phase transformer connection and winding types (example: Dy11)

The transformer connection Dy11 indicates

- ▶ D: delta connection on the primary side,
- ▶ y: star connection on the secondary side,
- ▶ 11: phase deviation of $11 \cdot 30^\circ = 330^\circ$ between the primary and secondary side.

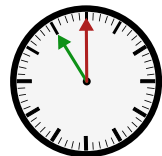
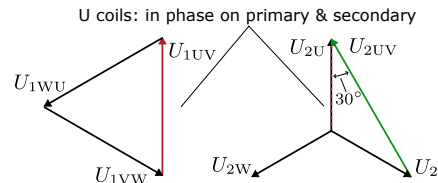
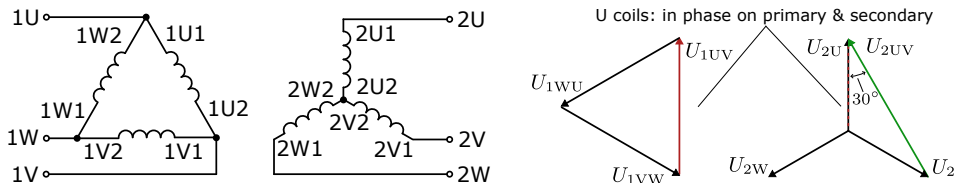


Fig. 4.30: Winding configuration and resulting phasor diagrams for Dy11 connection

Three-phase transformer connection and winding types (example: Dy5)

In this example, the primary and secondary side are still connected in a delta-star configuration, but, the polarity of the secondary side is reversed compared to the previous Dy11 connection. Consequently, the phase deviation is $5 \cdot 30^\circ = 150^\circ$.

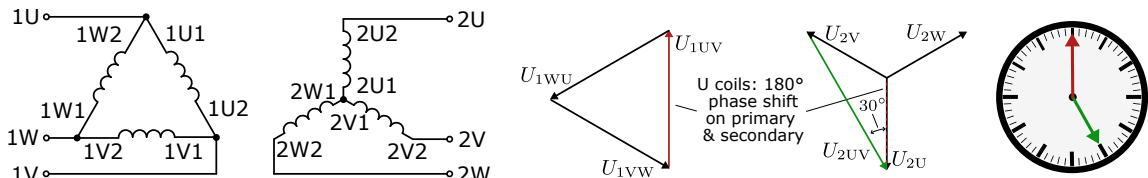


Fig. 4.31: Winding configuration and resulting phasor diagrams for Dy5 connection

Three-phase transformer connection symbols (vector groups)

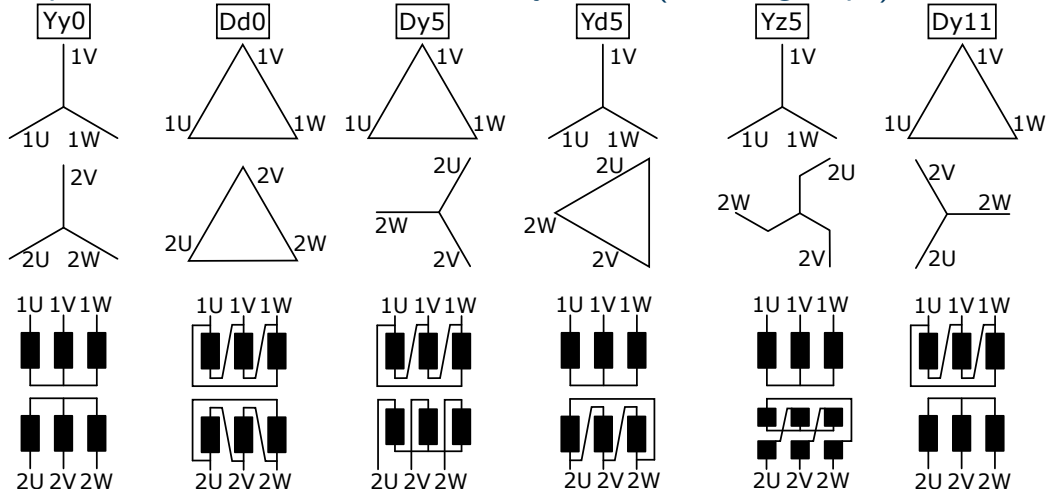


Fig. 4.32: Exemplary (simplified) connection symbols for three-phase transformers and the resulting phasor displacement representations

Three-phase transformer voltage ratio

If the three-phase connection type changes between the primary and secondary side, the voltage ratio between the primary and secondary side is affected – cf. Tab. 4.1.

primary	Y	D	Y	D	Y	D
secondary	y	y	d	d	z	z
$U_{1,\text{ll}}/U_{2,\text{ll}}$	1	$\sqrt{3}$	$1/\sqrt{3}$	1	$\sqrt{3}/2$	$3/2$

Tab. 4.1: Idealized voltage ratios between primary and secondary due to different connection types (assuming $N_1 = N_2$) with $U_{1,\text{ll}}$ and $U_{2,\text{ll}}$ being the line-to-line voltages on the primary and secondary side, respectively

Dynamic modeling of the three-phase transformer

Assuming a three-phase transformer without mutual coupling between the phases abc (as in the three independent single-phase transformers from Fig. 4.23) and without saturation, the magnetic flux linkage of the primary and secondary side can be expressed as

$$\psi(t) = \begin{bmatrix} \psi_{1a}(t) \\ \psi_{1b}(t) \\ \psi_{1c}(t) \\ \psi_{2a}(t) \\ \psi_{2b}(t) \\ \psi_{2c}(t) \end{bmatrix} = \begin{bmatrix} L_{1a} & 0 & 0 & M_a & 0 & 0 \\ 0 & L_{1b} & 0 & 0 & M_b & 0 \\ 0 & 0 & L_{1c} & 0 & 0 & M_c \\ M_a & 0 & 0 & L_{2a} & 0 & 0 \\ 0 & M_b & 0 & 0 & L_{2b} & 0 \\ 0 & 0 & M_c & 0 & 0 & L_{2c} \end{bmatrix} \begin{bmatrix} i_{1a}(t) \\ i_{1b}(t) \\ i_{1c}(t) \\ i_{2a}(t) \\ i_{2b}(t) \\ i_{2c}(t) \end{bmatrix} = \mathbf{L}\mathbf{i}(t). \quad (4.37)$$

If the transformer's magnetic three-phase circuit is ideally symmetric, also

$$M = M_a = M_b = M_c, \quad L_1 = L_{1a} = L_{1b} = L_{1c}, \quad L_2 = L_{2a} = L_{2b} = L_{2c}$$

holds.

Dynamic modeling of the three-phase transformer (cont.)

Hence, we have

$$\boldsymbol{\psi}(t) = \begin{bmatrix} \psi_{1a}(t) \\ \psi_{1b}(t) \\ \psi_{1c}(t) \\ \psi_{2a}(t) \\ \psi_{2b}(t) \\ \psi_{2c}(t) \end{bmatrix} = \begin{bmatrix} L_1 & 0 & 0 & M & 0 & 0 \\ 0 & L_1 & 0 & 0 & M & 0 \\ 0 & 0 & L_1 & 0 & 0 & M \\ M & 0 & 0 & L_2 & 0 & 0 \\ 0 & M & 0 & 0 & L_2 & 0 \\ 0 & 0 & M & 0 & 0 & L_2 \end{bmatrix} \begin{bmatrix} i_{1a}(t) \\ i_{1b}(t) \\ i_{1c}(t) \\ i_{2a}(t) \\ i_{2b}(t) \\ i_{2c}(t) \end{bmatrix} = \mathbf{L}\mathbf{i}(t). \quad (4.38)$$

The voltage equation results from Faraday's law and Ohm's law:

$$\mathbf{u}(t) = \mathbf{R}\mathbf{i}(t) + \mathbf{L}\frac{d}{dt}\mathbf{i}(t) = \begin{bmatrix} R_1 & 0 & 0 & 0 & 0 & 0 \\ 0 & R_1 & 0 & 0 & 0 & 0 \\ 0 & 0 & R_1 & 0 & 0 & 0 \\ 0 & 0 & 0 & R_2 & 0 & 0 \\ 0 & 0 & 0 & 0 & R_2 & 0 \\ 0 & 0 & 0 & 0 & 0 & R_2 \end{bmatrix} \mathbf{i}(t) + \mathbf{L}\frac{d}{dt}\mathbf{i}(t). \quad (4.39)$$

Dynamic modeling of the three-phase transformer (cont.)

Due to the ideal three-phase symmetry, the model relation per phase pair on the primary and secondary side are identical for all three phases, i.e., we can split up the model into:

$$\begin{bmatrix} u_{1a}(t) \\ u_{2a}(t) \end{bmatrix} = \begin{bmatrix} R_1 & 0 \\ 0 & R_2 \end{bmatrix} \begin{bmatrix} i_{1a}(t) \\ i_{2a}(t) \end{bmatrix} + \begin{bmatrix} L_1 & M \\ M & L_2 \end{bmatrix} \frac{d}{dt} \begin{bmatrix} i_{1a}(t) \\ i_{2a}(t) \end{bmatrix}, \quad (4.40)$$

$$\begin{bmatrix} u_{1b}(t) \\ u_{2b}(t) \end{bmatrix} = \begin{bmatrix} R_1 & 0 \\ 0 & R_2 \end{bmatrix} \begin{bmatrix} i_{1b}(t) \\ i_{2b}(t) \end{bmatrix} + \begin{bmatrix} L_1 & M \\ M & L_2 \end{bmatrix} \frac{d}{dt} \begin{bmatrix} i_{1b}(t) \\ i_{2b}(t) \end{bmatrix}, \quad (4.41)$$

$$\begin{bmatrix} u_{1c}(t) \\ u_{2c}(t) \end{bmatrix} = \begin{bmatrix} R_1 & 0 \\ 0 & R_2 \end{bmatrix} \begin{bmatrix} i_{1c}(t) \\ i_{2c}(t) \end{bmatrix} + \begin{bmatrix} L_1 & M \\ M & L_2 \end{bmatrix} \frac{d}{dt} \begin{bmatrix} i_{1c}(t) \\ i_{2c}(t) \end{bmatrix}. \quad (4.42)$$

Hence, under the made assumptions the same ECD from Fig. 4.4 for the single-phase transformer case can be also used to model the three-phase transformer.

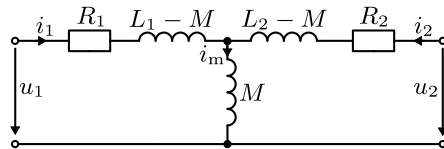


Table of contents

5 Rotating field theory

Rotating field theory

Oliver Wallscheid



Conceptual idea of a rotating magnetic field

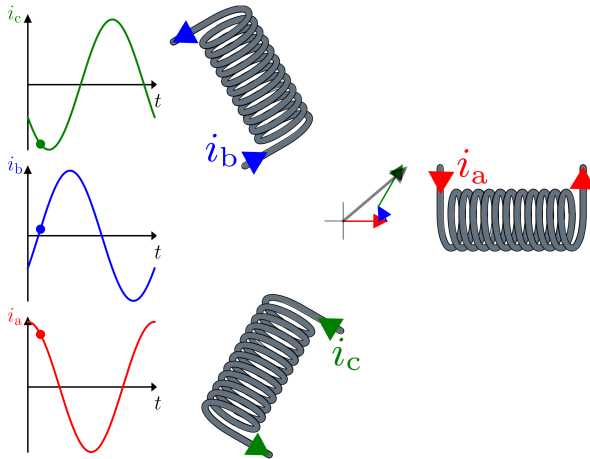


Fig. 5.1: Animation of a rotating magnetic field produced by three-phase currents in three coils both physically and electrically displaced by 120° (inspired by C. Joubert)

MMF distribution of a single-phase coil

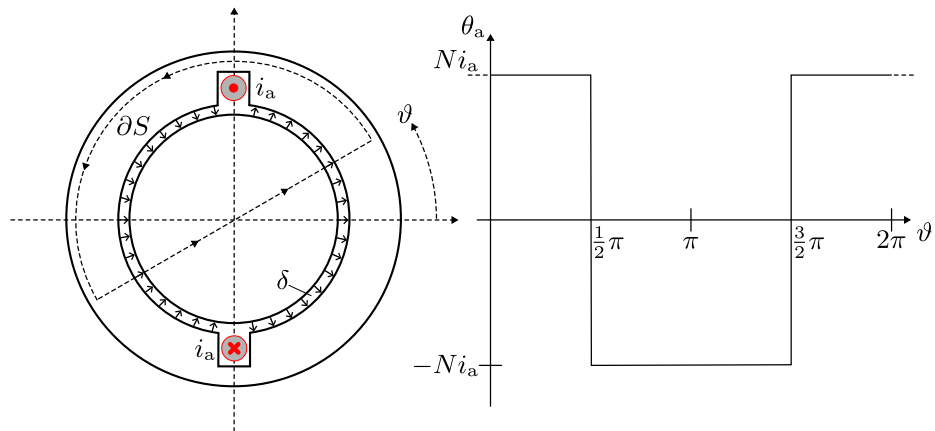


Fig. 5.2: MMF of a lumped single-phase coil with N turns for some current $i_a \neq 0$ with the rotating integration path ∂S along the circumference coordinate ϑ . The rotor is considered an unspecific solid iron dummy. Both stator and iron have infinite magnetic permeability.

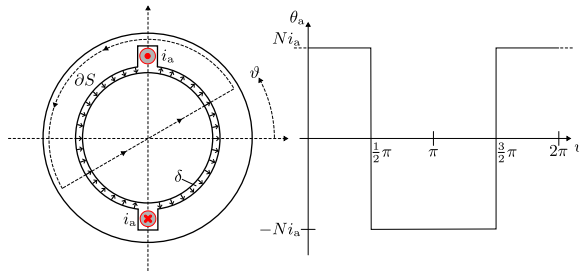
MMF distribution of a single-phase coil (cont.)

Utilizing Ampère's law in the magnetic network context from (2.36)

$$\oint_{\partial S} \mathbf{H} \cdot d\mathbf{s} = i_f = Ni = \sum_k \theta_k = \sum_k l_k H_k$$

and assuming that the air gap path along δ is dominating the magnetic circuit, we have

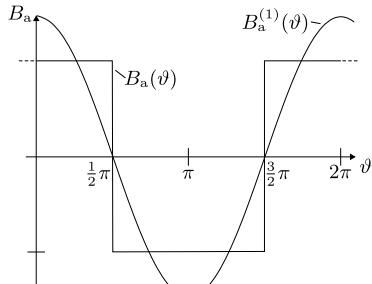
$$H_a(\vartheta) = \frac{1}{2\delta} \theta_a(\vartheta) = \frac{1}{2\delta} \begin{cases} Ni_a & \text{for } -\pi/2 \leq \vartheta < \pi/2, \\ -Ni_a & \text{for } \pi/2 \leq \vartheta < 3\pi/2. \end{cases} \quad (5.1)$$



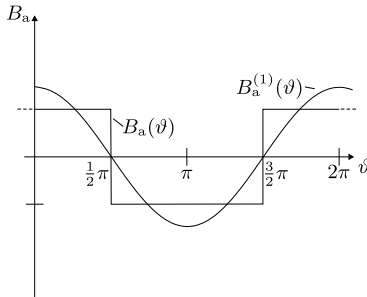
Air gap flux density distribution of a single-phase coil

With $B = \mu_0 H$ in the air gap and an alternating current $i_a = i_a(t)$, we have

$$B_a(\vartheta, t) = \frac{\mu_0}{2\delta} \begin{cases} Ni_a(t) & \text{for } -\pi/2 \leq \vartheta < \pi/2, \\ -Ni_a(t) & \text{for } \pi/2 \leq \vartheta < 3\pi/2. \end{cases} \quad (5.2)$$



(a) $i_a(t) = \hat{i}$



(b) $i_a(t) = \hat{i}/2$

Fig. 5.3: Air gap flux density distribution of a lumped single-phase coil representing a spatiotemporal function together with its fundamental component $B^{(1)}$

Fourier analysis of the air gap flux density distribution

Assuming a sinusoidal current $i_a(t) = \hat{i} \cos(\omega t)$, we have

$$B_a(\vartheta, t) = \underbrace{\frac{\mu_0 N \hat{i}}{2\delta}}_{\hat{B}} \begin{cases} \cos(\omega t) & \text{for } -\pi/2 \leq \vartheta < \pi/2, \\ -\cos(\omega t) & \text{for } \pi/2 \leq \vartheta < 3\pi/2. \end{cases} \quad (5.3)$$

The flux density distribution therefore is periodic and has a sinusoidal shape over t as well as a rectangular shape over ϑ . To analyze the latter in terms of its fundamental and harmonic components, we utilize the Fourier series expansion for some arbitrary $t \in \mathbb{R}$:

$$B_a(\vartheta, t) = B_a(\vartheta) = \hat{B}^{(0)} + \sum_{k=1}^{\infty} \hat{B}_c^{(k)} \cos(k\vartheta) + \hat{B}_s^{(k)} \sin(k\vartheta), \quad (5.4)$$

for harmonic order $k \in \mathbb{N}$ with amplitudes $\hat{B}_c^{(k)} \in \mathbb{R}$ and $\hat{B}_s^{(k)} \in \mathbb{R}$ as well as offset $\hat{B}^{(0)} \in \mathbb{R}$.

Fourier analysis of the air gap flux density distribution (cont.)

The coefficients of (5.4) are

$$\begin{aligned}\hat{B}^{(0)} &= \frac{1}{2\pi} \int_0^{2\pi} B(\vartheta) d\vartheta, \\ \hat{B}_c^{(k)} &= \frac{1}{\pi} \int_0^{2\pi} B(\vartheta) \cos(k\vartheta) d\vartheta, \\ \hat{B}_s^{(k)} &= \frac{1}{\pi} \int_0^{2\pi} B(\vartheta) \sin(k\vartheta) d\vartheta.\end{aligned}\tag{5.5}$$

Since the positive and negative areas under the MMF curve in Fig. 5.2 are identical in size, the magnetic field does not have any offset component:

$$\hat{B}^{(0)} = 0.$$

Furthermore, (5.3) is an even function, i.e., $B(\vartheta) = B(-\vartheta)$ (i.e., the function is mirror-symmetrical to the ϑ axis – cf. Fig. 5.3), leading to

$$\hat{B}_s^{(k)} = 0.$$

Fourier analysis of the air gap flux density distribution (cont.)

Finally, (5.3) is symmetrical w.r.t. the abscissa, i.e., $B(\vartheta) = -B(\vartheta + \pi)$ (mirrored positive and negative half-wave), leading to

$$\hat{B}_c^{(k)} = 0 \quad \text{for} \quad k = 2, 4, 6, \dots$$

Summarizing the above, the Fourier series for the air gap flux density boils down to

$$B_a(\vartheta) = \sum_{k=1,3,5,\dots}^{\infty} \hat{B}_c^{(k)} \cos(k\vartheta) \quad \text{with} \quad \hat{B}_c^{(k)} = \frac{1}{\pi} \int_0^{2\pi} B(\vartheta) \cos(k\vartheta) d\vartheta. \quad (5.6)$$

Utilizing symmetry of the flux distribution as shown in Fig. 5.3, we can calculate $\hat{B}_c^{(k)}$ for the remaining odd $k = 1, 3, 5, \dots$ harmonic orders as follows:

$$\begin{aligned} \hat{B}_c^{(k)} &= \frac{2}{\pi} \int_{-\pi/2}^{\pi/2} B(\vartheta) \cos(k\vartheta) d\vartheta = \frac{\mu_0 N \hat{i}}{\delta \pi} \cos(\omega t) \int_{-\pi/2}^{\pi/2} \cos(k\vartheta) d\vartheta \\ &= \frac{\mu_0 N \hat{i}}{k \delta \pi} \cos(\omega t) \left[\sin\left(\frac{k\pi}{2}\right) - \sin\left(-\frac{k\pi}{2}\right) \right] = \frac{2\mu_0 N \hat{i}}{\delta \pi k} \cos(\omega t) \sin\left(\frac{k\pi}{2}\right). \end{aligned} \quad (5.7)$$

Fourier analysis of the air gap flux density distribution (cont.)

The Fourier series describing the spatiotemporal air gap flux density distribution of a lumped single-phase coil is therefore

$$\begin{aligned} B_a(\vartheta, t) &= \frac{2\mu_0 N \hat{i}}{\delta\pi} \cos(\omega t) \sum_{k=1,3,5,\dots}^{\infty} \frac{1}{k} \sin\left(\frac{k\pi}{2}\right) \cos(k\vartheta) \\ &= \frac{4}{\pi} \hat{B} \cos(\omega t) \sum_{k=1,3,5,\dots}^{\infty} \frac{1}{k} \sin\left(\frac{k\pi}{2}\right) \cos(k\vartheta). \end{aligned} \tag{5.8}$$

One might note that

$$\sin\left(\frac{k\pi}{2}\right) = 1 \quad \text{for } k = 1, 5, 9, \dots, \quad \sin\left(\frac{k\pi}{2}\right) = -1 \quad \text{for } k = 3, 7, 11, \dots$$

applies above. Also, the fundamental component $\hat{B}^{(1)}$ of the air gap flux density distribution is $4/\pi$ times higher than the amplitude \hat{B} of the original square wave function from (5.3) while the harmonic amplitudes decrease with $1/k$.

Fourier analysis of the air gap flux density distribution (cont.)

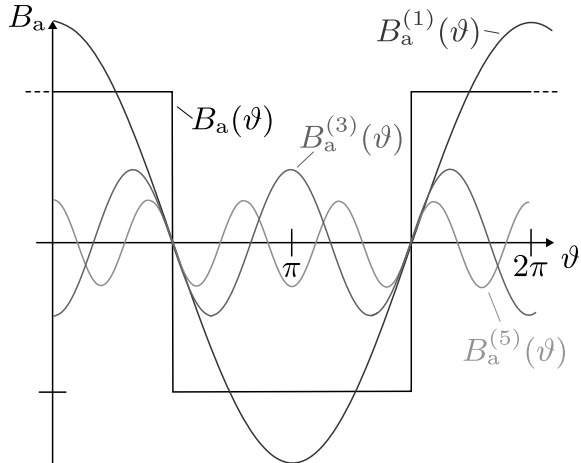


Fig. 5.4: Decomposition of $B(\vartheta, t)$ for $t = 0$ into its fundamental and its first harmonic components

Flux density harmonics

The existence of harmonics is to be attributed to the spatial layout of the winding. The phase current was assumed to be of pure sinusoidal form, i.e., is not causing the flux density harmonics (in our investigation).

Multipole stators

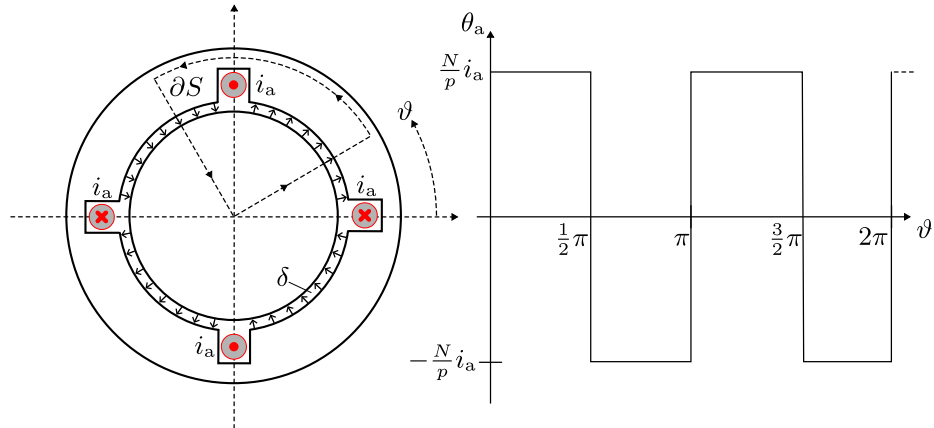


Fig. 5.5: MMF of a lumped single-phase coil with two pole pairs p and N/p turns per pole pair for some current $i_a \neq 0$ with the rotating integration path ∂S along the circumference coordinate ϑ

Multipole stators (cont.)

Following the same derivation as previously for machines with $p \geq 1$ pole pairs, we have

$$\begin{aligned} B_a(\vartheta, t) &= \frac{2\mu_0 N \hat{i}}{\delta \pi p} \cos(\omega t) \sum_{k=1,3,5,\dots}^{\infty} \frac{1}{k} \sin\left(\frac{k\pi}{2}\right) \cos(kp\vartheta) \\ &= \frac{4}{\pi p} \hat{B} \cos(\omega t) \sum_{k=1,3,5,\dots}^{\infty} \frac{1}{k} \sin\left(\frac{k\pi}{2}\right) \cos(kp\vartheta). \end{aligned} \quad (5.9)$$

Compared to the single-pole pair case, the flux density

- ▶ amplitude is reduced by $1/p$ (due to the winding turns being distributed over p pole pairs),
- ▶ spatial frequency is increased by p : $\vartheta \rightarrow p\vartheta$.

The latter implies that the fundamental and harmonics of $B(\vartheta)$ repeat p times more often over the (mechanical) stator circumference (compare Fig. 5.4).

Multipole stators (cont.)

From the previous finding

$$B_a(\vartheta, t) = \frac{4}{\pi p} \hat{B} \cos(\omega t) \sum_{k=1,3,5,\dots}^{\infty} \frac{1}{k} \sin\left(\frac{k\pi}{2}\right) \cos(kp\vartheta)$$

we can conclude that the field distribution for $p > 1$ is repeated p times over the mechanical stator circumference, assuming that the machine is ideally identical for each pole pair.

Electrical vs. mechanical angle

To simplify the following analysis, we introduce the electrical angle

$$\vartheta_{\text{el}} = p\vartheta, \quad (5.10)$$

i.e., to complete one mechanical revolution, the electrical angle has to complete p revolutions. The field description in the electrical coordinate system is therefore sufficient, as this is merely repeated in the mechanical system.

Basic rotating field model

We assume an ideal three-phase stator current:

$$\begin{aligned} i_{s,a}(t) &= \hat{i}_s \cos(\omega t), \\ i_{s,b}(t) &= \hat{i}_s \cos(\omega t - 2\pi/3), \\ i_{s,c}(t) &= \hat{i}_s \cos(\omega t + 2\pi/3). \end{aligned} \quad (5.11)$$

The index 's' indicates stator quantities, but is omitted in the following as we will only consider stator quantities until further notice, i.e.,

$$i_{s,a}(t) = i_a(t), \quad i_{s,b}(t) = i_b(t), \quad i_{s,c}(t) = i_c(t)$$

and $\hat{i}_s = \hat{i}$.

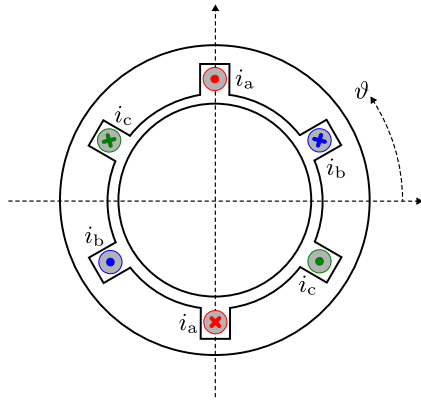


Fig. 5.6: Elementary three-phase stator winding with lumped coils displaced by 120° ($p = 1$ pole pair)

Basic rotating field model (cont.)

Transferring the finding (5.9) to the three-phase stator winding from Fig. 5.6 (considering an arbitrary number of $p \geq 1$ pole pairs), we have

$$\begin{aligned}B_a(\vartheta_{\text{el}}, t) &= \frac{4}{\pi p} \hat{B} \cos(\omega t) \sum_{k=1,3,5,\dots}^{\infty} \frac{1}{k} \sin\left(\frac{k\pi}{2}\right) \cos(k\vartheta_{\text{el}}), \\B_b(\vartheta_{\text{el}}, t) &= \frac{4}{\pi p} \hat{B} \cos\left(\omega t - \frac{2\pi}{3}\right) \sum_{k=1,3,5,\dots}^{\infty} \frac{1}{k} \left(\frac{k\pi}{2}\right) \cos\left(k\vartheta_{\text{el}} - k\frac{2\pi}{3}\right), \\B_c(\vartheta_{\text{el}}, t) &= \frac{4}{\pi p} \hat{B} \cos\left(\omega t + \frac{2\pi}{3}\right) \sum_{k=1,3,5,\dots}^{\infty} \frac{1}{k} \left(\frac{k\pi}{2}\right) \cos\left(k\vartheta_{\text{el}} + k\frac{2\pi}{3}\right).\end{aligned}\tag{5.12}$$

Basic rotating field model (cont.)

Applying the decomposition

$$\cos(x) \cos(y) = \frac{1}{2} [\cos(x - y) + \cos(x + y)]$$

to (5.12), we obtain

$$B_a(\vartheta_{\text{el}}, t) = \frac{2}{\pi p} \hat{B} \sum_{k=1,3,5,\dots}^{\infty} \frac{1}{k} \sin\left(\frac{k\pi}{2}\right) [\cos(\omega t - k\vartheta_{\text{el}}) + \cos(\omega t + k\vartheta_{\text{el}})],$$

$$B_b(\vartheta_{\text{el}}, t) = \frac{2}{\pi p} \hat{B} \sum_{k=1,3,5,\dots}^{\infty} \frac{1}{k} \sin\left(\frac{k\pi}{2}\right) \left[\cos(\omega t - k\vartheta_{\text{el}} - \frac{2\pi}{3}(1-k)) + \cos(\omega t + k\vartheta_{\text{el}} - \frac{2\pi}{3}(1+k)) \right],$$

$$B_c(\vartheta_{\text{el}}, t) = \frac{2}{\pi p} \hat{B} \sum_{k=1,3,5,\dots}^{\infty} \frac{1}{k} \sin\left(\frac{k\pi}{2}\right) \left[\cos(\omega t - k\vartheta_{\text{el}} + \frac{2\pi}{3}(1-k)) + \cos(\omega t + k\vartheta_{\text{el}} + \frac{2\pi}{3}(1+k)) \right].$$

Positive and negative sequence decomposition

Hence, the decomposition led to two sinusoidal fields rotating in opposite directions:

$$\underbrace{\cos(\omega t - k\vartheta_{el}) = \cos(k\vartheta_{el} - \omega t)}_{\text{positive sequence}} \quad \text{and} \quad \underbrace{\cos(\omega t + k\vartheta_{el})}_{\text{negative sequence}}.$$

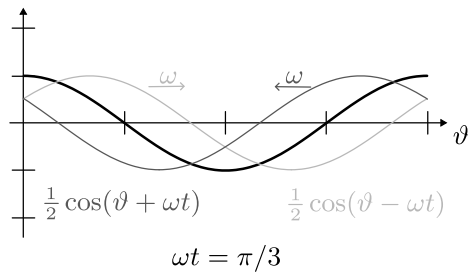
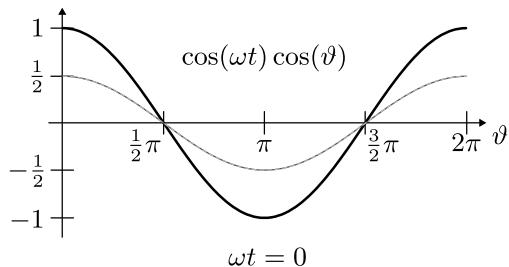


Fig. 5.7: Decomposition of the alternating field into positive and negative sequence components for $p = 1$ and $k = 1$

Resulting field: positive sequence part

To describe the resulting field distribution (as visualized in Fig. 5.1)

$$B(\vartheta_{\text{el}}, t) = B_a(\vartheta_{\text{el}}, t) + B_b(\vartheta_{\text{el}}, t) + B_c(\vartheta_{\text{el}}, t) \quad (5.13)$$

we analyze the positive and negative sequences separately. Utilizing

$$\cos(x \pm y) = \cos(x)\cos(y) \mp \sin(x)\sin(y)$$

we obtain for the positive sequence:

$$\begin{aligned} & \cos(\omega t - k\vartheta_{\text{el}}) + \cos(\omega t - k\vartheta_{\text{el}} - \frac{2\pi}{3}(1-k)) + \cos(\omega t - k\vartheta_{\text{el}} + \frac{2\pi}{3}(1-k)) \\ = & \cos(\omega t - k\vartheta_{\text{el}}) + \cos(\omega t - k\vartheta_{\text{el}}) \cos(\frac{2\pi}{3}(1-k)) + \sin(\omega t - k\vartheta_{\text{el}}) \sin(\frac{2\pi}{3}(1-k)) \\ & + \cos(\omega t - k\vartheta_{\text{el}}) \cos(\frac{2\pi}{3}(1-k)) - \sin(\omega t - k\vartheta_{\text{el}}) \sin(\frac{2\pi}{3}(1-k)). \end{aligned}$$

Hence, the sine terms cancel out each other.

Resulting field: positive sequence part (cont.)

Summarizing the above, we have

$$\begin{aligned} & \cos(\omega t - k\vartheta_{\text{el}}) \cos(\omega t - k\vartheta_{\text{el}} - \frac{2\pi}{3}(1-k)) + \cos(\omega t - k\vartheta_{\text{el}} + \frac{2\pi}{3}(1-k)) \\ = & \cos(\omega t - k\vartheta_{\text{el}})(1 + 2 \cos(\frac{2\pi}{3}(1-k))). \end{aligned}$$

Considering $\cos(n2\pi) = 1$ and $\cos(4\pi/3 + n2\pi) = \cos(2\pi/3 + n2\pi) = -1/2$ for $n \in \mathbb{Z}$ we observe the following for the positive sequence

$$\cos(\omega t - k\vartheta_{\text{el}})(1 + 2 \cos(\frac{2\pi}{3}(1-k))) = \begin{cases} 3 \cos(\omega t - k\vartheta_{\text{el}}) & \text{for } k = 1, 7, 13, 19, \dots, \\ 0 & \text{for } k = 3, 5, 9, 11, 15, 17, \dots \end{cases} \quad (5.14)$$

Hence, there are multiple harmonic orders which cancel out each other, among others, any multiple of $k = 3$. Moreover, the positive sequences of all three phases carries the fundamental component for $k = 1$.

Resulting field: negative sequence part

For the negative sequence part of

$$B(\vartheta_{\text{el}}, t) = B_a(\vartheta_{\text{el}}, t) + B_b(\vartheta_{\text{el}}, t) + B_c(\vartheta_{\text{el}}, t)$$

we rewrite the following terms

$$\begin{aligned} & \cos(\omega t + k\vartheta_{\text{el}}) + \cos(\omega t + k\vartheta_{\text{el}} - \frac{2\pi}{3}(1+k)) + \cos(\omega t + k\vartheta_{\text{el}} + \frac{2\pi}{3}(1+k)) \\ = & \cos(\omega t + k\vartheta_{\text{el}}) + \cos(\omega t + k\vartheta_{\text{el}}) \cos(\frac{2\pi}{3}(1+k)) + \sin(\omega t + k\vartheta_{\text{el}}) \sin(\frac{2\pi}{3}(1+k)) \\ & + \cos(\omega t + k\vartheta_{\text{el}}) \cos(\frac{2\pi}{3}(1+k)) - \sin(\omega t + k\vartheta_{\text{el}}) \sin(\frac{2\pi}{3}(1+k)) \end{aligned}$$

and find for the negative sequence

$$\cos(\omega t + k\vartheta_{\text{el}})(1 + 2 \cos(\frac{2\pi}{3}(1+k))) = \begin{cases} 3 \cos(\omega t + k\vartheta_{\text{el}}) & \text{for } k = 5, 11, 17, \dots, \\ 0 & \text{for } k = 1, 3, 7, 9, 15, \dots. \end{cases} \quad (5.15)$$

Resulting field: summary

Combining the positive and negative sequences, we receive

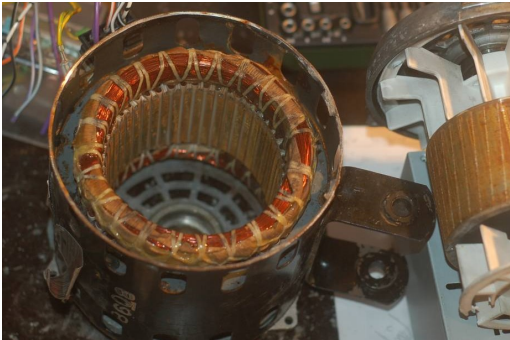
$$B(\vartheta_{\text{el}}, t) = \frac{6}{\pi p} \hat{B} \sum_k^{\infty} \frac{1}{k} \sin\left(\frac{k\pi}{2}\right) \begin{cases} \cos(\omega t - k\vartheta_{\text{el}}) & \text{for } k = 1, 7, 13, 19, \dots, \\ \cos(\omega t + k\vartheta_{\text{el}}) & \text{for } k = 5, 11, 17, \dots, \\ 0 & \text{otherwise.} \end{cases} \quad (5.16)$$

Utilizing $\cos(-x) = \cos(x)$ and $\sin(-x) = -\sin(x)$, we can rewrite the above as

$$B(\vartheta_{\text{el}}, t) = \frac{6}{\pi p} \hat{B} \sum_k^{\infty} \frac{1}{k} \sin\left(\frac{k\pi}{2}\right) \cos(\omega t - k\vartheta_{\text{el}}) \quad \text{for } k = 1, -5, 7, -11, 13, -17, \dots \quad (5.17)$$

Here, the negative sequences are represented by the negative harmonic orders. Finally, one can note that the amplitudes of the resulting field from the three-phase excitation (5.17) are $3/2$ times higher than in the single-phase case from (5.9).

Stator winding examples



(a) Induction machine with fed-in stator winding
(source: [Wikimedia Commons](#), J. Pharos,
CC BY-SA 3.0)



(b) Hydrogenerator with form-found stator winding
(source: [Wikimedia Commons](#), Astronmyinertia,
CC BY-SA 3.0)

Fig. 5.8: Examples of three-phase stator windings with different configurations

Winding as a distributed coil system

In contrast to the lumped-coil representation from Fig. 5.6, the stator coils per phase are distributed over the stator circumference. To describe the winding layout, we (re-)introduce:

Q : number of slots, m : number of phases (usually $m = 3$),

$q = \frac{Q}{2pm}$: number of notches (number of slots per phase and pole), ρ_p : pole pitch (elec.).

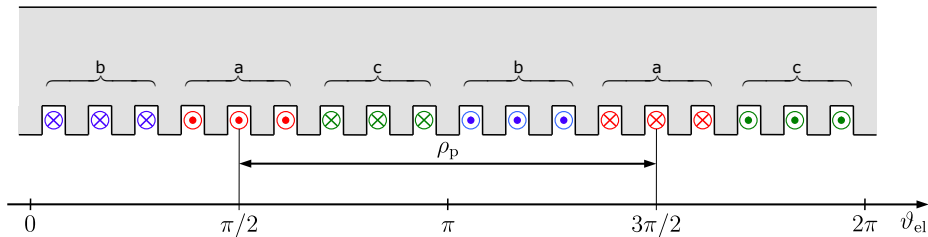
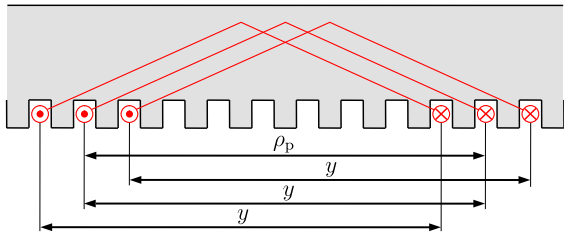
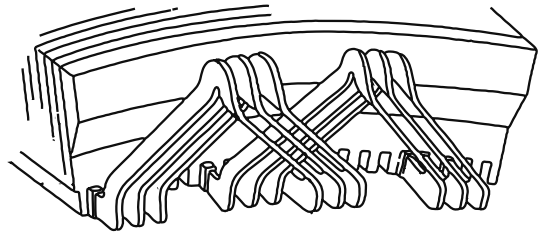


Fig. 5.9: Example scheme of a distributed winding with $Q = 18, p = 1, q = 3$ (adapted from J. Böcker, *Controlled Three-Phase Drives*, Paderborn University, 2021)

Distributed winding: same width coils



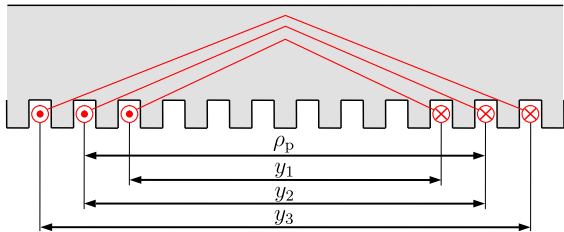
(a) Simplified unwound cross-section view (adapted from J. Böcker, *Controlled Three-Phase Drives*, Paderborn University, 2021)



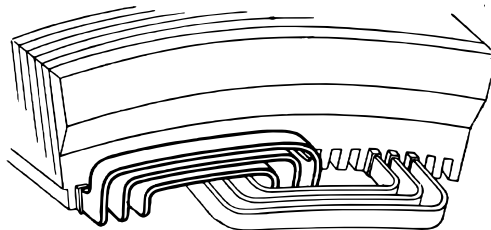
(b) Front view on end winding (adapted from W. Novender, *Elektrische Maschinen*, Technische Hochschule Mittelhessen, 2023)

Fig. 5.10: Realization of a distributed winding through windings of same width y

Distributed winding: varying width coils



(a) Simplified unwound cross-section view (adapted from J. Böcker, *Controlled Three-Phase Drives*, Paderborn University, 2021)



(b) Front view on end winding (adapted from W. Novender, *Elektrische Maschinen*, Technische Hochschule Mittelhessen, 2023)

Fig. 5.11: Realization of a distributed winding through windings of varying widths y_i

Distribution factor

As a result of the winding distribution, the MMF results in a staircase form as shown in Fig. 5.12. Hence, the field distribution calculation from (5.8) has to be adapted.

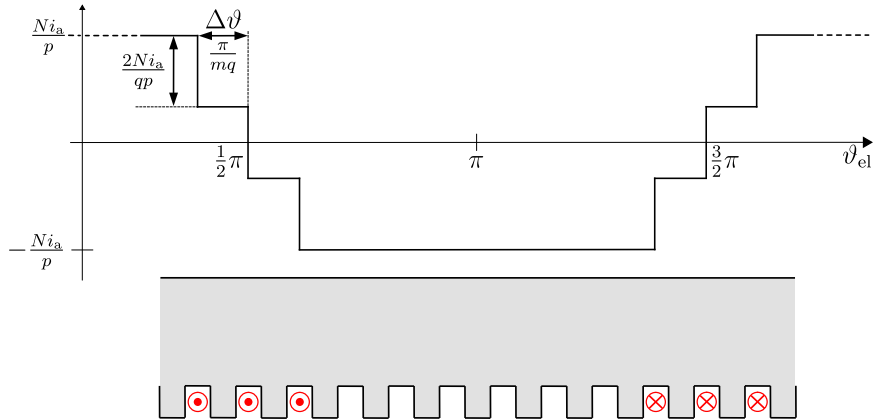


Fig. 5.12: Example of the MMF of a distributed winding scheme

Distribution factor (cont.)

Starting from

$$B_a(\vartheta_{\text{el}}) = \sum_{k=1,3,5,\dots}^{\infty} \hat{B}_c^{(k)} \cos(k\vartheta_{\text{el}})$$

$$\hat{B}_c^{(k)} = \frac{2}{\pi} \int_{-\pi/2}^{\pi/2} B(\vartheta_{\text{el}}) \cos(k\vartheta_{\text{el}}) d\vartheta_{\text{el}}$$

we rewrite the integral considering shifted coils by $\Delta\vartheta$ steps (i.e., $k\Delta\vartheta$ steps for the k -th harmonic order) with N/q turns per coil based on the distribution of a single lumped coil B' from (5.7):

$$\hat{B}_c^{(k)} = \frac{2}{\pi q} \operatorname{Re} \left\{ \sum_{l=0}^{q-1} e^{j\Delta\vartheta_l k} \int_{-\pi/2}^{\pi/2} B'(\vartheta_{\text{el}}) \cos(k\vartheta_{\text{el}}) d\vartheta_{\text{el}} \right\}.$$

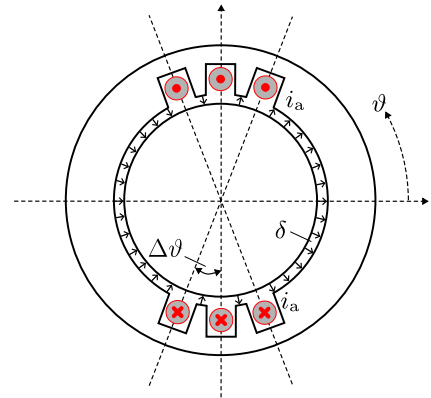


Fig. 5.13: Representation of the coil displacement by $\Delta\vartheta$ steps for a distributed winding with $q = 3$ and $p = 1$

Distribution factor (cont.)

The discrete coil displacement angles are (assuming that the Q slots are evenly distributed over the stator circumference, i.e., $\Delta\vartheta = p2\pi/Q$)

$$\Delta\vartheta_l = -\frac{q-1}{2}\frac{\pi}{mq} + l\frac{\pi}{mq} = -\frac{q-1}{2}p\frac{2\pi}{Q} + lp\frac{2\pi}{Q} \quad \text{for } l = 0, 1, \dots, q-1. \quad (5.18)$$

Hence, we can rewrite the Fourier series coefficient integral as:

$$\hat{B}_c^{(k)} = \underbrace{\frac{1}{q} \operatorname{Re} \left\{ \sum_{l=0}^{q-1} e^{j\Delta\vartheta_l k} \right\}}_{\xi_{d,k}} \underbrace{\frac{2}{\pi} \int_{-\pi/2}^{\pi/2} B'(\vartheta_{\text{el}}) \cos(k\vartheta_{\text{el}}) d\vartheta_{\text{el}}}_{\text{single lumped-coil integral}}. \quad (5.19)$$

Hence, the Fourier coefficient of every harmonic order k is multiplied by the distribution factor $\xi_{d,k}$.

Distribution factor (cont.)

To write this $\xi_{d,k}$ more compactly, we rearrange

$$\sum_{l=0}^{q-1} e^{\mathrm{j}\Delta\vartheta_l k} = \sum_{l=0}^{q-1} e^{\mathrm{j}k(-\frac{q-1}{2}p\frac{2\pi}{Q} + lp\frac{2\pi}{Q})} = e^{-\mathrm{j}k\frac{q-1}{2}p\frac{2\pi}{Q}} \sum_{l=0}^{q-1} \left(e^{\mathrm{j}kp\frac{2\pi}{Q}}\right)^l \quad (5.20)$$

and utilize the finite geometric series expression

$$\sum_{l=0}^{q-1} x^l = \frac{1-x^q}{1-x}$$

to rewrite

$$\sum_{l=0}^{q-1} \left(e^{\mathrm{j}kp\frac{2\pi}{Q}}\right)^l = \frac{1 - e^{\mathrm{j}kqp\frac{2\pi}{Q}}}{1 - e^{\mathrm{j}kp\frac{2\pi}{Q}}}.$$

Distribution factor (cont.)

The latter can be further rewritten as

$$\frac{1 - e^{jkqp\frac{2\pi}{Q}}}{1 - e^{jkp\frac{2\pi}{Q}}} = \frac{e^{jkqp\frac{2\pi}{Q}\frac{1}{2}} \left(e^{-jkqp\frac{2\pi}{Q}\frac{1}{2}} - e^{jkqp\frac{2\pi}{Q}\frac{1}{2}} \right)}{e^{jkp\frac{2\pi}{Q}\frac{1}{2}} \left(e^{-j kp\frac{2\pi}{Q}\frac{1}{2}} - e^{j kp\frac{2\pi}{Q}\frac{1}{2}} \right)}.$$

Utilizing the identity

$$\sin(x) = \frac{e^{jx} - e^{-jx}}{2j}$$

we can further rewrite

$$\sum_{l=0}^{q-1} \left(e^{jkp\frac{2\pi}{Q}} \right)^l = \frac{1 - e^{jkqp\frac{2\pi}{Q}}}{1 - e^{jkp\frac{2\pi}{Q}}} = \frac{e^{jkqp\frac{2\pi}{Q}\frac{1}{2}} (-2j) \sin(kqp\frac{2\pi}{Q}\frac{1}{2})}{e^{jkp\frac{2\pi}{Q}\frac{1}{2}} (-2j) \sin(kp\frac{2\pi}{Q}\frac{1}{2})} = e^{jk\frac{2\pi}{Q}\frac{q-1}{2}} \frac{\sin(kqp\frac{2\pi}{Q}\frac{1}{2})}{\sin(kp\frac{2\pi}{Q}\frac{1}{2})}. \quad (5.21)$$

Distribution factor (cont.)

Inserting (5.21) into (5.20) we finally receive

$$\begin{aligned}\xi_{d,k} &= \frac{1}{q} \operatorname{Re} \left\{ \sum_{l=0}^{q-1} e^{j\Delta\vartheta_l k} \right\} = \frac{1}{q} e^{-jkp \frac{2\pi}{Q} \frac{q-1}{2}} e^{jk \frac{2\pi}{Q} \frac{q-1}{2}} \frac{\sin(kqp \frac{2\pi}{Q} \frac{1}{2})}{\sin(kp \frac{2\pi}{Q} \frac{1}{2})} \\ &= \frac{\sin(kqp \frac{2\pi}{Q} \frac{1}{2})}{q \sin(kp \frac{2\pi}{Q} \frac{1}{2})} = \frac{\sin(kqp \frac{\pi}{Q})}{q \sin(kp \frac{\pi}{Q})} \\ &= \frac{\sin\left(\frac{k\pi}{2m}\right)}{q \sin\left(\frac{k\pi}{2mq}\right)}.\end{aligned}\tag{5.22}$$

- ▶ $|\xi_{d,k}| \leq 1$ holds for all parameter combinations.
- ▶ The factor describes the change of each harmonic component due to the distributed winding compared to the (idealized) lumped-coil case.

Pitch factor

If windings are not implemented as diametral winding, i.e., the winding width y is smaller than the pole pitch ρ_p ,

$$y < \rho_p = \pi,$$

the winding is called chorded. Hence, the starting and end position of the coil are shifted towards $\pm(y/\rho_p)(\pi/2)$ along the circumference. Consequently, the Fourier coefficients of the chorded winding are:

$$\hat{B}_c^{(k)} = \frac{2}{\pi} \int_{-\frac{\pi}{2} \frac{y}{\rho_p}}^{\frac{\pi}{2} \frac{y}{\rho_p}} B(\vartheta_{el}) \cos(k\vartheta_{el}) d\vartheta_{el}. \quad (5.23)$$

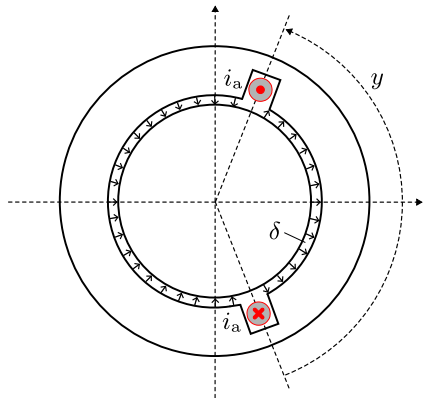


Fig. 5.14: Representation of a chorded coil for a distributed winding with $q = 3$ and $p = 1$

Pitch factor (cont.)

Continuing from (5.23), we can rewrite the integral as

$$\begin{aligned}\hat{B}_c^{(k)} &= \frac{2}{\pi} \int_{-\frac{\pi}{2} \frac{y}{\rho_p}}^{\frac{\pi}{2} \frac{y}{\rho_p}} B(\vartheta_{el}) \cos(k\vartheta_{el}) d\vartheta_{el} = \frac{2}{\pi} \hat{B} \cos(\omega t) \int_{-\frac{\pi}{2} \frac{y}{\rho_p}}^{\frac{\pi}{2} \frac{y}{\rho_p}} \cos(k\vartheta_{el}) d\vartheta_{el} \\ &= \frac{2}{\pi} \hat{B} \cos(\omega t) \frac{1}{k} \left[\sin\left(k \frac{\pi}{2} \frac{y}{\rho_p}\right) - \sin\left(-k \frac{\pi}{2} \frac{y}{\rho_p}\right) \right] = \frac{4}{\pi} \hat{B} \cos(\omega t) \frac{1}{k} \sin\left(k \frac{\pi}{2} \frac{y}{\rho_p}\right).\end{aligned}\tag{5.24}$$

Compared to the unchored case (5.7), the Fourier coefficients are

$$\frac{\sin\left(k \frac{\pi}{2} \frac{y}{\rho_p}\right)}{\sin\left(k \frac{\pi}{2}\right)}$$

smaller. As the magnitude of the denominator is always one, we define

$$\xi_{p,k} = \sin\left(k \frac{\pi}{2} \frac{y}{\rho_p}\right)\tag{5.25}$$

as the pitch factor.

Winding factor

Considering both, a distributed and chorded winding, we receive

$$\begin{aligned}\hat{B}_c^{(k)} &= \frac{1}{q} \operatorname{Re} \left\{ \sum_{l=0}^{q-1} e^{j\Delta\vartheta_l k} \right\} \frac{2}{\pi} \int_{-\frac{\pi}{2} \frac{y}{\rho_p}}^{\frac{\pi}{2} \frac{y}{\rho_p}} B(\vartheta_{el}) \cos(k\vartheta_{el}) d\vartheta_{el} \\ &= \dots \\ &= \frac{4}{\pi} \hat{B} \cos(\omega t) \frac{1}{k} \sin \left(k \frac{\pi}{2} \frac{y}{\rho_p} \right) \frac{\sin \left(\frac{k\pi}{2m} \right)}{q \sin \left(\frac{k\pi}{2mq} \right)} \\ &= \frac{4}{\pi} \hat{B} \cos(\omega t) \frac{1}{k} \underbrace{\xi_{d,k} \xi_{p,k}}_{\xi_{w,k}}\end{aligned}\tag{5.26}$$

with $\xi_{w,k} = \xi_{d,k} \xi_{p,k}$ being the winding factor. It describes the change of each harmonic component due to the distributed and chorded winding compared to the (idealized) lumped-coil case (which would be equivalent to $\xi_{w,k} = 1$).

Winding factor: examples

Machine A				Machine B			Machine C		
k	$\xi_{d,k}$	$\xi_{p,k}$	$\xi_{w,k}$	$\xi_{d,k}$	$\xi_{p,k}$	$\xi_{w,k}$	$\xi_{d,k}$	$\xi_{p,k}$	$\xi_{w,k}$
$q = 1, \quad y/\rho_p = 2/3, \quad Q/p = 6$				$q = 2, \quad y/\rho_p = 5/6, \quad Q/p = 12$			$q = 3, \quad y/\rho_p = 7/9, \quad Q/p = 18$		
1	1	0.866	0.866	0.966	0.966	0.933	0.960	0.940	0.902
3	1	0	0	0.707	-0.707	-0.500	0.667	-0.500	-0.333
5	1	-0.866	-0.866	0.259	0.259	0.067	0.218	-0.174	-0.038
7	1	0.866	0.866	-0.259	0.259	-0.067	-0.177	0.766	-0.136
9	1	0	0	-0.707	-0.707	0.500	-0.333	-1.000	0.333
11	1	-0.866	-0.866	-0.966	0.966	-0.933	-0.177	0.776	-0.136
13	1	0.866	0.866	-0.966	-0.966	0.933	0.218	-0.174	-0.038
15	1	0	0	-0.707	0.707	-0.500	0.667	-0.500	-0.333

Tab. 5.1: Winding factors for different winding configurations for three-phase machines ($m = 3$)

Winding factor interpretation

The winding factor $\xi_{w,k}$ mathematically maps a (real-world) distributed (and eventually charded) winding with N turns in slots distributed over the stator circumference to an idealized (abstract) lumped-coil representation with $N \cdot \xi_{w,k}$ (effective) turns. For following calculation steps (e.g., in a three-phase machine model – compare Fig. 5.6), one can utilize the simplified lumped-coil representation without systematic modeling errors thanks to the winding factor concept.

- ▶ With respect to Tab. 5.1 one can also observe that the winding configuration choice has a direct impact on the harmonic content of the flux density distribution.
- ▶ As those will also influence the production of torque and induced voltage (harmonics), the winding factor is a crucial parameter for the design of electrical machines.

Winding factor: limitations

The winding factor approach leading to (5.26) was based on several (implicit) assumptions:

- The number of slots per phase and pole is a (positive) integer: $q \in \mathbb{N}$.
- The slot distribution is even over the stator circumference.

However, these assumptions do not apply to all (typical) winding configurations, in particular fractional slot windings where

$$q = \frac{Q}{2pm} \in \mathbb{Q}$$

is represented by a common fraction, i.e., rational number.

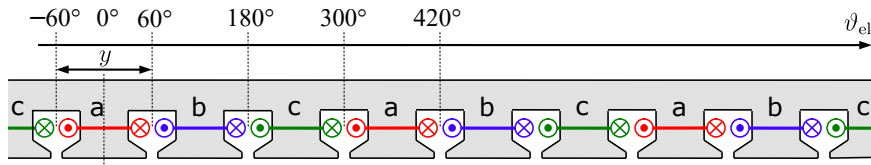


Fig. 5.15: Example scheme of a fractional slot concentrated winding with $Q = 9$, $p = 3$, $q = 1/2$
(adapted from J. Böcker, *Controlled Three-Phase Drives*, Paderborn University, 2021)

Concentrated winding

- ▶ Concentrated winding: the coils per phase are wound around single stator teeth.
- ▶ Allows for smaller end windings (i.e., less copper and reduced motor length) compared to distributed windings.



Fig. 5.16: Example of a concentrated winding where conductors form coils centered around single stator teeth
(source: Chan-Ho Baek et al., *Iron Loss Analysis of a Concentrated Winding Type Interior Permanent Magnet Synchronous Motor with Single and Dual Layer Magnet Shape*, MDPI Machines, 2021, CC BY 4.0)

Complex winding factor

The complex winding factor (here: for phase a) is defined as

$$\underline{\xi}_{a,k} = \frac{1}{jN_a} \sum_{i=1}^Q N_{a,i} e^{jk\vartheta_{el,a,i}} \quad (5.27)$$

with $N_{a,i} \in \mathbb{Z}$ being the number of conductors in slot i at the position $\vartheta_{el,a,i}$ with

$$N_a = \sum_{i=1}^Q |N_{a,i}| \quad (5.28)$$

being the total number of conductors. Moreover, $N_{a,i}$ represents the orientation of each conductor by

- ▶ $N_{a,i} = 0$: no conductor is in slot i ,
- ▶ $N_{a,i} > 0$: conductor is oriented towards the positive z -axis (directed towards reader),
- ▶ $N_{a,i} < 0$: conductor is oriented towards the negative z -axis (directed away from reader).

Complex winding factor (cont.)

The complex winding factor is a generalization of (5.19) weighting the contribution of each conductor to the k -th harmonic (compare Fig. 5.17). Hence,

- ▶ the conductor positions $\vartheta_{\text{el},a,i}$ are arbitrary and do not need to follow a specific distribution pattern (i.e., applicable to arbitrary slot configurations),
- ▶ the magnitude of the complex winding factor $|\xi_{a,k}| \in [0, 1]$ indicates the dampening of the harmonic component k due to the winding configuration,
- ▶ the phase of the complex winding factor $\angle \xi_{a,k}$ indicates the phase shift of the harmonic component k compared to the winding layout.

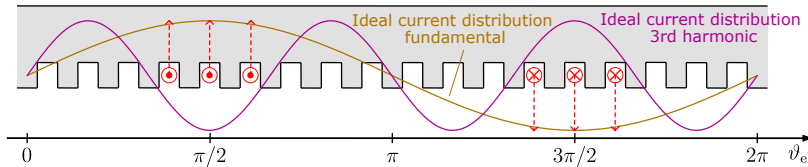


Fig. 5.17: Qualitative illustration of the complex winding factor as a comparison of the actual current distribution compared to the ideal distribution belonging to a certain flux harmonic

Complex winding factor (cont.)

While (5.27) represents the complex winding factor for phase a, the complex winding factor for phase b and c can be derived by rotating the coordinate system by $\pm 2\pi/3$:

$$\underline{\xi}_{b,k} = \frac{1}{jN_b} \sum_{i=1}^Q N_{b,i} e^{jk(\vartheta_{el,a,i} + \frac{2\pi}{3})}, \quad \underline{\xi}_{c,k} = \frac{1}{jN_c} \sum_{i=1}^Q N_{c,i} e^{jk(\vartheta_{el,a,i} - \frac{2\pi}{3})}. \quad (5.29)$$

Hence,

$$\underline{\xi}_{a,k} = e^{-jk\frac{2\pi}{3}} \underline{\xi}_{b,k} = e^{jk\frac{2\pi}{3}} \underline{\xi}_{c,k} \quad (5.30)$$

applies.

Harmonic orders

While regular symmetrical windings with $q \in \mathbb{N}$ will only produce certain harmonic orders ($k = 1, 3, 5, 7, \dots$ – cf. (5.12)), arbitrary winding configurations can produce further harmonic orders $k \in \mathbb{Q}$ (in particular if q is a common fraction).

Complex winding factor: example

Based on the below table describing the winding scheme information from Fig. 5.15 we have

$$\underline{\xi}_{a,k} = \frac{1}{j6} \left(-1e^{j\frac{k\pi}{3}} + 1e^{j\frac{k5\pi}{3}} - e^{j\frac{k7\pi}{3}} + e^{j\frac{k11\pi}{3}} - e^{j\frac{k13\pi}{3}} + e^{j\frac{k17\pi}{3}} \right),$$

$$\underline{\xi}_{a,1} = \frac{1}{j6} \left(-1e^{j\frac{\pi}{3}} + 1e^{j\frac{5\pi}{3}} - e^{j\frac{7\pi}{3}} + e^{j\frac{11\pi}{3}} - e^{j\frac{13\pi}{3}} + e^{j\frac{17\pi}{3}} \right) = -0.866,$$

$$\underline{\xi}_{a,2} = \frac{1}{j6} \left(-1e^{j\frac{2\pi}{3}} + 1e^{j\frac{10\pi}{3}} - e^{j\frac{14\pi}{3}} + e^{j\frac{22\pi}{3}} - e^{j\frac{26\pi}{3}} + e^{j\frac{34\pi}{3}} \right) = -0.866,$$

$$\underline{\xi}_{a,3} = \frac{1}{j6} \left(-1e^{j\pi} + 1e^{j5\pi} - e^{j7\pi} + e^{j11\pi} - e^{j13\pi} + e^{j17\pi} \right) = 0.$$

<i>i</i> -th slot	1	2	3	4	5	6	7	8	9
$\vartheta_{el,a,i}$	$\frac{1}{3}\pi$	π	$\frac{5}{3}\pi$	$\frac{7}{3}\pi$	3π	$\frac{11}{3}\pi$	$\frac{13}{3}\pi$	5π	$\frac{17}{3}\pi$
$N_{a,i}$	-1	0	1	-1	0	1	-1	0	1
$N_{b,i}$	1	-1	0	1	-1	0	1	-1	0
$N_{c,i}$	0	1	-1	0	1	-1	0	1	-1

Table of contents

6 Induction machines

Induction machines

Oliver Wallscheid



Basic induction machine (IM) representation

- ▶ Three-phase stator + three-phase rotor:
“rotating three-phase transformer”
(plus air gap)
- ▶ Rotor angular speed: ω_r
- ▶ Rotor angular displacement: ε_r
- ▶ Index “s” for stator, “r” for rotor quantities

Fundamental wave model

While the previous chapter has revealed that the magnetic flux distribution in the air gap is subject to plentiful harmonics, the following model limits itself to the fundamental wave.

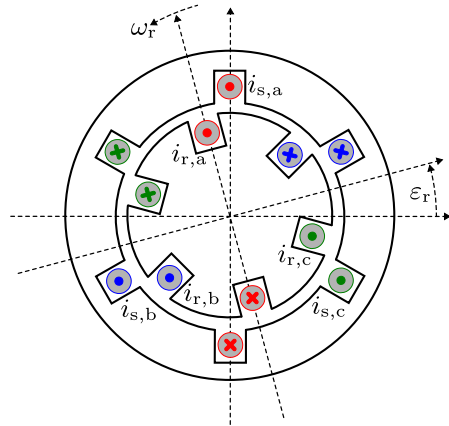
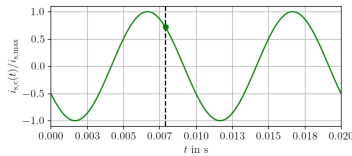
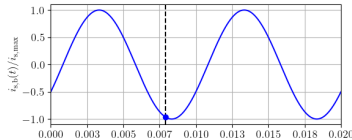
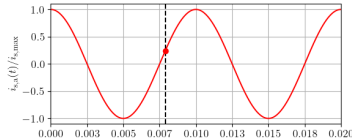


Fig. 6.1: Elementary three-phase induction machine (IM) lumped-coil representation ($p = 1$ pole pair)

Visualization of the asynchronous IM operation



B field (stator normal component, fundamental)
Lorentz Force

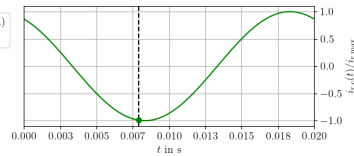
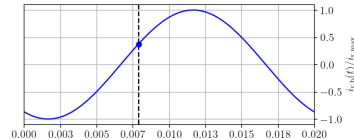
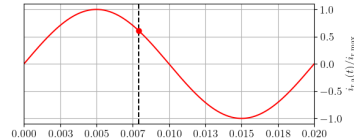


Fig. 6.2: Exemplary IM operation at $\omega = 2\pi 50 \frac{1}{s}$ in motoric operation (positive average torque)

Visualization of the asynchronous IM operation (cont.)

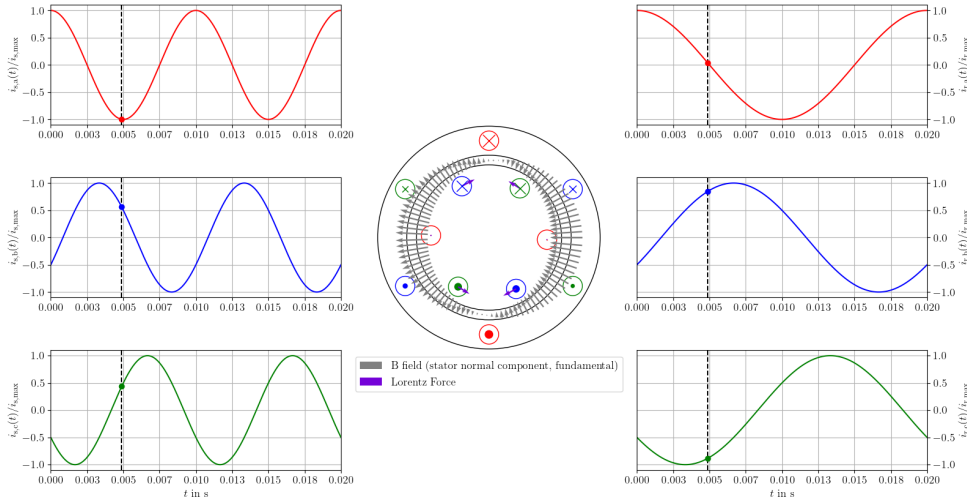


Fig. 6.3: Exemplary IM operation at $\omega = 2\pi 50 \frac{1}{s}$ in no-load operation (zero average torque)

Dynamical IM model

Based on Faraday's and Ohm's laws, we can write the following equations for the stator

$$\mathbf{u}_{s,abc}^s(t) = R_s \mathbf{i}_{s,abc}^s(t) + \frac{d}{dt} \boldsymbol{\psi}_{s,abc}^s(t) \Leftrightarrow \begin{bmatrix} u_{s,a}^s(t) \\ u_{s,b}^s(t) \\ u_{s,c}(t) \end{bmatrix} = R_s \begin{bmatrix} i_{s,a}^s(t) \\ i_{s,b}^s(t) \\ i_{s,c}^s(t) \end{bmatrix} + \frac{d}{dt} \begin{bmatrix} \psi_{s,a}^s(t) \\ \psi_{s,b}^s(t) \\ \psi_{s,c}^s(t) \end{bmatrix} \quad (6.1)$$

and rotor

$$\mathbf{u}_{r,abc}^r(t) = R_r \mathbf{i}_{r,abc}^r(t) + \frac{d}{dt} \boldsymbol{\psi}_{r,abc}^r(t) \Leftrightarrow \begin{bmatrix} u_{r,a}^r(t) \\ u_{r,b}^r(t) \\ u_{r,c}^r(t) \end{bmatrix} = R_r \begin{bmatrix} i_{r,a}^r(t) \\ i_{r,b}^r(t) \\ i_{r,c}^r(t) \end{bmatrix} + \frac{d}{dt} \begin{bmatrix} \psi_{r,a}^r(t) \\ \psi_{r,b}^r(t) \\ \psi_{r,c}^r(t) \end{bmatrix} \quad (6.2)$$

which are generally applicable as only identical resistances per phase on the stator and rotor are assumed. Above, the lower index denotes the physical location of the quantities, while the upper index indicates the coordinate system orientation.

Flux linkage model

In contrast to the simple three-phase transformer model (4.38), the flux linkage model of the IM is more complex:

- ▶ Due to the spatial 120° phase shift between the windings of the stator and rotor, the abc phases are all mutually coupled.
- ▶ The flux paths and physical dimensions of the stator and rotor are not identical, i.e., the rotor and stator inductances are different (even if the winding turns N_s and N_r are identical).
- ▶ The coupling between the stator and rotor is rotor position-dependent (not explicitly shown on the right due to space limitations).

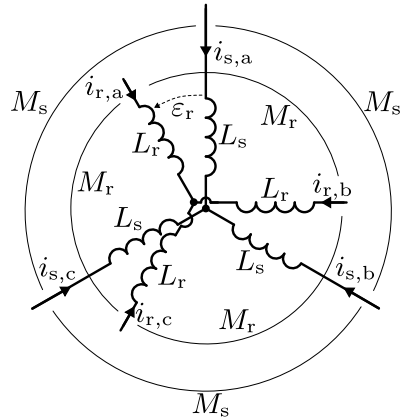


Fig. 6.4: Simplified representation of the inductive coupling between the stator/rotor phases of the IM

Flux linkages of the three-phase model

Based on the previous considerations, the flux linkages are given by

$$\begin{aligned}\psi_{s,abc}^s(t) &= \begin{bmatrix} L_s & -\frac{M_s}{2} & -\frac{M_s}{2} \\ -\frac{M_s}{2} & L_s & -\frac{M_s}{2} \\ -\frac{M_s}{2} & -\frac{M_s}{2} & L_s \end{bmatrix} \mathbf{i}_{s,abc}^s(t) + M_r \frac{N_s}{N_r} \mathcal{R}_{abc}(\varepsilon_{r,el}(t)) \mathbf{i}_{r,abc}^r(t), \\ \psi_{r,abc}^r(t) &= \begin{bmatrix} L_r & -\frac{M_r}{2} & -\frac{M_r}{2} \\ -\frac{M_r}{2} & L_r & -\frac{M_r}{2} \\ -\frac{M_r}{2} & -\frac{M_r}{2} & L_r \end{bmatrix} \mathbf{i}_{r,abc}^r(t) + M_s \frac{N_r}{N_s} \mathcal{R}_{abc}(\varepsilon_{r,el}(t))^T \mathbf{i}_{s,abc}^s(t)\end{aligned}\quad (6.3)$$

with $\varepsilon_{r,el}(t) = p\varepsilon_r(t)$ and the transformation matrix

$$\mathcal{R}_{abc}(\varepsilon_{r,el}(t)) = \begin{bmatrix} \cos(\varepsilon_{r,el}(t)) & \cos(\varepsilon_{r,el}(t) + \frac{2\pi}{3}) & \cos(\varepsilon_{r,el}(t) - \frac{2\pi}{3}) \\ \cos(\varepsilon_{r,el}(t) - \frac{2\pi}{3}) & \cos(\varepsilon_{r,el}(t)) & \cos(\varepsilon_{r,el}(t) + \frac{2\pi}{3}) \\ \cos(\varepsilon_{r,el}(t) + \frac{2\pi}{3}) & \cos(\varepsilon_{r,el}(t) - \frac{2\pi}{3}) & \cos(\varepsilon_{r,el}(t)) \end{bmatrix}. \quad (6.4)$$

Inductance matrices of the three-phase model

The inductance matrices

$$\boldsymbol{L}_{s,abc} = \begin{bmatrix} L_s & -\frac{M_s}{2} & -\frac{M_s}{2} \\ -\frac{M_s}{2} & L_s & -\frac{M_s}{2} \\ -\frac{M_s}{2} & -\frac{M_s}{2} & L_s \end{bmatrix}, \quad \boldsymbol{L}_{r,abc} = \begin{bmatrix} L_r & -\frac{M_r}{2} & -\frac{M_r}{2} \\ -\frac{M_r}{2} & L_r & -\frac{M_r}{2} \\ -\frac{M_r}{2} & -\frac{M_r}{2} & L_r \end{bmatrix}$$

are based on the following considerations.

- ▶ The self-inductances cover both the leakage and mutual coupling to other windings:
 $L_{s/r} = L_{s/r,\sigma} + M_{s/r}$.
- ▶ The mutual inductances on the stator/rotor $M_{s/r}$ are identical, as all three phases share the same magnetic paths and have the same winding turns $N_{s/r}$.
- ▶ The mutual inductances on the off diagonal represent the spatial displacement of the stator/rotor coils by $\pm 120^\circ$, which is why they are multiplied by $\cos(\pm 120^\circ) = -0.5$.
- ▶ In (6.3), the coupling term between stator and rotor is multiplied by the turn ratio to account for the different winding turns $N_{s/r}$ (i.e., mapping the mutual inductances between stator/rotor).

Orthogonal representation: alpha-beta coordinates

- ▶ The three-phase IM model is obviously quite unhandy: six differential equations plus a rather complicated magnetic circuit representation.
- ▶ Remedy: transform the three-phase model into the orthogonal $\alpha\beta$ coordinates.
- ▶ Advantage: only four differential equations and a simpler magnetic circuit representation (as one will see on the next slides).

Coordinate transformations

The following transformations of the IM model into different coordinate systems are pure mathematical “tricks” to simplify the analysis. The IM remains a three-phase machine.

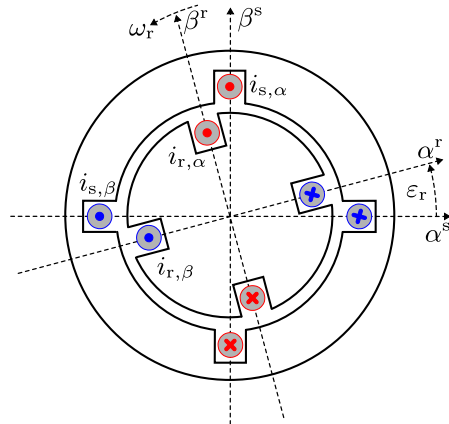


Fig. 6.5: Conceptual IM representation within the orthogonal $\alpha\beta$ coordinates ($p = 1$ pole pair)

Clarke transformation

To transform the three-phase model into the orthogonal $\alpha\beta$ coordinates, the Clarke transformation is applied. Consider any $\mathbf{x}_{abc} \in \mathbb{R}^3$, then the Clarke transformation is given by

$$\mathbf{x}_{\alpha\beta 0} = \begin{bmatrix} x_\alpha \\ x_\beta \\ x_0 \end{bmatrix} = \begin{bmatrix} 2/3 & -1/3 & -1/3 \\ 0 & 1/\sqrt{3} & -1/\sqrt{3} \\ \sqrt{2}/3 & \sqrt{2}/3 & \sqrt{2}/3 \end{bmatrix} \begin{bmatrix} x_a \\ x_b \\ x_c \end{bmatrix} = \mathbf{T}_c \mathbf{x}_{abc} \quad (6.5)$$

with the inverse transformation

$$\mathbf{x}_{abc} = \begin{bmatrix} 1 & 0 & 1/\sqrt{2} \\ -1/2 & \sqrt{3}/2 & 1/\sqrt{2} \\ -1/2 & -\sqrt{3}/2 & 1/\sqrt{2} \end{bmatrix} \begin{bmatrix} x_\alpha \\ x_\beta \\ x_0 \end{bmatrix} = \mathbf{T}_c^{-1} \mathbf{x}_{\alpha\beta 0}. \quad (6.6)$$

Above, $\mathbf{T}_c \in \mathbb{R}^{3 \times 3}$ is the Clarke transformation matrix and $\mathbf{x}_{\alpha\beta 0} \in \mathbb{R}^3$ the transformed vector.

Clarke transformation: amplitude and power scaling

The transformation (6.5) is amplitude-preserving, i.e., the amplitude of the $\alpha\beta$ vector is identical to the amplitude of the original abc vector. On the other hand, the power is not preserved, as can be seen from the inner product of the transformed vectors (which commonly occurs in power calculations):

$$\mathbf{x}_{\text{abc}}^T \mathbf{y}_{\text{abc}} = \mathbf{x}_{\alpha\beta 0}^T (\mathbf{T}_c^{-1})^T \mathbf{T}_c^{-1} \mathbf{y}_{\alpha\beta 0} \quad \Leftrightarrow \quad x_a y_a + x_b y_b + x_c y_c = \frac{3}{2} (x_\alpha y_\alpha + x_\beta y_\beta + x_0 y_0).$$

The alternative power-preserving Clarke transformation variant is given by

$$\mathbf{T}'_c = \frac{\sqrt{3}}{2} \mathbf{T}_c \quad (\mathbf{T}'_c)^{-1} = (\mathbf{T}'_c)^T, \quad (6.7)$$

which utilizes an orthogonal transformation matrix. However, when using \mathbf{T}'_c the amplitude of the transformed vector is not preserved. While being an arbitrary choice, we will stick to (6.5) as a convention for the following.

Clarke transformation: simplification for zero-component-free vectors

If the abc vector \mathbf{x}_{abc} is zero-component-free, i.e.,

$$x_a + x_b + x_c = 0,$$

e.g., the phase currents of a star connected system, the Clarke transformation simplifies to

$$\mathbf{x}_{\alpha\beta} = \begin{bmatrix} x_\alpha \\ x_\beta \end{bmatrix} = \begin{bmatrix} 2/3 & -1/3 & -1/3 \\ 0 & 1/\sqrt{3} & -1/\sqrt{3} \end{bmatrix} \begin{bmatrix} x_a \\ x_b \\ x_c \end{bmatrix} = \mathbf{T}_{23}\mathbf{x}_{abc} \quad (6.8)$$

and

$$\mathbf{x}_{abc} = \begin{bmatrix} 1 & 0 \\ -1/2 & \sqrt{3}/2 \\ -1/2 & -\sqrt{3}/2 \end{bmatrix} \begin{bmatrix} x_\alpha \\ x_\beta \end{bmatrix} = \mathbf{T}_{32}\mathbf{x}_{\alpha\beta}. \quad (6.9)$$

Clarke transformation: simplification for zero-component-free vectors

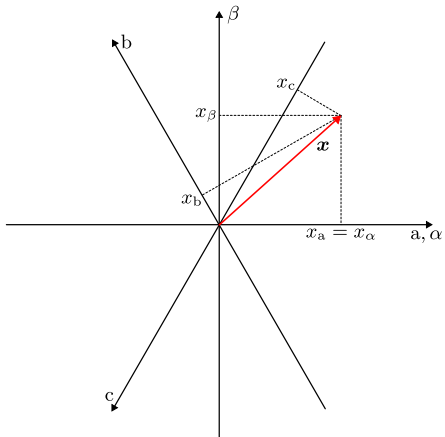


Fig. 6.6: Geometrical interpretation of the Clarke transformation without zero components: mapping $\mathbf{x}_{abc} \in \mathbb{R}^3$ to $\mathbf{x}_{\alpha\beta} \in \mathbb{R}^2$ without information loss (adapted from J. Böcker, *Controlled Three-Phase Drives*, Paderborn University, 2021)

Park transformation

The Park transform rotates a vector $\mathbf{x}_{\alpha\beta} \in \mathbb{R}^2$ by a certain angle ε to obtain $\mathbf{x}_{dq} \in \mathbb{R}^2$, that is,

$$\mathbf{x}_{dq} = \begin{bmatrix} x_d \\ x_q \end{bmatrix} = \begin{bmatrix} \cos(\varepsilon) & \sin(\varepsilon) \\ -\sin(\varepsilon) & \cos(\varepsilon) \end{bmatrix} \begin{bmatrix} x_\alpha \\ x_\beta \end{bmatrix} = \mathbf{T}_p^{-1}(\varepsilon) \mathbf{x}_{\alpha\beta} \quad (6.10)$$

with the counter rotation

$$\mathbf{x}_{\alpha\beta} = \begin{bmatrix} \cos(\varepsilon) & -\sin(\varepsilon) \\ \sin(\varepsilon) & \cos(\varepsilon) \end{bmatrix} \begin{bmatrix} x_d \\ x_q \end{bmatrix} = \mathbf{T}_p(\varepsilon) \mathbf{x}_{dq}. \quad (6.11)$$

Above, $\mathbf{T}_p \in \mathbb{R}^{2 \times 2}$ is the Park transformation matrix. It might be noted that this is a (historical) convention to define that \mathbf{T}_p rotates into the mathematically positive direction. Depending on the application background and choice of ε , the interpretation of \mathbf{x}_{dq} can vary.

Park transformation (cont.)

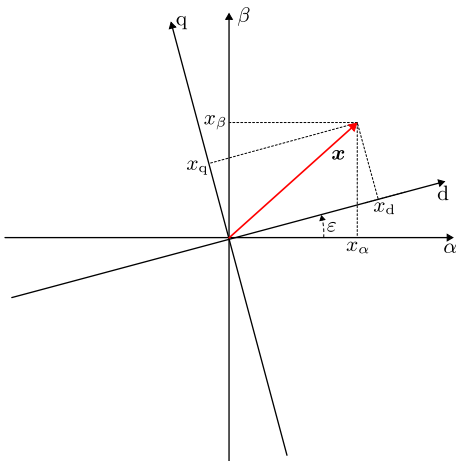


Fig. 6.7: Geometrical interpretation of the Park transformation: mapping $x_{\alpha\beta} \in \mathbb{R}^2$ to $x_{dq} \in \mathbb{R}^2$
(adapted from J. Böcker, *Controlled Three-Phase Drives*, Paderborn University, 2021)

Park transformation: some properties

Performing the Park and inverse Park transformation sequentially, does not change the vector:

$$\mathbf{x}_{\alpha\beta} = \mathbf{T}_p \mathbf{T}_p^{-1} \mathbf{x}_{\alpha\beta} = \mathbf{T}_p^{-1} \mathbf{T}_p \mathbf{x}_{\alpha\beta}. \quad (6.12)$$

A frequent rotation within the electric machines and drives context is

$$\mathbf{T}_p(\varepsilon = \pi/2) = \begin{bmatrix} \cos(\pi/2) & -\sin(\pi/2) \\ \sin(\pi/2) & \cos(\pi/2) \end{bmatrix} = \begin{bmatrix} 0 & -1 \\ 1 & 0 \end{bmatrix} = \mathbf{J} \quad (6.13)$$

leading to the definition of $\mathbf{J} \in \mathbb{R}^{2 \times 2}$ which will be used for brevity in the following. Moreover, if ε results from some rotation, i.e., $d/dt \varepsilon(t) = \omega(t)$, we have:

$$\frac{d}{dt} \mathbf{T}_p(\varepsilon(t)) = \begin{bmatrix} -\sin(\varepsilon(t)) & -\cos(\varepsilon(t)) \\ \cos(\varepsilon(t)) & -\sin(\varepsilon(t)) \end{bmatrix} \frac{d}{dt} \varepsilon(t) = \mathbf{T}_p(\varepsilon(t)) \mathbf{J} \omega(t), \quad (6.14)$$

$$\frac{d}{dt} \mathbf{T}_p^{-1}(\varepsilon(t)) = \begin{bmatrix} -\sin(\varepsilon(t)) & \cos(\varepsilon(t)) \\ -\cos(\varepsilon(t)) & -\sin(\varepsilon(t)) \end{bmatrix} \frac{d}{dt} \varepsilon(t) = -\mathbf{T}_p^{-1}(\varepsilon(t)) \mathbf{J} \omega(t). \quad (6.15)$$

Visualization of different coordinate systems

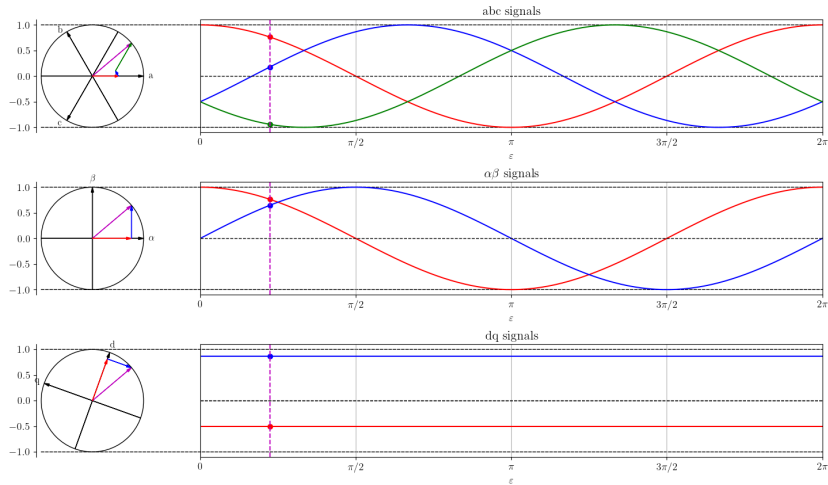


Fig. 6.8: Representation of a rotating phasor (without zero component) in different coordinate systems

IM model $\alpha\beta$ coordinates

Assuming zero-component-free three-phase quantities, multiplying the three-phase IM model (6.1) and (6.2) with T_{23} results in

$$\begin{aligned} \mathbf{T}_{23}\mathbf{u}_{s,abc}^s(t) &= R_s \mathbf{T}_{23}\mathbf{i}_{s,abc}^s(t) + \mathbf{T}_{23} \frac{d}{dt} \boldsymbol{\psi}_{s,abc}^s(t) \\ \Leftrightarrow \quad \mathbf{u}_{s,\alpha\beta}^s(t) &= R_s \mathbf{i}_{s,\alpha\beta}^s(t) + \frac{d}{dt} \boldsymbol{\psi}_{s,\alpha\beta}^s(t) \end{aligned} \tag{6.16}$$

and

$$\begin{aligned} \mathbf{T}_{23}\mathbf{u}_{r,abc}^r(t) &= R_r \mathbf{T}_{23}\mathbf{i}_{r,abc}^r(t) + \mathbf{T}_{23} \frac{d}{dt} \boldsymbol{\psi}_{r,abc}^r(t) \\ \Leftrightarrow \quad \mathbf{u}_{r,\alpha\beta}^r(t) &= R_r \mathbf{i}_{r,\alpha\beta}^r(t) + \frac{d}{dt} \boldsymbol{\psi}_{r,\alpha\beta}^r(t). \end{aligned} \tag{6.17}$$

Here, it must be noted that the two voltage equations are still represented in their own stator or rotor coordinate system. In particular, the rotor's $\alpha\beta$ axes are rotating (compare Fig. 6.5).

IM model $\alpha\beta$ coordinates: transformation of rotor quantities

To bring both model parts into the same coordinate system, the rotor quantities will be transformed into the stator's $\alpha\beta$ coordinates. This is done by applying the Park transformation with $\varepsilon(t) = \varepsilon_{r,el}(t) = p\varepsilon_r(t)$:

$$\begin{aligned} T_p(\varepsilon_{r,el}(t)) \mathbf{u}_{r,\alpha\beta}^r(t) &= T_p(\varepsilon_{r,el}(t)) R_r \mathbf{i}_{r,\alpha\beta}^r(t) + T_p(\varepsilon_{r,el}(t)) \frac{d}{dt} \boldsymbol{\psi}_{r,\alpha\beta}^r(t) \\ \Leftrightarrow \quad \mathbf{u}_{r,\alpha\beta}^s(t) &= R_r \mathbf{i}_{r,\alpha\beta}^s(t) + T_p(\varepsilon_{r,el}(t)) \frac{d}{dt} \boldsymbol{\psi}_{r,\alpha\beta}^r(t). \end{aligned} \tag{6.18}$$

The last term of (6.18) is rewritten as

$$\begin{aligned} T_p(\varepsilon_{r,el}(t)) \frac{d}{dt} \boldsymbol{\psi}_{r,\alpha\beta}^r(t) &= T_p(\varepsilon_{r,el}(t)) \frac{d}{dt} [T_p^{-1}(\varepsilon_{r,el}(t)) \boldsymbol{\psi}_{r,\alpha\beta}^s(t)] \\ &= T_p(\varepsilon_{r,el}(t)) \left[\frac{d}{dt} (T_p^{-1}(\varepsilon_{r,el}(t))) \boldsymbol{\psi}_{r,\alpha\beta}^s(t) + T_p^{-1}(\varepsilon_{r,el}(t)) \frac{d}{dt} (\boldsymbol{\psi}_{r,\alpha\beta}^s(t)) \right] \\ &= -\omega_{r,el}(t) \mathbf{J} \boldsymbol{\psi}_{r,\alpha\beta}^s(t) + \frac{d}{dt} \boldsymbol{\psi}_{r,\alpha\beta}^s(t). \end{aligned}$$

IM model $\alpha\beta$ coordinates: transformation of rotor quantities (cont.)

Hence, the IM model voltage equations in the stator-oriented $\alpha\beta$ coordinates are

$$\begin{aligned}\mathbf{u}_{s,\alpha\beta}^s(t) &= R_s \mathbf{i}_{s,\alpha\beta}^s(t) + \frac{d}{dt} \boldsymbol{\psi}_{s,\alpha\beta}^s(t), \\ \mathbf{u}_{r,\alpha\beta}^s(t) &= R_r \mathbf{i}_{r,\alpha\beta}^s(t) - \omega_{r,el}(t) \mathbf{J} \boldsymbol{\psi}_{r,\alpha\beta}^s(t) + \frac{d}{dt} \boldsymbol{\psi}_{r,\alpha\beta}^s(t).\end{aligned}\quad (6.19)$$

Furthermore, the flux linkages representation (6.3) should be also transformed into the stator-oriented $\alpha\beta$ coordinates. Hence, (6.3) is multiplied with \mathbf{T}_{23} :

$$\begin{aligned}\boldsymbol{\psi}_{s,\alpha\beta}^s(t) &= \mathbf{T}_{23} \boldsymbol{\psi}_{s,abc}^s(t) = \underbrace{\mathbf{T}_{23} \mathbf{L}_{s,abc} \mathbf{T}_{32}}_{\mathbf{L}_{s,\alpha\beta}} \mathbf{i}_{s,\alpha\beta}^s(t) + M_r \frac{N_s}{N_r} \underbrace{\mathbf{T}_{23} \mathcal{R}_{abc}(\varepsilon_{r,el}(t)) \mathbf{T}_{32}}_{\mathcal{R}_{\alpha\beta}^s(\varepsilon_{r,el}(t))} \mathbf{i}_{r,\alpha\beta}^s(t), \\ \boldsymbol{\psi}_{r,\alpha\beta}^s(t) &= \mathbf{T}_{23} \boldsymbol{\psi}_{r,abc}^s(t) = \underbrace{\mathbf{T}_{23} \mathbf{L}_{r,abc} \mathbf{T}_{32}}_{\mathbf{L}_{r,\alpha\beta}} \mathbf{i}_{r,\alpha\beta}^s(t) + M_s \frac{N_r}{N_s} \underbrace{\mathbf{T}_{23} \mathcal{R}_{abc}(\varepsilon_{r,el}(t))^T \mathbf{T}_{32}}_{\mathcal{R}_{\alpha\beta}^r(\varepsilon_{r,el}(t))} \mathbf{i}_{s,\alpha\beta}^s(t).\end{aligned}\quad (6.20)$$

IM model $\alpha\beta$ coordinates: transformation of rotor quantities (cont.)

Continuing from the previous slide, we can rewrite the newly defined inductance matrices as

$$\begin{aligned}\mathbf{L}_{s,\alpha\beta} &= \mathbf{T}_{23}\mathbf{L}_{s,abc}\mathbf{T}_{32} = \begin{bmatrix} L_s + M_s/2 & 0 \\ 0 & L_s + M_s/2 \end{bmatrix} = (L_s + M_s/2)\mathbf{I}, \\ \mathbf{L}_{r,\alpha\beta} &= \mathbf{T}_{23}\mathbf{L}_{r,abc}\mathbf{T}_{32} = \begin{bmatrix} L_r + M_r/2 & 0 \\ 0 & L_r + M_r/2 \end{bmatrix} = (L_r + M_r/2)\mathbf{I}\end{aligned}\quad (6.21)$$

and the rotation matrices as

$$\begin{aligned}\mathcal{R}_{\alpha\beta}^s(\varepsilon_{r,el}(t)) &= \mathbf{T}_{23}\mathcal{R}_{abc}(\varepsilon_{r,el}(t))\mathbf{T}_{32} = \frac{3}{2} \begin{bmatrix} \cos(\varepsilon_{r,el}(t)) & -\sin(\varepsilon_{r,el}(t)) \\ \sin(\varepsilon_{r,el}(t)) & \cos(\varepsilon_{r,el}(t)) \end{bmatrix} = \frac{3}{2}\mathbf{T}_p(\varepsilon_{r,el}(t)), \\ \mathcal{R}_{\alpha\beta}^r(\varepsilon_{r,el}(t)) &= \mathbf{T}_{23}\mathcal{R}_{abc}(\varepsilon_{r,el}(t))^T\mathbf{T}_{32} = \frac{3}{2} \begin{bmatrix} \cos(\varepsilon_{r,el}(t)) & \sin(\varepsilon_{r,el}(t)) \\ -\sin(\varepsilon_{r,el}(t)) & \cos(\varepsilon_{r,el}(t)) \end{bmatrix} = \frac{3}{2}\mathbf{T}_p^{-1}(\varepsilon_{r,el}(t)).\end{aligned}\quad (6.22)$$

IM model $\alpha\beta$ coordinates: transformation of rotor quantities (cont.)

Inserting (6.21) and (6.22) into the flux linkage model (6.20) yields

$$\begin{aligned}\psi_{s,\alpha\beta}^s(t) &= (L_s + M_s/2)\mathbf{i}_{s,\alpha\beta}^s(t) + M_r \frac{3}{2} \frac{N_s}{N_r} \mathbf{T}_p(\varepsilon_{r,el}(t)) \mathbf{i}_{r,\alpha\beta}^r(t), \\ \psi_{r,\alpha\beta}^r(t) &= (L_r + M_r/2)\mathbf{i}_{r,\alpha\beta}^r(t) + M_s \frac{3}{2} \frac{N_r}{N_s} \mathbf{T}_p^{-1}(\varepsilon_{r,el}(t)) \mathbf{i}_{s,\alpha\beta}^s(t).\end{aligned}\quad (6.23)$$

Multiplying the second equation with $\mathbf{T}_p(\varepsilon_{r,el}(t))$ from the left allows transforming the rotor flux linkage into the stator's $\alpha\beta$ coordinates

$$\mathbf{T}_p(\varepsilon_{r,el}(t)) \psi_{r,\alpha\beta}^r(t) = (L_r + M_r/2) \mathbf{T}_p(\varepsilon_{r,el}(t)) \mathbf{i}_{r,\alpha\beta}^r(t) + M_s \frac{3}{2} \frac{N_r}{N_s} \mathbf{T}_p(\varepsilon_{r,el}(t)) \mathbf{T}_p^{-1}(\varepsilon_{r,el}(t)) \mathbf{i}_{s,\alpha\beta}^s(t)$$

resulting in a mutual flux linkage model in the stator's $\alpha\beta$ coordinates:

$$\begin{aligned}\psi_{s,\alpha\beta}^s(t) &= (L_s + M_s/2)\mathbf{i}_{s,\alpha\beta}^s(t) + M_r \frac{3}{2} \frac{N_s}{N_r} \mathbf{i}_{r,\alpha\beta}^r(t), \\ \psi_{r,\alpha\beta}^s(t) &= (L_r + M_r/2)\mathbf{i}_{r,\alpha\beta}^r(t) + M_s \frac{3}{2} \frac{N_r}{N_s} \mathbf{i}_{s,\alpha\beta}^s(t).\end{aligned}\quad (6.24)$$

IM model $\alpha\beta$ coordinates: torque

To obtain the IM's torque equation, a power balance is performed w.r.t. (6.19). Dropping the time dependency for brevity, the power terms (transposed current times voltage) are

$$\begin{aligned}(\mathbf{i}_{s,\alpha\beta}^s)^T \mathbf{u}_{s,\alpha\beta}^s &= R_s (\mathbf{i}_{s,\alpha\beta}^s)^T \mathbf{i}_{s,\alpha\beta}^s + (\mathbf{i}_{s,\alpha\beta}^s)^T \frac{d}{dt} \boldsymbol{\psi}_{s,\alpha\beta}^s, \\(\mathbf{i}_{r,\alpha\beta}^s)^T \mathbf{u}_{r,\alpha\beta}^s &= R_r (\mathbf{i}_{r,\alpha\beta}^s)^T \mathbf{i}_{r,\alpha\beta}^s - \omega_{r,el} (\mathbf{i}_{r,\alpha\beta}^s)^T \mathbf{J} \boldsymbol{\psi}_{r,\alpha\beta}^s + (\mathbf{i}_{r,\alpha\beta}^s)^T \frac{d}{dt} \boldsymbol{\psi}_{r,\alpha\beta}^s.\end{aligned}\tag{6.25}$$

Considering Fig. 1.5 and the Clarke transf. power mapping, one can identify the following:

$$\begin{aligned}\text{Input power: } \quad \frac{2}{3} P_{el} &= (\mathbf{i}_{s,\alpha\beta}^s)^T \mathbf{u}_{s,\alpha\beta}^s + (\mathbf{i}_{r,\alpha\beta}^s)^T \mathbf{u}_{r,\alpha\beta}^s, \\ \text{Losses: } \quad \frac{2}{3} P_l &= R_s (\mathbf{i}_{s,\alpha\beta}^s)^T \mathbf{i}_{s,\alpha\beta}^s + R_r (\mathbf{i}_{r,\alpha\beta}^s)^T \mathbf{i}_{r,\alpha\beta}^s, \\ \text{Change of stored energy: } \quad \frac{2}{3} \frac{d}{dt} E_i &= (\mathbf{i}_{s,\alpha\beta}^s)^T \frac{d}{dt} \boldsymbol{\psi}_{s,\alpha\beta}^s + (\mathbf{i}_{r,\alpha\beta}^s)^T \frac{d}{dt} \boldsymbol{\psi}_{r,\alpha\beta}^s, \\ \text{Mechanical power: } \quad \frac{2}{3} P_{me} &= -\omega_{r,el} (\mathbf{i}_{r,\alpha\beta}^s)^T \mathbf{J} \boldsymbol{\psi}_{r,\alpha\beta}^s.\end{aligned}\tag{6.26}$$

IM model $\alpha\beta$ coordinates: torque (cont.)

From (6.26) one can compare the mechanical power representations

$$\frac{2}{3}P_{\text{me}} = \frac{2}{3}\omega_r T = -p\omega_r (\mathbf{i}_{r,\alpha\beta}^s)^T \mathbf{J} \boldsymbol{\psi}_{r,\alpha\beta}^s \quad (6.27)$$

and find the torque expression

$$T = -\frac{3}{2}p(\mathbf{i}_{r,\alpha\beta}^s)^T \mathbf{J} \boldsymbol{\psi}_{r,\alpha\beta}^s = \frac{3}{2}p(\psi_{r,\beta}^s i_{r,\alpha}^s - \psi_{r,\alpha}^s i_{r,\beta}^s). \quad (6.28)$$

As all terms in (6.28) are invariant with respect to the choice of the coordinate system, the superscript labeling can be omitted:

$$T = \frac{3}{2}p(\psi_{r,\beta} i_{r,\alpha} - \psi_{r,\alpha} i_{r,\beta}). \quad (6.29)$$

If one would transform the model (6.19) into the rotor-oriented $\alpha\beta$ coordinates and redo the torque derivation, one would find the alternative torque expression

$$T = \frac{3}{2}p(\mathbf{i}_{s,\alpha\beta})^T \mathbf{J} \boldsymbol{\psi}_{s,\alpha\beta} = \frac{3}{2}p(\psi_{s,\alpha} i_{s,\beta} - \psi_{s,\beta} i_{s,\alpha}). \quad (6.30)$$

Summary: IM model in stator-oriented $\alpha\beta$ coordinates

The most important equations of the IM model in the stator-oriented $\alpha\beta$ coordinates are:

$$\text{Stator voltage: } \mathbf{u}_{s,\alpha\beta}^s(t) = R_s \mathbf{i}_{s,\alpha\beta}^s(t) + \frac{d}{dt} \boldsymbol{\psi}_{s,\alpha\beta}^s(t),$$

$$\text{Rotor voltage: } \mathbf{u}_{r,\alpha\beta}^s(t) = R_r \mathbf{i}_{r,\alpha\beta}^s(t) - \omega_{r,\text{el}}(t) \mathbf{J} \boldsymbol{\psi}_{r,\alpha\beta}^s(t) + \frac{d}{dt} \boldsymbol{\psi}_{r,\alpha\beta}^s(t),$$

$$\text{Stator flux linkage: } \boldsymbol{\psi}_{s,\alpha\beta}^s(t) = (L_s + M_s/2) \mathbf{i}_{s,\alpha\beta}^s(t) + M_r \frac{3}{2} \frac{N_s}{N_r} \mathbf{i}_{r,\alpha\beta}^s(t),$$

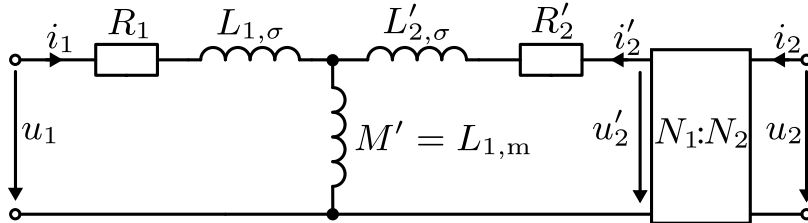
$$\text{Rotor flux linkage: } \boldsymbol{\psi}_{r,\alpha\beta}^s(t) = (L_r + M_r/2) \mathbf{i}_{r,\alpha\beta}^s(t) + M_s \frac{3}{2} \frac{N_r}{N_s} \mathbf{i}_{s,\alpha\beta}^s(t),$$

$$\text{Torque: } T(t) = \frac{3}{2} p (\mathbf{i}_{s,\alpha\beta}^s)^T \mathbf{J} \boldsymbol{\psi}_{s,\alpha\beta}^s = -\frac{3}{2} p (\mathbf{i}_{r,\alpha\beta}^s)^T \mathbf{J} \boldsymbol{\psi}_{r,\alpha\beta}^s.$$

It may be noted that the voltage and torque equations are independent of any linearity assumption, i.e., also apply to IMs with magnetic saturation. Only if the above flux linkage models are utilized, magnetic linearity is assumed.

Transformation of the rotor quantities based on the turn ratio

- ▶ The previous model depends on the physical parameters of the rotor: R_r , L_r , and M_r .
- ▶ Those parameters might not be accessible or known in practice (in particular when direct rotor measurements are not possible).
- ▶ Remedy: Transform the rotor quantities into the stator side based on the turn ratio N_s/N_r .
- ▶ Identical procedure to the transformer approach as from Fig. 4.6.
- ▶ Hence, stator-based measurements can be used to infer the rotor quantities (compare open-circuit test Fig. 4.12 and short-circuit test Fig. 4.13).



Transformation of the rotor quantities based on the turn ratio (cont.)

Applying (4.14) with $\alpha = N_s/N_r$ to the IM model interpreting the rotor as the secondary side results in

$$\begin{aligned} \mathbf{u}'_r &= \frac{N_s}{N_r} \mathbf{u}_r, & \mathbf{i}'_r &= \frac{N_r}{N_s} \mathbf{i}_r, & \boldsymbol{\psi}'_{r,\alpha\beta} &= \frac{N_s}{N_r} \boldsymbol{\psi}_{r,\alpha\beta}, \\ R'_r &= \frac{N_s^2}{N_r^2} R_r, & L'_r &= \frac{N_s^2}{N_r^2} L_r, & M'_r &= \frac{N_s}{N_r} M_r. \end{aligned} \tag{6.31}$$

Above, the indices representing the coordinate system are omitted as the transformation is independent of the chosen coordinate system.

Utilizing also $L_s = L_{\sigma,s} + M_s$ and $L_r = L_{\sigma,r} + M_r$, the flux linkage equations in the stator-oriented $\alpha\beta$ coordinates are then

$$\begin{aligned} \boldsymbol{\psi}_{s,\alpha\beta}^s(t) &= (L_{\sigma,s} + \frac{3}{2}M_s)\mathbf{i}_{s,\alpha\beta}^s(t) + M'_r \frac{3}{2}\mathbf{i}_{r,\alpha\beta}^{s'}(t), \\ \boldsymbol{\psi}_{r,\alpha\beta}^{s'}(t) &= (L'_{\sigma,r} + \frac{3}{2}M'_r)\mathbf{i}_{r,\alpha\beta}^{s'}(t) + M_s \frac{3}{2}\mathbf{i}_{s,\alpha\beta}^s(t). \end{aligned}$$

Transformation of the rotor quantities based on the turn ratio (cont.)

Analyzing the (magnetic) power balance reveals

$$\frac{3}{2}M_s = \frac{3}{2}M'_r = M, \quad (6.32)$$

that is, the mutual inductance is identical for both the stator and (transformed) rotor side. Hence, we can rewrite the flux linkage equations as

$$\psi_{s,\alpha\beta}^s(t) = (L_{\sigma,s} + M)\mathbf{i}_{s,\alpha\beta}^s(t) + M\mathbf{i}_{r,\alpha\beta}^{s'}(t), \quad (6.33)$$

$$\psi_{r,\alpha\beta}^{s'}(t) = (L'_{\sigma,r} + M)\mathbf{i}_{r,\alpha\beta}^{s'}(t) + M\mathbf{i}_{s,\alpha\beta}^s(t). \quad (6.34)$$

Alternatively, we can express the currents as a function of the flux linkages:

$$\mathbf{i}_{s,\alpha\beta}^s(t) = \frac{(L_{\sigma,s} + M)\psi_{s,\alpha\beta}^s(t) - M\psi_{r,\alpha\beta}^{s'}(t)}{M(L_{\sigma,s} + L'_{\sigma,r}) + L_{\sigma,s}L'_{\sigma,r}}, \quad (6.35)$$

$$\mathbf{i}_{r,\alpha\beta}^{s'}(t) = \frac{(L'_{\sigma,r} + M)\psi_{r,\alpha\beta}^{s'}(t) - M\psi_{s,\alpha\beta}^s(t)}{M(L'_{\sigma,r} + L_{\sigma,s}) + L'_{\sigma,r}L_{\sigma,s}}. \quad (6.36)$$

Transformation of the rotor quantities based on the turn ratio (cont.)

Rewriting the transformer's leakage coefficient definition (4.5) for the IM model as

$$\sigma = \frac{(L_{\sigma,s} + L'_{\sigma,r})M + L'_{\sigma,r}L_{\sigma,s}}{(M + L_{\sigma,s})(M + L'_{\sigma,r})} = 1 - \frac{M^2}{(M + L_{\sigma,s})(M + L'_{\sigma,r})} \quad (6.37)$$

allows expressing the currents as

$$\mathbf{i}_{s,\alpha\beta}^s(t) = \frac{1}{\sigma(L_{\sigma,s} + M)} \left(\boldsymbol{\psi}_{s,\alpha\beta}^s(t) - \frac{M}{M + L'_{\sigma,r}} \boldsymbol{\psi}_{r,\alpha\beta}^{s'}(t) \right), \quad (6.38)$$

$$\mathbf{i}_{r,\alpha\beta}^{s'}(t) = \frac{1}{\sigma(L'_{\sigma,r} + M)} \left(\boldsymbol{\psi}_{r,\alpha\beta}^{s'}(t) - \frac{M}{M + L_{\sigma,s}} \boldsymbol{\psi}_{s,\alpha\beta}^s(t) \right). \quad (6.39)$$

ECD of transformed IM model in general $\alpha\beta$ coordinates

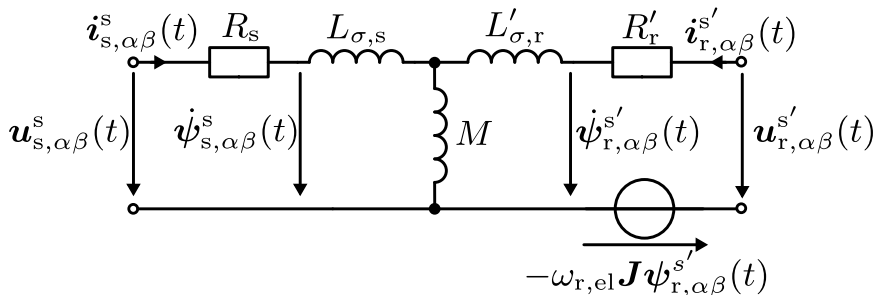


Fig. 6.9: T-type ECD of an IM in stator-oriented $\alpha\beta$ coordinates with rotor quantities transformed using $\alpha = N_s/N_r$

Summary: transformed IM model in stator-oriented $\alpha\beta$ coordinates

The most important equations of the IM model in the stator-oriented $\alpha\beta$ coordinates with all rotor quantities transformed to the stator side are:

$$\text{Stator voltage: } \mathbf{u}_{s,\alpha\beta}^s(t) = R_s \mathbf{i}_{s,\alpha\beta}^s(t) + \frac{d}{dt} \boldsymbol{\psi}_{s,\alpha\beta}^s(t),$$

$$\text{Rotor voltage: } \mathbf{u}_{r,\alpha\beta}^{s'}(t) = R_r \mathbf{i}_{r,\alpha\beta}^{s'}(t) - \omega_{r,\text{el}}(t) \mathbf{J} \boldsymbol{\psi}_{r,\alpha\beta}^{s'}(t) + \frac{d}{dt} \boldsymbol{\psi}_{r,\alpha\beta}^{s'}(t),$$

$$\text{Stator flux linkage: } \boldsymbol{\psi}_{s,\alpha\beta}^s(t) = (L_{\sigma,s} + M) \mathbf{i}_{s,\alpha\beta}^s(t) + M \mathbf{i}_{r,\alpha\beta}^{s'}(t),$$

$$\text{Rotor flux linkage: } \boldsymbol{\psi}_{r,\alpha\beta}^{s'}(t) = (L'_{\sigma,r} + M) \mathbf{i}_{r,\alpha\beta}^{s'}(t) + M \mathbf{i}_{s,\alpha\beta}^s(t),$$

$$\text{Torque: } T(t) = \frac{3}{2} p (\mathbf{i}_{s,\alpha\beta}^s(t))^T \mathbf{J} \boldsymbol{\psi}_{s,\alpha\beta}^s(t) = -\frac{3}{2} p (\mathbf{i}_{r,\alpha\beta}^{s'}(t))^T \mathbf{J} \boldsymbol{\psi}_{r,\alpha\beta}^{s'}(t).$$

The transformed rotor quantities are $\mathbf{u}'_r = \alpha \mathbf{u}_r$, $\mathbf{i}'_r = 1/\alpha \mathbf{i}_r$, $\boldsymbol{\psi}'_r = \alpha \boldsymbol{\psi}_r$, $R'_r = \alpha^2 R_r$, $L'_r = \alpha^2 L_r$, and $M'_r = \alpha M_r$ with $\alpha = N_s/N_r$.

General rotating coordinate system k

- ▶ In $\alpha\beta$ coordinates, all quantities have sinusoidal trajectory under regular IM operation.
- ▶ Compare rotating field theory: sinusoidal phase currents lead to sinusoidal $\alpha\beta$ currents.

K coordinate system

To simplify the machine analysis, a general rotating coordinate system k is introduced. The orientation of the d-axis of that coordinate system can be chosen freely, however, if aligned to the stator or rotor flux linkage vector all quantities become constant during steady state (cf. Fig. 6.8).

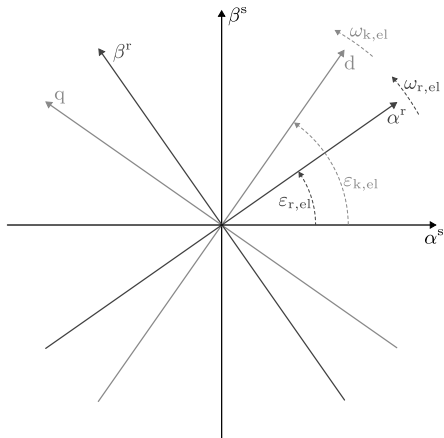


Fig. 6.10: Comparison of coordinate systems

IM model in coordinate system k

Applying the Park transformation to the IM model in the stator-oriented $\alpha\beta$ coordinates results in (dropping the time dependency for brevity):

$$\begin{aligned} \mathbf{u}_{s,dq}^k &= \mathbf{T}_p^{-1}(\varepsilon_{k,el}) \mathbf{u}_{s,\alpha\beta}^s, & \mathbf{i}_{s,dq}^k &= \mathbf{T}_p^{-1}(\varepsilon_{k,el}) \mathbf{i}_{s,\alpha\beta}^s, & \boldsymbol{\psi}_{s,dq}^k &= \mathbf{T}_p^{-1}(\varepsilon_{k,el}) \boldsymbol{\psi}_{s,\alpha\beta}^s, \\ \mathbf{u}_{r,dq}^k &= \mathbf{T}_p^{-1}(\varepsilon_{k,el}) \mathbf{u}_{r,\alpha\beta}^s, & \mathbf{i}_{r,dq}^k &= \mathbf{T}_p^{-1}(\varepsilon_{k,el}) \mathbf{i}_{r,\alpha\beta}^s, & \boldsymbol{\psi}_{r,dq}^k &= \mathbf{T}_p^{-1}(\varepsilon_{k,el}) \boldsymbol{\psi}_{r,\alpha\beta}^s. \end{aligned} \quad (6.40)$$

The transformed flux linkage model in the k coordinate system remains structurally unaffected by the coordinate transformation

$$\begin{aligned} \boldsymbol{\psi}_{s,dq}^k &= (L_s + M_s/2) \mathbf{i}_{s,dq}^k + M_r \frac{3}{2} \frac{N_s}{N_r} \mathbf{i}_{r,dq}^k, \\ \boldsymbol{\psi}_{r,dq}^k &= (L_r + M_r/2) \mathbf{i}_{r,dq}^k + M_s \frac{3}{2} \frac{N_r}{N_s} \mathbf{i}_{s,dq}^k \end{aligned} \quad (6.41)$$

since both the current and flux linkage vectors are transformed in the same way starting from (6.24).

IM model in coordinate system k (cont.)

Likewise, the torque is invariant with respect to the chosen coordinate system:

$$T = \frac{3}{2}p (\mathbf{i}_{s,dq})^T \mathbf{J} \boldsymbol{\psi}_{s,dq} = -\frac{3}{2}p (\mathbf{i}_{r,dq})^T \mathbf{J} \boldsymbol{\psi}_{r,dq}. \quad (6.42)$$

Applying the Park transformation derivative rule (6.15) to the voltage equations in the k coordinate system yields

$$\begin{aligned} \mathbf{u}_{s,dq}^k &= R_s \mathbf{i}_{s,dq}^k + \omega_{k,el} \mathbf{J} \boldsymbol{\psi}_{s,dq}^k + \frac{d}{dt} \boldsymbol{\psi}_{s,dq}^k, \\ \mathbf{u}_{r,dq}^k &= R_r \mathbf{i}_{r,dq}^k + (\omega_{k,el} - \omega_{r,el}) \mathbf{J} \boldsymbol{\psi}_{r,dq}^k + \frac{d}{dt} \boldsymbol{\psi}_{r,dq}^k. \end{aligned} \quad (6.43)$$

Likewise, the transformation of the rotor quantities based on the turn ratio $\alpha = N_s/N_r$ can be applied to the k coordinate system:

$$\begin{aligned} \mathbf{u}_{r,dq}^{k'} &= \alpha \mathbf{u}_{r,dq}^k, \quad \mathbf{i}_{r,dq}^{k'} = 1/\alpha \mathbf{i}_{r,dq}^k, \quad \boldsymbol{\psi}_{r,dq}^{k'} = \alpha \boldsymbol{\psi}_{r,dq}^k, \\ R'_r &= \alpha^2 R_r, \quad L'_r = \alpha^2 L_r, \quad M'_r = \alpha M_r. \end{aligned} \quad (6.44)$$

Summary: IM model in general dq coordinates

The most important equations of the IM model in the general k coordinate system with dq coordinates are:

Stator voltage: $\mathbf{u}_{s,dq}^k(t) = R_s \mathbf{i}_{s,dq}^k(t) + \omega_{k,el}(t) \mathbf{J} \boldsymbol{\psi}_{s,dq}^k(t) + \frac{d}{dt} \boldsymbol{\psi}_{s,dq}^k(t),$

Rotor voltage: $\mathbf{u}_{r,dq}^k(t) = R_r \mathbf{i}_{r,dq}^k(t) + (\omega_{k,el}(t) - \omega_{r,el}(t)) \mathbf{J} \boldsymbol{\psi}_{r,dq}^k(t) + \frac{d}{dt} \boldsymbol{\psi}_{r,dq}^k(t),$

Stator flux linkage: $\boldsymbol{\psi}_{s,dq}^k(t) = (L_s + M_s/2) \mathbf{i}_{s,dq}^k(t) + M_r \frac{3}{2} \frac{N_s}{N_r} \mathbf{i}_{r,dq}^k(t),$

Rotor flux linkage: $\boldsymbol{\psi}_{r,dq}^k(t) = (L_r + M_r/2) \mathbf{i}_{r,dq}^k(t) + M_s \frac{3}{2} \frac{N_r}{N_s} \mathbf{i}_{s,dq}^k(t),$

Torque: $T(t) = \frac{3}{2} p(\mathbf{i}_{s,dq}^k(t))^T \mathbf{J} \boldsymbol{\psi}_{s,dq}^k(t) = -\frac{3}{2} p(\mathbf{i}_{r,dq}^k(t))^T \mathbf{J} \boldsymbol{\psi}_{r,dq}^k(t).$

Likewise in the stator-oriented $\alpha\beta$ coordinates, one can further transform the rotor quantities based on the turn ratio $\alpha = N_s/N_r$ to infer the rotor parameters from stator-based measurements (cf. next slide).

Summary: transformed IM model in general dq coordinates

The most important equations of the IM model in the general k coordinate system with dq coordinates with all rotor quantities transformed to the stator side are:

$$\text{Stator voltage: } \mathbf{u}_{s,dq}^k(t) = R_s \mathbf{i}_{s,dq}^k(t) + \omega_{k,el}(t) \mathbf{J} \boldsymbol{\psi}_{s,dq}^k(t) + \frac{d}{dt} \boldsymbol{\psi}_{s,dq}^k(t),$$

$$\text{Rotor voltage: } \mathbf{u}_{r,dq}^{k'}(t) = R_r \mathbf{i}_{r,dq}^{k'}(t) + (\omega_{k,el}(t) - \omega_{r,el}(t)) \mathbf{J} \boldsymbol{\psi}_{r,dq}^{k'}(t) + \frac{d}{dt} \boldsymbol{\psi}_{r,dq}^{k'}(t),$$

$$\text{Stator flux linkage: } \boldsymbol{\psi}_{s,dq}^k(t) = (L_{\sigma,s} + M) \mathbf{i}_{s,dq}^k(t) + M \mathbf{i}_{r,dq}^{k'}(t),$$

$$\text{Rotor flux linkage: } \boldsymbol{\psi}_{r,dq}^{k'}(t) = (L'_{\sigma,r} + M) \mathbf{i}_{r,dq}^{k'}(t) + M \mathbf{i}_{s,dq}^k(t),$$

$$\text{Torque: } T(t) = \frac{3}{2} p (\mathbf{i}_{s,dq}^k(t))^T \mathbf{J} \boldsymbol{\psi}_{s,dq}^k(t) = -\frac{3}{2} p (\mathbf{i}_{r,dq}^{k'}(t))^T \mathbf{J} \boldsymbol{\psi}_{r,dq}^{k'}(t).$$

The transformed rotor quantities are $\mathbf{u}'_r = \alpha \mathbf{u}_r$, $\mathbf{i}'_r = 1/\alpha \mathbf{i}_r$, $\boldsymbol{\psi}'_r = \alpha \boldsymbol{\psi}_r$, $R'_r = \alpha^2 R_r$, $L'_r = \alpha^2 L_r$, and $M'_r = \alpha M_r$ with $\alpha = N_s/N_r$.

ECD of transformed IM model in general dq coordinates

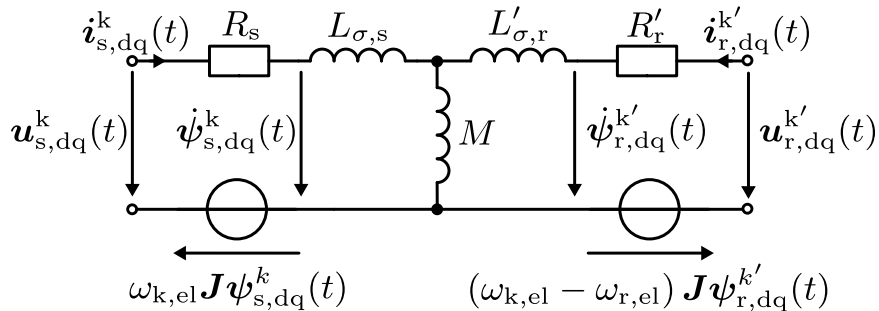


Fig. 6.11: T-type ECD of an IM in general dq coordinates with rotor quantities transformed using
$$\alpha = N_s/N_r$$

Stator flux orientation in the k coordinate system

Per definition we can assign the stator flux linkage vector to the d-axis of the k coordinate system:

$$\begin{aligned}\psi_{s,dq}^k(t) &= \begin{bmatrix} \psi_{s,d}^k(t) \\ \psi_{s,q}^k(t) \end{bmatrix} = \begin{bmatrix} \psi_{s,d}^k(t) \\ 0 \end{bmatrix} \\ &= \begin{bmatrix} |\psi_{s,dq}^k(t)| \\ 0 \end{bmatrix}. \quad (6.45)\end{aligned}$$

In this case, the torque expression simplifies to

$$\begin{aligned}T(t) &= \frac{3}{2}p(\mathbf{i}_{s,dq}^k(t))^T \mathbf{J} \psi_{s,dq}^k(t) \\ &= \frac{3}{2}p i_{s,q}^k(t) \psi_{s,d}^k(t).\end{aligned} \quad (6.46)$$

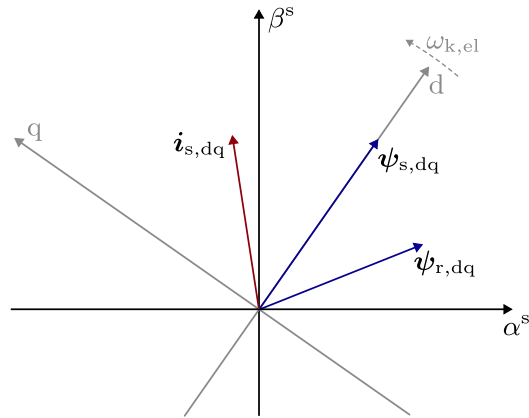


Fig. 6.12: Stator flux-oriented coordinate system

Rotor flux orientation in the k coordinate system

Per definition we can also assign the rotor flux linkage vector to the d-axis of the k coordinate system:

$$\begin{aligned}\psi_{r,dq}^k(t) &= \begin{bmatrix} \psi_{r,d}^k(t) \\ \psi_{r,q}^k(t) \end{bmatrix} = \begin{bmatrix} \psi_{r,d}^k(t) \\ 0 \end{bmatrix} \\ &= \begin{bmatrix} |\psi_{r,dq}^k(t)| \\ 0 \end{bmatrix}. \quad (6.47)\end{aligned}$$

In this case, the torque expression simplifies to

$$\begin{aligned}T(t) &= -\frac{3}{2}p(\mathbf{i}_{r,dq}^k(t))^T \mathbf{J} \psi_{r,dq}^k(t) \\ &= -\frac{3}{2}p i_{r,q}^k(t) \psi_{r,d}^k(t). \quad (6.48)\end{aligned}$$

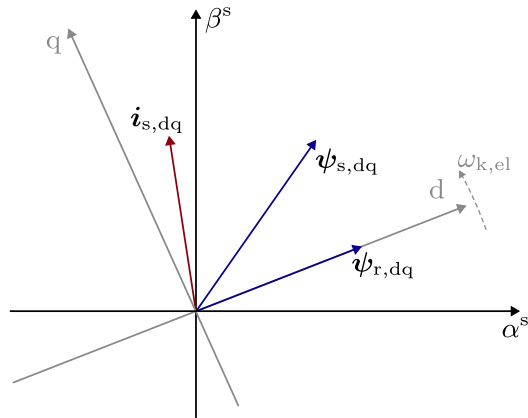


Fig. 6.13: Rotor flux-oriented coordinate system

Steady-state behavior

Starting from the general IM model voltage equations in the transformed k coordinate system (6.44), the steady-state ($\frac{dx(t)}{dt}=0$) behavior is described by

$$\begin{aligned}\mathbf{u}_{s,dq}^k &= R_s \mathbf{i}_{s,dq}^k + \omega_{k,el} \mathbf{J} \boldsymbol{\psi}_{s,dq}^k, \\ \mathbf{u}_{r,dq}^{k'} &= R'_r \mathbf{i}_{r,dq}^{k'} + (\omega_{k,el} - \omega_{r,el}) \mathbf{J} \boldsymbol{\psi}_{r,dq}^{k'}.\end{aligned}\quad (6.49)$$

During steady state the stator is excited by a constant three-phase voltage with the stator frequency ω_s while the rotor is excited with the rotor or slip frequency ω_{slip} :

$$\omega_{k,el} \rightarrow \omega_s, \quad \omega_{k,el} - \omega_{r,el} \rightarrow \omega_{\text{slip}}. \quad (6.50)$$

Dropping the coordinate system indices, we have

$$\mathbf{u}_s = R_s \mathbf{i}_s + \omega_s \mathbf{J} \boldsymbol{\psi}_s, \quad \mathbf{u}'_r = R'_r \mathbf{i}'_r + \omega_{\text{slip}} \mathbf{J} \boldsymbol{\psi}'_r. \quad (6.51)$$

Rewriting the vectorial quantities as complex phasors $\underline{X}_{dq} = X e^{j\phi} = X_d + jX_q$, we obtain

$$\underline{U}_s = R_s \underline{I}_s + j\omega_s \underline{\Psi}_s, \quad \underline{U}'_r = R'_r \underline{I}'_r + j\omega_{\text{slip}} \underline{\Psi}'_r. \quad (6.52)$$

Steady-state behavior (cont.)

In (6.52) the complex rotor and stator fluxes rotate with different frequencies. To simplify the analysis, we introduce the slip ratio

$$s = \frac{\omega_{\text{slip}}}{\omega_s}. \quad (6.53)$$

Multiplying (6.52) with the inverse slip ratio delivers then

$$\underline{U}_s = R_s \underline{I}_s + j\omega_s \underline{\Psi}_s, \quad \frac{1}{s} \underline{U}'_r = \frac{1}{s} R'_r \underline{I}'_r + j\omega_s \underline{\Psi}'_r. \quad (6.54)$$

Here, both the stator and rotor fluxes rotate with the same frequency ω_s . Additionally, we can insert the current-to-flux linkage relationships

$$\underline{\Psi}_s = (L_{\sigma,s} + M) \underline{I}_s + M \underline{I}'_r, \quad \underline{\Psi}'_r = (L'_{\sigma,r} + M) \underline{I}'_r + M \underline{I}_s \quad (6.55)$$

leading to

$$\begin{aligned} \underline{U}_s &= R_s \underline{I}_s + j\omega_s [(L_{\sigma,s} + M) \underline{I}_s + M \underline{I}'_r], \\ \frac{1}{s} \underline{U}'_r &= \frac{1}{s} R'_r \underline{I}'_r + j\omega_s [(L'_{\sigma,r} + M) \underline{I}'_r + M \underline{I}_s]. \end{aligned} \quad (6.56)$$

Steady-state behavior: equivalent circuit diagram

The complex steady-state phasor model (6.56) can be represented by the following equivalent circuit diagram. Here, one can note the striking similarity to the T-type ECD of a transformer.

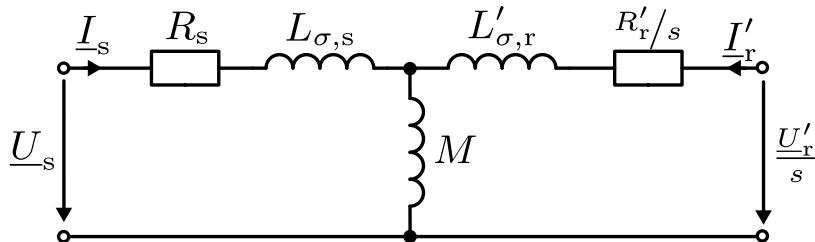


Fig. 6.14: T-type ECD of an IM in steady state represented by complex phasors

IM rotor types



(a) Squirrel cage rotor (source: [Wikimedia Commons](#),
Zurek, CC BY-SA 3.0)



(b) Wound or
slip ring rotor

Fig. 6.15: IM rotor variants

Squirrel cage IM torque-speed characteristic

Utilizing the stator flux orientation we define

$$\underline{\Psi}_s = \Psi_{s,d} + j\Psi_{s,q} = \Psi_{s,d} = \Psi_s.$$

Assuming that the stator ohmic voltage drop is negligible ($R_s = 0$), we get from (6.54)

$$\underline{U}_s = U_{s,d} + jU_{s,q} = j\omega_s \underline{\Psi}_s = j\omega_s \Psi_d \quad (6.57)$$

and, therefore,

$$U_{s,d} = 0, \quad \Psi_{s,d} = \frac{U_{s,q}}{\omega_s} = \frac{U_s}{\omega_s} = \Psi_s. \quad (6.58)$$

Hence, the stator voltage phasor is purely imaginary and the stator flux phasor is real due to the chosen orientation. From (6.55) we can rewrite the flux-to-current relationships as

$$\begin{aligned} \underline{I}_s &= \frac{1}{\sigma(L_{\sigma,s} + M)} \underline{\Psi}_s - \frac{M}{\sigma(L_{\sigma,s} + M)(L'_{\sigma,r} + M)} \underline{\Psi}'_r, \\ \underline{I}'_r &= \frac{1}{\sigma(L'_{\sigma,r} + M)} \underline{\Psi}'_r - \frac{M}{\sigma(L_{\sigma,s} + M)(L'_{\sigma,r} + M)} \underline{\Psi}_s. \end{aligned} \quad (6.59)$$

Squirrel cage IM torque-speed characteristic (cont.)

Furthermore, the rotor voltage for the squirrel cage IM is

$$\underline{U}'_r = 0$$

due to the short-circuited rotor winding. The rotor voltage equation (6.54) then simplifies to

$$0 = \frac{1}{s} R'_r \underline{I}'_r + j\omega_s \underline{\Psi}'_r \Leftrightarrow \underline{\Psi}'_r = \frac{j}{\omega_s} \frac{R'_r}{s} \underline{I}'_r. \quad (6.60)$$

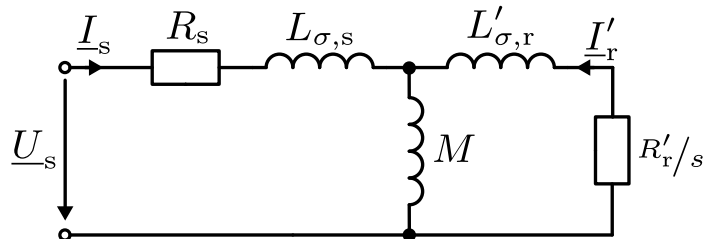


Fig. 6.16: T-type ECD of a squirrel cage IM in steady state represented by complex phasors

Squirrel cage IM torque-speed characteristic (cont.)

Combining (6.58), (6.59), and (6.60) we have a linear equation system resulting in

$$I_{s,d} = \frac{U_s}{\omega_s} \frac{\sigma^2 \omega_{\text{slip}}^2 (L'_{\sigma,s} + M)(L'_{\sigma,r} + M)^3 + (L'_{\sigma,r} + M)(L'_{\sigma,s} + M)(R'_r)^2 - M^2(R'_r)^2}{\sigma(L'_{\sigma,s} + M)^2(L'_{\sigma,r} + M)\omega_{\text{slip}}(\sigma^2 \omega_{\text{slip}}^2 (L'_{\sigma,r} + M)^2 + (R'_r)^2)}, \quad (6.61)$$

$$I_{s,q} = \frac{U_s}{\omega_s} \frac{M^2 \omega_{\text{slip}} R'_r}{(L'_{\sigma,s} + M)^2(\sigma^2 (L'_{\sigma,r} + M)^2 \omega_{\text{slip}}^2 + (R'_r)^2)}, \quad (6.62)$$

$$I_{r,d} = -\frac{U_s}{\omega_s} \frac{\sigma M \omega_{\text{slip}}^2 (L'_{\sigma,r} + M)}{(L'_{\sigma,s} + M)(\sigma^2 (L'_{\sigma,r} + M)^2 \omega_{\text{slip}}^2 + (R'_r)^2)}, \quad (6.63)$$

$$I_{r,q} = -\frac{U_s}{\omega_s} \frac{M R'_r \omega_{\text{slip}}}{(L'_{\sigma,s} + M)(\sigma^2 (L'_{\sigma,r} + M)^2 \omega_{\text{slip}}^2 + (R'_r)^2)}, \quad (6.64)$$

$$\Psi_{r,d} = \frac{U_s}{\omega_s} \frac{M (R'_r)^2}{(L'_{\sigma,s} + M)(\sigma^2 (L'_{\sigma,r} + M)^2 \omega_{\text{slip}}^2 + (R'_r)^2)}, \quad (6.65)$$

$$\Psi_{r,q} = -\frac{U_s}{\omega_s} \frac{\sigma M (L'_{\sigma,r} + M) R'_r \omega_{\text{slip}}}{(L'_{\sigma,s} + M)((L'_{\sigma,r} + M)^2 \sigma^2 \omega_{\text{slip}}^2 + (R'_r)^2)}. \quad (6.66)$$

Squirrel cage IM torque-speed characteristic (cont.)

With the definition of $\omega_{\max} = R'_r / \sigma(L'_{\sigma,r} + M)$ we can rewrite and receive

$$I_{s,d} = \frac{U_s}{\omega_s} \frac{\sigma^2 \omega_{\text{slip}}^2 (L_{\sigma,s} + M)(L'_{\sigma,r} + M)^3 + (L'_{\sigma,r} + M)(L_{\sigma,s} + M)(R'_r)^2 - M^2(R'_r)^2}{\sigma(L_{\sigma,s} + M)^2(L'_{\sigma,r} + M)\omega_{\text{slip}}(\sigma^2 \omega_{\text{slip}}^2 (L'_{\sigma,r} + M)^2 + (R'_r)^2)}, \quad (6.67)$$

$$I_{s,q} = \frac{U_s}{\omega_s} \frac{M^2}{\sigma(L_{\sigma,s} + M)^2(L'_{\sigma,r} + M)} \frac{1}{\frac{\omega_{\text{slip}}}{\omega_{\max}} + \frac{\omega_{\max}}{\omega_{\text{slip}}}}, \quad (6.68)$$

$$I_{r,d} = -U_s \frac{Ms}{(L_{\sigma,s} + M)R'_r} \frac{1}{\frac{\omega_{\text{slip}}}{\omega_{\max}} + \frac{\omega_{\max}}{\omega_{\text{slip}}}}, \quad (6.69)$$

$$I_{r,q} = -\frac{U_s}{\omega_s} \frac{M}{\sigma(L_{\sigma,s} + M)(L'_{\sigma,r} + M)} \frac{1}{\frac{\omega_{\text{slip}}}{\omega_{\max}} + \frac{\omega_{\max}}{\omega_{\text{slip}}}}, \quad (6.70)$$

$$\Psi_{r,d} = \frac{U_s}{\omega_s} \frac{MR'_r}{\sigma(L_{\sigma,s} + M)(L'_{\sigma,r} + M)\omega_{\text{slip}}} \frac{1}{\frac{\omega_{\text{slip}}}{\omega_{\max}} + \frac{\omega_{\max}}{\omega_{\text{slip}}}}, \quad (6.71)$$

$$\Psi_{r,q} = -\frac{U_s}{\omega_s} \frac{M}{(L_{\sigma,s} + M)} \frac{1}{\frac{\omega_{\text{slip}}}{\omega_{\max}} + \frac{\omega_{\max}}{\omega_{\text{slip}}}}. \quad (6.72)$$

Squirrel cage IM torque-speed characteristic (cont.)

The torque expression is then

$$T = \frac{3}{2}p\sqrt{2}\Psi_s\sqrt{2}I_{s,q} = \frac{3}{2}p\frac{U_s^2}{\omega_s^2} \frac{M^2}{\sigma(L_{\sigma,s} + M)^2(L'_{\sigma,r} + M)} \frac{2}{\frac{\omega_{\text{slip}}}{\omega_{\text{max}}} + \frac{\omega_{\text{max}}}{\omega_{\text{slip}}}}. \quad (6.73)$$

Hence, the maximum achievable torque for a constant stator excitation is

$$T_{\text{max}} = \frac{3}{2}p\frac{U_s^2}{\omega_s^2} \frac{M^2}{\sigma(L_{\sigma,s} + M)^2(L'_{\sigma,r} + M)} \quad (6.74)$$

since

$$\max_{\omega_{\text{slip}}} \left\{ \frac{2}{\frac{\omega_{\text{slip}}}{\omega_{\text{max}}} + \frac{\omega_{\text{max}}}{\omega_{\text{slip}}}} \right\} = 1, \quad \arg \max_{\omega_{\text{slip}}} \left\{ \frac{2}{\frac{\omega_{\text{slip}}}{\omega_{\text{max}}} + \frac{\omega_{\text{max}}}{\omega_{\text{slip}}}} \right\} = \omega_{\text{max}} = \frac{R'_r}{\sigma(L'_{\sigma,r} + M)}$$

applies. Above, Ψ_s and $I_{s,q}$ are RMS values according to the complex phasor definitions, which is why the factor $\sqrt{2}$ appears in the torque expression.

Squirrel cage IM torque-speed characteristic (cont.)

The torque expression

$$T = T_{\max} \frac{2}{\frac{\omega_{\text{slip}}}{\omega_{\max}} + \frac{\omega_{\max}}{\omega_{\text{slip}}}} \quad (6.75)$$

can be also alternatively expressed as a function of the slip ratio s by utilizing

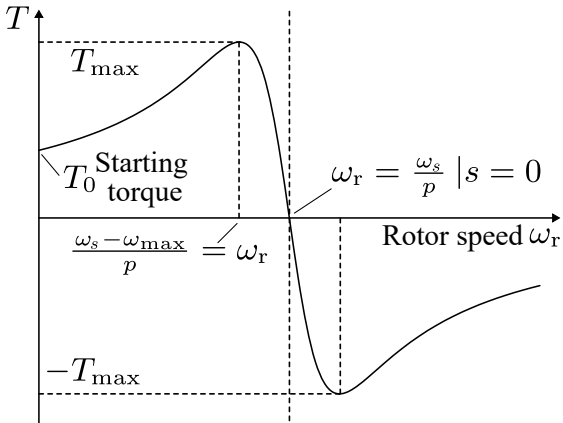
$$\omega_{\text{slip}} = s\omega_s, \quad s_{\max} = \frac{\omega_{\max}}{\omega_s} = \frac{R'_r}{\sigma(L'_{\sigma,r} + M)\omega_s}$$

leading to

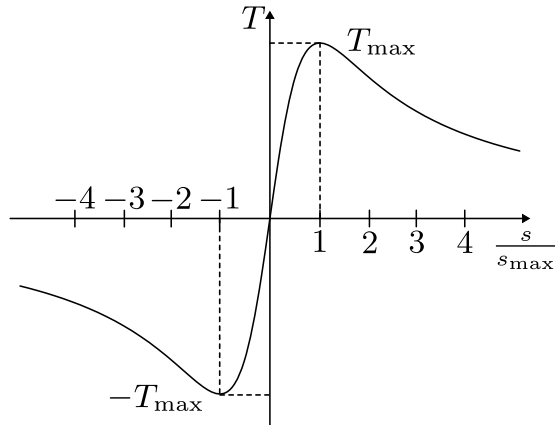
$$T = T_{\max} \frac{2}{\frac{s}{s_{\max}} + \frac{s_{\max}}{s}}. \quad (6.76)$$

The torque-speed characteristic of a squirrel cage IM is also known as Kloss's formula. It should be noted that ω_{\max} and s_{\max} are machine-dependent parameters (for a constant stator excitation), i.e., constants. Contrary, the slip ratio s and slip frequency ω_{slip} depend on the IM's shaft speed and vary during operation.

Kloss's formula: visual representation



(a) Illustration based on the mechanical speed



(b) Illustration based on the slip ratio

Fig. 6.17: Steady-state torque-speed characteristic of a squirrel cage IM for a fixed stator excitation

Squirrel cage IM torque-speed characteristic: rotor resistance

The starting torque, i.e., the torque at motor standstill ($\omega_r = 0$), is given by

$$T_0 = T_{\max} \frac{2s_{\max}}{1 + s_{\max}^2} = T_{\max} \frac{2\omega_{\max}}{1 + \omega_{\max}^2} \quad (6.77)$$

since

$$\omega_{\text{slip}} = \omega_s - p\omega_r = \omega_s - 0 = \omega_s$$

holds. Depending on the machine design T_0 can be significantly lower than T_{\max} , which might be a disadvantage for certain applications. Since

$$\omega_{\max} = \frac{R'_r}{\sigma(L'_{\sigma,r} + M)}, \quad s_{\max} = \frac{R'_r}{\sigma(L'_{\sigma,r} + M)\omega_s}$$

depend on the rotor resistance R'_r , the starting torque can be modified by changing the rotor resistance, e.g., via a dropping resistor or potentiometer (which would require a slip ring rotor).

Squirrel cage IM torque-speed characteristic: rotor resistance (cont.)

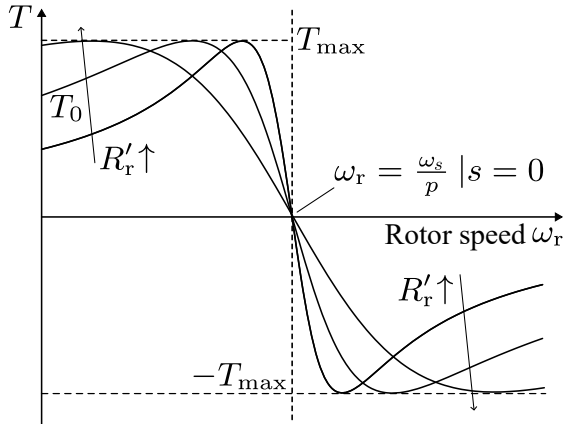


Fig. 6.18: Steady-state torque-speed characteristic of a squirrel cage IM for a fixed stator excitation with varying rotor resistance R'_r – note that the synchronous speed $\omega_r = \omega_s/p$ and the maximum torque T_{\max} are independent of the rotor resistance variation

Slip frequency-dependent rotor skin effect

- ▶ If $\omega_{\text{slip}} \neq 0$, the rotor bars are exposed to a time-varying magnetic field.
- ▶ This induces eddy currents leading to an uneven current distribution within the bars.
- ▶ As a result, the effective rotor resistance increases with the slip frequency:

$$\frac{R_r(\omega_{\text{slip}})}{R_{r,\text{DC}}} = \delta \frac{\sinh(2\delta) + \sin(2\delta)}{\cosh(2\delta) - \cos(2\delta)} \quad (6.78)$$

with

$$\delta = h_{\text{bar}} \sqrt{\omega_{\text{slip}} \frac{\mu_0 \kappa}{2} \frac{w_{\text{bar}}}{w_{\text{slot}}}}$$

being the skin depth. Here, μ_0 is the vacuum permeability and κ is the bar's conductivity.

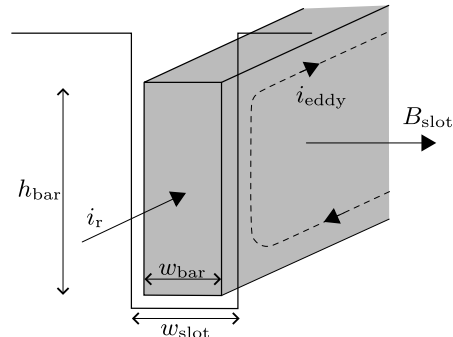


Fig. 6.19: Rotor bar with eddy currents induced by the rotating magnetic field (inspired from A. Binder, *Elektrische Maschinen und Antriebe*, Vol. 2, Springer, 2017)

Slip frequency-dependent rotor skin effect (cont.)

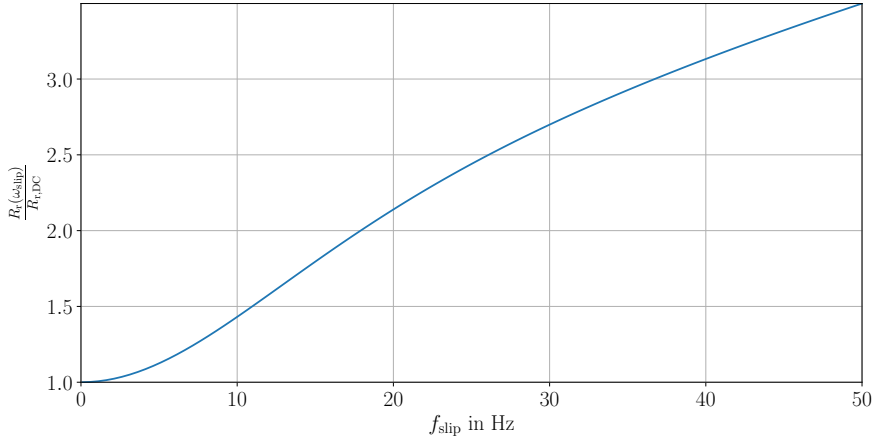


Fig. 6.20: Rotor resistance of a squirrel cage IM as a function of the slip frequency (example based on the following values: $\kappa = 3.7 \cdot 10^7 \frac{\text{S}}{\text{m}}$, $h_{\text{bar}} = 50 \text{ mm}$, $w_{\text{bar}} = 10 \text{ mm}$, $w_{\text{slot}} = 15 \text{ mm}$)

Squirrel cage IM torque-speed characteristic: varying stator frequency

- ▶ Adaption of rotor resistance might be technically tricky.
- ▶ Alternative: vary stator frequency ω_s .
- ▶ Shift of the torque-speed characteristic along the speed axis, i.e., the synchronous speed $\omega_r = \omega_s/p$.
- ▶ Allows utilizing T_{\max} at different speeds (including initial starting torque).
- ▶ Requires a variable frequency source, e.g., a power electronic converter.

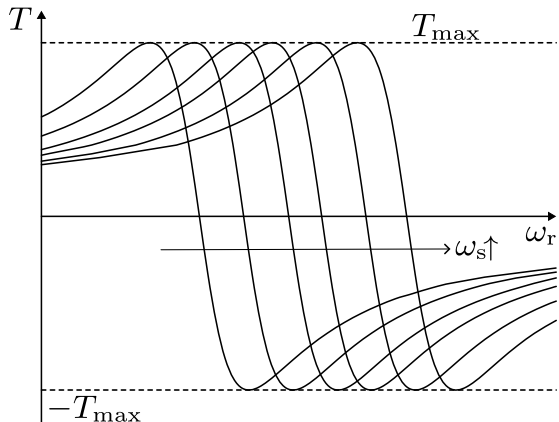


Fig. 6.21: Steady-state torque-speed characteristic of a squirrel cage IM with varying ω_s while keeping $U_s/\omega_s = \text{const.}$

Squirrel cage IM torque-speed characteristic: flux weakening

- ▶ The previous consideration from Fig. 6.21 assumed that $U_s/\omega_s = \text{const.}$ applies, that is, the stator voltage amplitude is adjusted according to the frequency.
- ▶ Obviously, this is only possible to a certain extent due to the voltage source limitations.
- ▶ Hence, at some point, the torque-speed characteristic is limited by the available voltage leading to a flux weakening operation mode (cf. right figure).

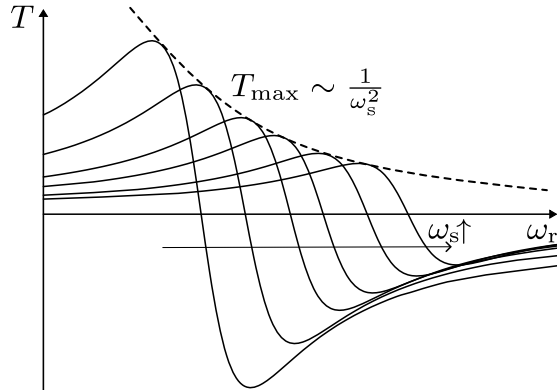


Fig. 6.22: Steady-state torque-speed characteristic of a squirrel cage IM with varying ω_s while keeping $U_s = \text{const.}$, i.e., field weakening operation ($\Psi_s \sim 1/\omega_s$)

Squirrel cage IM torque-speed characteristic: air gap harmonics

- The rotating field analysis (5.17) revealed that the air gap magnetic field contains harmonics:

$$B = \frac{6}{\pi p} \hat{B} \sum_{k=1}^{\infty} \frac{1}{k} \sin\left(\frac{k\pi}{2}\right) \cos(\omega t - k\vartheta_{\text{el}})$$

- This induces rotor currents with the harmonic slip frequency $\omega_{\text{slip}}^{(k)}$.
- Likewise the IM fundamental torque, these air gap field and rotor current harmonics lead to constant, i.e., non-harmonic, torque contributions distorting the torque-speed characteristic.

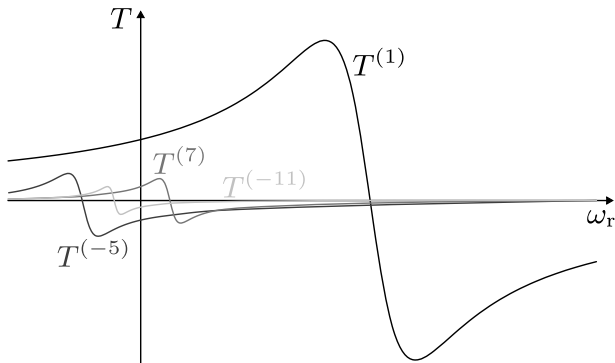


Fig. 6.23: Steady-state torque-speed characteristic of a squirrel cage IM considering torque harmonics due to stator magnetic field harmonics of order
 $k = 1, -5, 7, -11$

Table of contents

7

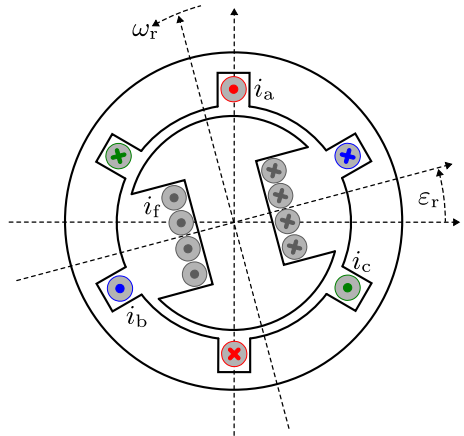
Synchronous machines

Synchronous machines

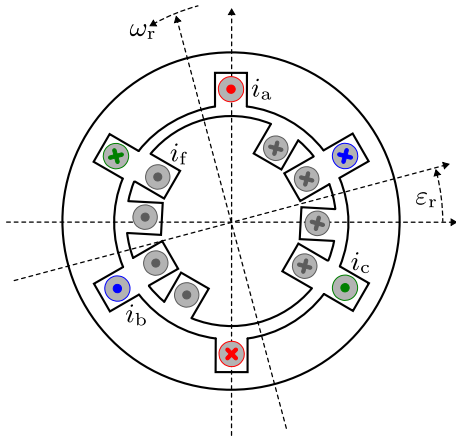
Oliver Wallscheid



Synchronous machine (SM) rotor types



(a) Salient pole rotor



(b) Cylindrical rotor

Fig. 7.1: Major rotor types of synchronous machines (SM)

SM application examples



(a) 2 MVA generator from 1920 (source: [Wikimedia Commons](#), Kolosso, CC BY-SA 3.0)



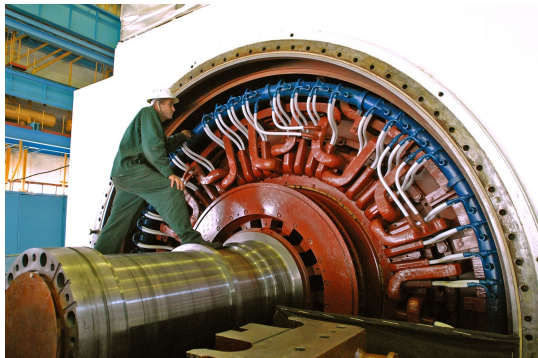
(b) 36 MVA Pelton wheel generator (source: [Wikimedia Commons](#), Asurnipal, CC BY-SA 4.0)

Fig. 7.2: SM examples with salient pole rotor type

SM application examples (cont.)



(a) 650 MVA turbogenerator from Cernavodă nuclear power plant (source: [Wikimedia Commons](#), R. Lavinia, CC BY-SA 4.0)



(b) 1 GVA turbogenerator SM rotor from Balakovo nuclear power plant (source: [Wikimedia Commons](#), A. Seetenky, CC BY-SA 3.0)

Fig. 7.3: SM examples with cylindrical rotor type

Visualization of the synchronous machine operation

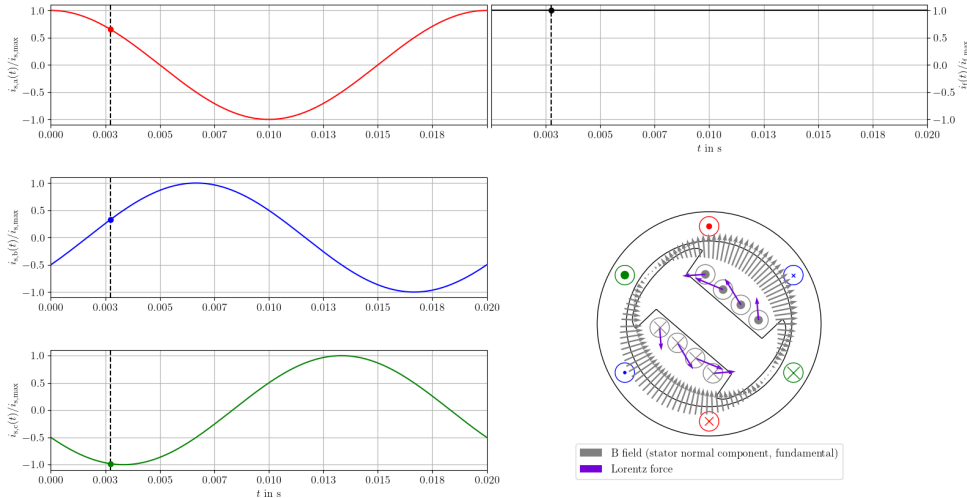


Fig. 7.4: Exemplary SM operation at $\omega = 2\pi 50 \frac{1}{s}$ in motoric operation (positive average torque)

Visualization of the synchronous machine operation (cont.)

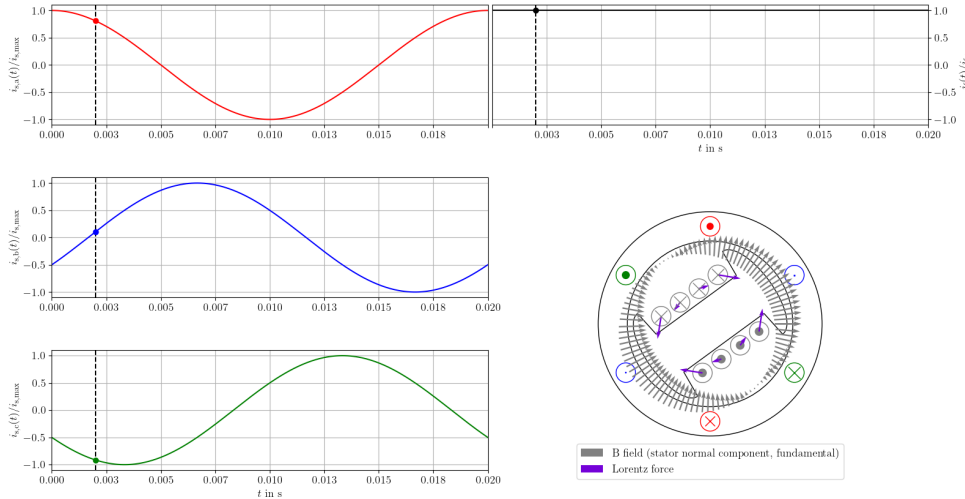


Fig. 7.5: Exemplary SM operation at $\omega = 2\pi 50 \frac{1}{s}$ in no-load operation (zero average torque)

Dynamical SM model

Based on Faraday's and Ohm's laws, we can write the following equations for the stator

$$\mathbf{u}_{s,abc}^s(t) = R_s \mathbf{i}_{s,abc}^s(t) + \frac{d}{dt} \boldsymbol{\psi}_{s,abc}^s(t) \Leftrightarrow \begin{bmatrix} u_{s,a}^s(t) \\ u_{s,b}^s(t) \\ u_{s,c}^s(t) \end{bmatrix} = R_s \begin{bmatrix} i_{s,a}^s(t) \\ i_{s,b}^s(t) \\ i_{s,c}^s(t) \end{bmatrix} + \frac{d}{dt} \begin{bmatrix} \psi_{s,a}^s(t) \\ \psi_{s,b}^s(t) \\ \psi_{s,c}^s(t) \end{bmatrix} \quad (7.1)$$

and rotor field winding

$$u_f^r(t) = R_f i_f^r(t) + \frac{d}{dt} \boldsymbol{\psi}_f^r(t) \quad (7.2)$$

which are generally applicable as only identical resistances per phase on the stator are assumed. In contrast to the induction motor, only a single rotor field winding is present.

Flux linkage model

The SM flux linkage model is similar to the IM model:

- ▶ Assuming a cylindrical rotor, the self-induced stator flux remains identical to the IM model (derived from rotating field theory chapter).
- ▶ In contrast to the IM model Fig. 6.4, the SM's rotor field coil is represented by a single winding.
- ▶ The coupling of the stator and rotor remains rotor position-dependent (not explicitly shown on the right due to space limitations).

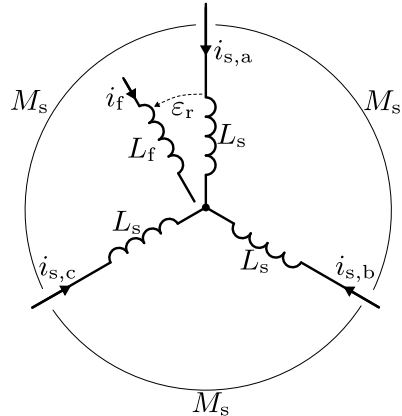


Fig. 7.6: Simplified representation of the inductive coupling between the stator/rotor phases of the cylindrical rotor SM

Flux linkages of the three-phase model

Based on the previous considerations, the flux linkages of the cylindrical SM are given by

$$\begin{aligned}\psi_{s,abc}^s(t) &= \begin{bmatrix} L_s & -\frac{M_s}{2} & -\frac{M_s}{2} \\ -\frac{M_s}{2} & L_s & -\frac{M_s}{2} \\ -\frac{M_s}{2} & -\frac{M_s}{2} & L_s \end{bmatrix} i_{s,abc}^s(t) + M_r \frac{N_s}{N_r} \begin{bmatrix} \cos(\varepsilon_{r,el}(t)) \\ \cos(\varepsilon_{r,el}(t) - \frac{2\pi}{3}) \\ \cos(\varepsilon_{r,el}(t) + \frac{2\pi}{3}) \end{bmatrix} i_f^r(t), \\ \psi_f^r(t) &= L_f i_f^r(t) \\ &\quad + M_s \frac{N_r}{N_s} \begin{bmatrix} \cos(\varepsilon_{r,el}(t)) & \cos(\varepsilon_{r,el}(t) - \frac{2\pi}{3}) & \cos(\varepsilon_{r,el}(t) + \frac{2\pi}{3}) \end{bmatrix} i_{s,abc}^s(t)\end{aligned}\tag{7.3}$$

with $\varepsilon_{r,el}(t) = p\varepsilon_r(t)$. Consequently, (7.3) is a reduced representation of the IM's flux linkage model (6.3).

Cylindrical SM model in alpha-beta coordinates: voltage equations

Similar to the IM, we can represent the SM model in orthogonal $\alpha\beta$ -coordinates. For the SM this only applies to the three-phase stator, as the rotor has only a single phase winding. The $\alpha\beta$ -coordinates voltage equation is given by (compare to (6.16))

$$\mathbf{u}_{s,\alpha\beta}^s(t) = R_s \mathbf{i}_{s,\alpha\beta}^s(t) + \frac{d}{dt} \boldsymbol{\psi}_{s,\alpha\beta}^s(t) \quad (7.4)$$

while the rotor field winding voltage equation remains identical to (7.2):

$$u_f^r(t) = R_f i_f^r(t) + \frac{d}{dt} \boldsymbol{\psi}_f^r(t).$$

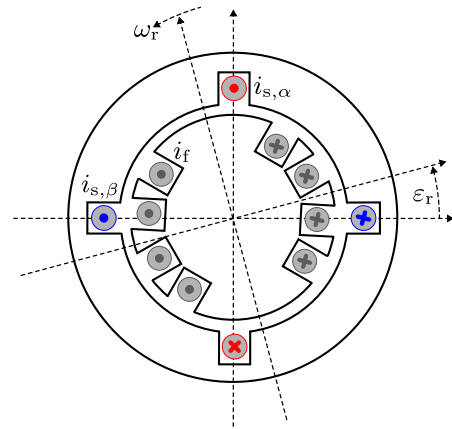


Fig. 7.7: Conceptual cylindrical SM representation within the orthogonal $\alpha\beta$ coordinates ($p = 1$ pole pair)

Cylindrical SM model in alpha-beta coordinates: flux linkage

For the flux linkage model in $\alpha\beta$ -coordinates, we multiply the stator flux equations from (7.3) with \mathbf{T}_{23} from the right

$$\begin{aligned}\psi_{s,\alpha\beta}^s(t) &= \mathbf{T}_{23}\psi_{s,abc}^s(t) = \overbrace{\mathbf{T}_{23}\mathbf{L}_{s,abc}\mathbf{T}_{32}}^{\mathbf{L}_{s,\alpha\beta}} \mathbf{i}_{s,\alpha\beta}^s(t) + M_r \frac{N_s}{N_r} \mathbf{T}_{23} \begin{bmatrix} \cos(\varepsilon_{r,el}(t)) \\ \cos(\varepsilon_{r,el}(t) - \frac{2\pi}{3}) \\ \cos(\varepsilon_{r,el}(t) + \frac{2\pi}{3}) \end{bmatrix} i_f^r(t) \\ &= (L_s + M_s/2)\mathbf{i}_{s,\alpha\beta}^s(t) + M_r \frac{N_s}{N_r} \begin{bmatrix} \cos(\varepsilon_{r,el}(t)) \\ \sin(\varepsilon_{r,el}(t)) \end{bmatrix} i_f^r(t)\end{aligned}\quad (7.5)$$

and utilize $\mathbf{i}_{s,abc}^s(t) = \mathbf{T}_{32}\mathbf{i}_{s,\alpha\beta}^s(t)$ to modify the rotor flux linkage equation accordingly:

$$\psi_f^r(t) = L_f i_f^r(t) + M_s \frac{N_r}{N_s} [\cos(\varepsilon_{r,el}(t)) \quad \sin(\varepsilon_{r,el}(t))] \mathbf{i}_{s,\alpha\beta}^s(t). \quad (7.6)$$

In contrast to the IM $\alpha\beta$ -coordinates flux linkage model, the SM flux-to-current coupling is rotor position-dependent.

Cylindrical SM model in alpha-beta coordinates: flux linkage (cont.)

Analyzing the (magnetic) power balance reveals

$$M_r \frac{N_s}{N_r} = M_s \frac{N_r}{N_s} \stackrel{!}{=} M_{fs}, \quad (7.7)$$

and with the shorter notation

$$L'_s = (L_s + M_s/2) \quad (7.8)$$

we can rewrite the flux linkage model in $\alpha\beta$ -coordinates to

$$\begin{aligned} \psi_{s,\alpha\beta}^s(t) &= L'_s \mathbf{i}_{s,\alpha\beta}^s(t) + M_{fs} \begin{bmatrix} \cos(\varepsilon_{r,el}(t)) \\ \sin(\varepsilon_{r,el}(t)) \end{bmatrix} i_f^r(t), \\ \psi_f^r(t) &= L_f i_f^r(t) + M_{fs} \begin{bmatrix} \cos(\varepsilon_{r,el}(t)) \\ \sin(\varepsilon_{r,el}(t)) \end{bmatrix}^T \mathbf{i}_{s,\alpha\beta}^s(t). \end{aligned} \quad (7.9)$$

Cylindrical SM model in alpha-beta coordinates: torque

Following the same power balance approach as from the IM, the SM's torque equation is given by

$$T(t) = \frac{3}{2}p(\mathbf{i}_{s,\alpha\beta}^s(t))^\top \mathbf{J} \boldsymbol{\psi}_{s,\alpha\beta}^s(t). \quad (7.10)$$

The equivalent representation with the rotor current and flux linkage as in the IM case is not applicable in the SM case, as the rotor has only a single field winding, i.e., is lacking an $\alpha\beta$ representation. Inserting the linear flux linkage model from (7.9) into the torque equation yields

$$\begin{aligned} T(t) &= \frac{3}{2}p(\mathbf{i}_{s,\alpha\beta}^s(t))^\top \mathbf{J} \boldsymbol{\psi}_{s,\alpha\beta}^s(t) \\ &= \frac{3}{2}p(\mathbf{i}_{s,\alpha\beta}^s(t))^\top \mathbf{J} \left(L'_s \mathbf{i}_{s,\alpha\beta}^s(t) + M_{fs} \begin{bmatrix} \cos(\varepsilon_{r,el}(t)) \\ \sin(\varepsilon_{r,el}(t)) \end{bmatrix} i_f^r(t) \right) \\ &= \frac{3}{2}pM_{fs} i_f^r (\cos(\varepsilon_{r,el}(t)) i_{s,\beta}^s(t) - \sin(\varepsilon_{r,el}(t)) i_{s,\alpha}^s(t)). \end{aligned} \quad (7.11)$$

Cylindrical SM model in alpha-beta coordinates: torque interpretation

In (7.11) the term

$$M_{fs} \begin{bmatrix} \cos(\varepsilon_{r,el}(t)) \\ \sin(\varepsilon_{r,el}(t)) \end{bmatrix} i_f^r(t) = \psi_f^s(t) \quad (7.12)$$

can be interpreted as the field winding flux linkage coupled with the stator winding. Hence, the torque expression can be rewritten as:

$$\begin{aligned} T(t) &= \frac{3}{2} p \|\psi_f^s(t) \times \mathbf{i}_{s,\alpha\beta}^s(t)\| \\ &= \frac{3}{2} p \|\psi_f^s(t)\| \|\mathbf{i}_{s,\alpha\beta}^s(t)\| \sin(\theta(t)) \end{aligned} \quad (7.13)$$

with θ being the angle between the field winding flux linkage and the stator current vectors, also known as the load angle.

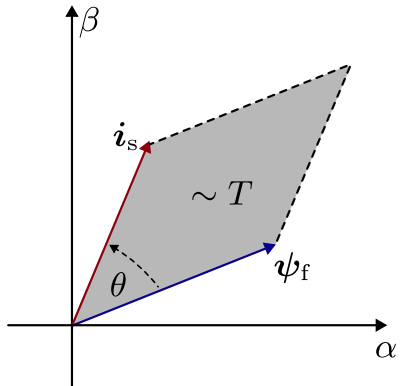


Fig. 7.8: Interpretation of the torque as the parallelogram area spanned by the vectors of the field winding flux and the stator current

Summary: cylindrical SM model in $\alpha\beta$ coordinates

The most important equations of the cylindrical SM model in the $\alpha\beta$ coordinates are:

Stator voltage: $u_{s,\alpha\beta}^s(t) = R_s i_{s,\alpha\beta}^s(t) + \frac{d}{dt} \psi_{s,\alpha\beta}^s(t),$

Rotor / field winding voltage: $u_f^r(t) = R_f i_f^r(t) + \frac{d}{dt} \psi_f^r(t),$

Stator flux linkage: $\psi_{s,\alpha\beta}^s(t) = L'_s i_{s,\alpha\beta}^s(t) + M_{fs} \begin{bmatrix} \cos(\varepsilon_{r,el}(t)) \\ \sin(\varepsilon_{r,el}(t)) \end{bmatrix} i_f^r(t),$

Rotor / field winding flux linkage: $\psi_f^r(t) = L_f i_f^r(t) + M_{fs} \begin{bmatrix} \cos(\varepsilon_{r,el}(t)) \\ \sin(\varepsilon_{r,el}(t)) \end{bmatrix}^T i_{s,\alpha\beta}^s(t),$

Torque: $T(t) = \frac{3}{2} p (\dot{i}_{s,\alpha\beta}^s)^T \mathbf{J} \psi_{s,\alpha\beta}^s.$

Rotor flux orientation: the dq coordinate system

- ▶ In the SM case the rotor flux orientation is directly related to the rotor position (cf. Fig. 7.1).
- ▶ Hence, to transfer the rotor and stator equations into a mutual coordinate system, the rotor flux orientation is typically used as a reference.
- ▶ In contrast to the $\alpha\beta$ -coordinates, where the stator quantity signals are of sinusoidal shape during steady state, the rotor flux-oriented signals are constant during steady state.

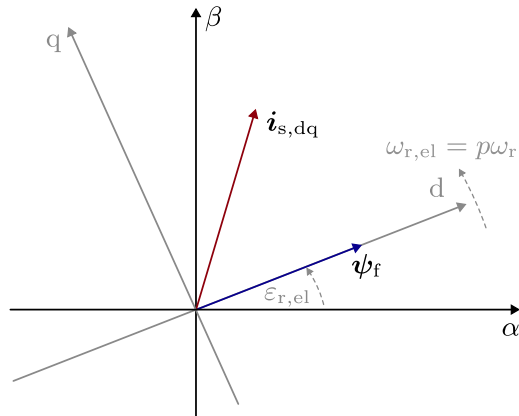


Fig. 7.9: Rotor flux-oriented coordinate system

Rotor flux orientation: the dq coordinate system (cont.)

Transferring the stator voltage equation into the dq coordinate system results in

$$\begin{aligned} \mathbf{u}_{s,\alpha\beta}^s(t) &= R_s \mathbf{i}_{s,\alpha\beta}^s(t) + \frac{d}{dt} \boldsymbol{\psi}_{s,\alpha\beta}^s(t) \\ \Leftrightarrow \quad \mathbf{T}_p^{-1}(\varepsilon_{r,el}) \mathbf{u}_{s,dq}^s(t) &= R_s \mathbf{T}_p^{-1}(\varepsilon_{r,el}) \mathbf{i}_{s,dq}^s(t) + \frac{d}{dt} (\mathbf{T}_p^{-1}(\varepsilon_{r,el}) \boldsymbol{\psi}_{s,dq}^s(t)) \quad (7.14) \\ \Leftrightarrow \quad \mathbf{u}_{s,dq}^r(t) &= R_s \mathbf{i}_{s,dq}^r(t) + \omega_{r,el}(t) \mathbf{J} \boldsymbol{\psi}_{s,dq}^r(t) + \frac{d}{dt} \boldsymbol{\psi}_{s,dq}^r(t). \end{aligned}$$

Since the dq coordinate system is always aligned with the rotor flux in the SM case, one can also drop the superscript r:

$$\mathbf{u}_{s,dq}(t) = R_s \mathbf{i}_{s,dq}(t) + \omega_{r,el}(t) \mathbf{J} \boldsymbol{\psi}_{s,dq}(t) + \frac{d}{dt} \boldsymbol{\psi}_{s,dq}(t).$$

Rotor flux orientation: the dq coordinate system (cont.)

The stator flux linkage model in the dq coordinate system is given by

$$\begin{aligned}
 \psi_{s,\alpha\beta}^s(t) &= L'_s \mathbf{i}_{s,\alpha\beta}^s(t) + M_{fs} \begin{bmatrix} \cos(\varepsilon_{r,el}(t)) \\ \sin(\varepsilon_{r,el}(t)) \end{bmatrix} i_f^r(t), \\
 \Leftrightarrow \quad \mathbf{T}_p^{-1}(\varepsilon_{r,el}) \psi_{s,dq}(t) &= L'_s \mathbf{T}_p^{-1}(\varepsilon_{r,el}) \mathbf{i}_{s,dq}(t) + M_{fs} \begin{bmatrix} \cos(\varepsilon_{r,el}(t)) \\ \sin(\varepsilon_{r,el}(t)) \end{bmatrix} i_f^r(t) \quad (7.15) \\
 \Leftrightarrow \quad \psi_{s,dq}(t) &= L'_s \mathbf{i}_{s,dq}(t) + M_{fs} \underbrace{\begin{bmatrix} 1 \\ 0 \end{bmatrix}}_{M_{fs}} i_f^r(t) = L'_s \mathbf{i}_{s,dq}(t) + \mathbf{M}_{fs} i_f^r(t).
 \end{aligned}$$

while the field winding flux results in

$$\begin{aligned}
 \psi_f^r(t) &= L_f i_f^r(t) + M_{fs} \begin{bmatrix} \cos(\varepsilon_{r,el}(t)) & \sin(\varepsilon_{r,el}(t)) \end{bmatrix} \mathbf{i}_{s,\alpha\beta}^s(t) \\
 \Leftrightarrow \quad \psi_f^r(t) &= L_f i_f^r(t) + M_{fs} \begin{bmatrix} \cos(\varepsilon_{r,el}(t)) & \sin(\varepsilon_{r,el}(t)) \end{bmatrix} \mathbf{T}_p^{-1}(\varepsilon_{r,el}) \mathbf{i}_{s,dq}^s(t) \quad (7.16) \\
 \Leftrightarrow \quad \psi_f^r(t) &= L_f i_f^r(t) + M_{fs} \begin{bmatrix} 1 & 0 \end{bmatrix} \mathbf{i}_{s,dq}(t) = L_f i_f^r(t) + \mathbf{M}_{fs}^\top \mathbf{i}_{s,dq}(t).
 \end{aligned}$$

Summary: cylindrical SM model in dq coordinates

The most important equations of the cylindrical SM model in the dq coordinates are:

Stator voltage: $\mathbf{u}_{\text{s},\text{dq}}(t) = R_{\text{s}} \mathbf{i}_{\text{s},\text{dq}}(t) + \omega_{\text{r},\text{el}}(t) \mathbf{J} \boldsymbol{\psi}_{\text{s},\text{dq}}(t) + \frac{d}{dt} \boldsymbol{\psi}_{\text{s},\text{dq}}(t),$

Rotor / field winding voltage: $u_{\text{f}}(t) = R_{\text{f}} i_{\text{f}}(t) + \frac{d}{dt} \psi_{\text{f}}(t),$

Stator flux linkage: $\boldsymbol{\psi}_{\text{s},\text{dq}}(t) = L'_{\text{s}} \mathbf{i}_{\text{s},\text{dq}}(t) + \mathbf{M}_{\text{fs}} i_{\text{f}}(t),$

Rotor / field winding flux linkage: $\psi_{\text{f}}(t) = L_{\text{f}} i_{\text{f}}^{\text{r}}(t) + \mathbf{M}_{\text{fs}}^{\text{T}} \mathbf{i}_{\text{s},\text{dq}}(t),$

Torque: $T(t) = \frac{3}{2} p (\mathbf{i}_{\text{s},\text{dq}})^{\text{T}} \mathbf{J} \boldsymbol{\psi}_{\text{s},\text{dq}}.$

Here, one can observe that the d component of the stator flux linkage is directly coupled with the field winding flux and vice versa, which was to be expected due to the rotor flux orientation of the chosen coordinate system.

ECD of cylindrical SM model in dq coordinates

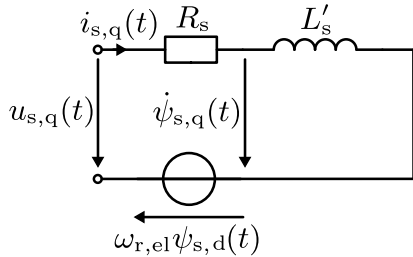
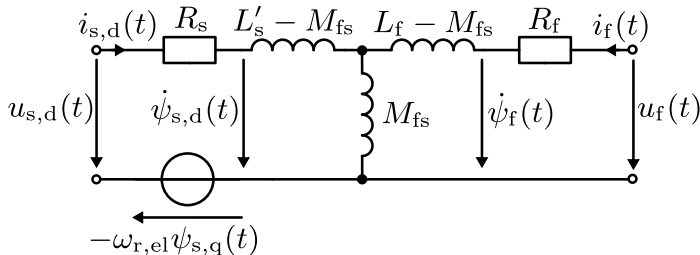


Fig. 7.10: T-type ECD of a cylindrical SM in dq coordinates (note that this ECD is represented with scalar values and not as vectors or complex numbers as in the IM case).

Salient pole SM model

- ▶ The cylindrical rotor SM model (7.15) considered an identical stator inductance L'_s for the d and q axis.
- ▶ In the cylindrical SM case this is a valid assumption, as the rotor is symmetrical.
- ▶ However, in the case of a salient pole SM, the rotor is not symmetrical and the flux path per axis is different (cf. Fig. 7.11).
- ▶ The q-axis reluctance is larger than the d-axis reluctance due to the larger air gap in the q-axis direction.
- ▶ Consequently, the inductance per axis is different.

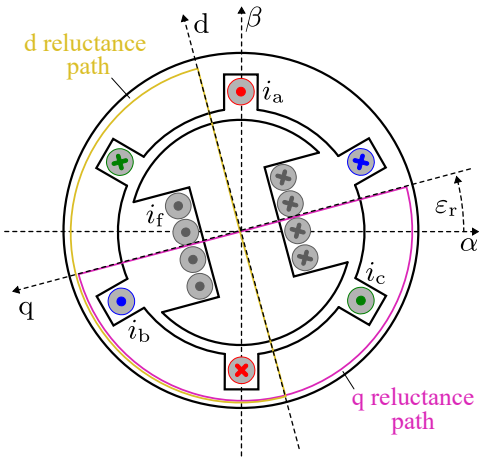


Fig. 7.11: Effective reluctance paths of the salient pole SM in the dq coordinate system

Salient pole SM model (cont.)

From Fig. 7.11 we derive the following stator flux linkage model for the salient pole SM:

$$\boldsymbol{\psi}_{s,dq}(t) = \underbrace{\begin{bmatrix} L'_{s,d} & 0 \\ 0 & L'_{s,q} \end{bmatrix}}_{\boldsymbol{L}_{s,dq}} \boldsymbol{i}_{s,dq}(t) + M_{fs} \begin{bmatrix} 1 \\ 0 \end{bmatrix} i_f(t) = \boldsymbol{L}_{s,dq} \boldsymbol{i}_{s,dq}(t) + \boldsymbol{M}_{fs} i_f(t) \quad (7.17)$$

while the rotor field winding flux linkage remains identical to the cylindrical SM case. Inserting the stator flux linkage model into the torque equation yields

$$\begin{aligned} T(t) &= \frac{3}{2} p (\boldsymbol{i}_{s,dq})^\top \boldsymbol{J} \boldsymbol{\psi}_{s,dq} = \frac{3}{2} p i_{s,q} [M_{fs} i_f + (L'_{s,d} - L'_{s,q}) i_{s,d}] \\ &= \underbrace{\frac{3}{2} p M_{fs} i_{s,q} i_f}_{\text{main torque}} + \underbrace{\frac{3}{2} p i_{s,q} i_{s,d} (L'_{s,d} - L'_{s,q})}_{\text{reluctance torque}}. \end{aligned} \quad (7.18)$$

The latter part is specific to the salient pole SM since $L'_{s,d} \neq L'_{s,q}$ holds, while $L'_{s,d} = L'_{s,q} = L'_s$ applies to the cylindrical SM, that is, the reluctance torque is zero.

Summary: salient pole SM model in dq coordinates

The most important equations of the salient pole SM model in the dq coordinates are:

Stator voltage: $\mathbf{u}_{s,dq}(t) = R_s \mathbf{i}_{s,dq}(t) + \omega_{r,el}(t) \mathbf{J} \boldsymbol{\psi}_{s,dq}(t) + \frac{d}{dt} \boldsymbol{\psi}_{s,dq}(t),$

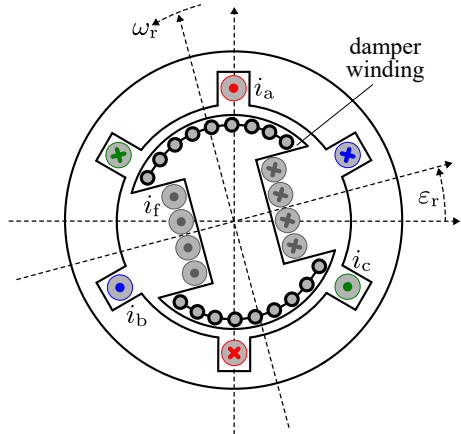
Rotor / field winding voltage: $u_f(t) = R_f i_f(t) + \frac{d}{dt} \psi_f(t),$

Stator flux linkage: $\boldsymbol{\psi}_{s,dq}(t) = \mathbf{L}_{s,dq} \mathbf{i}_{s,dq}(t) + \mathbf{M}_{fs} i_f(t),$

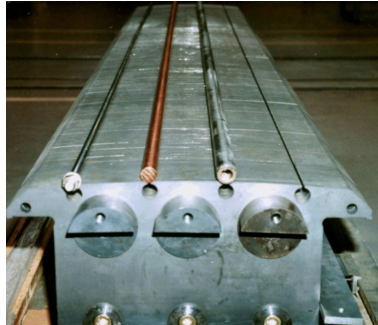
Rotor / field winding flux linkage: $\psi_f(t) = L_f i_f^r(t) + \mathbf{M}_{fs}^\top \mathbf{i}_{s,dq}(t),$

Torque:
$$\begin{aligned} T(t) &= \frac{3}{2} p (\mathbf{i}_{s,dq})^\top \mathbf{J} \boldsymbol{\psi}_{s,dq} \\ &= \frac{3}{2} p i_{s,q} [M_{fs} i_f + (L'_{s,d} - L'_{s,q}) i_{s,d}] . \end{aligned}$$

Damper winding



(a) Salient pole SM with damper winding



(b) Salient pole with dismantled damper winding
(source: L. Frosini, *Novel Diagnostic Techniques for Rotating Electrical Machines – A Review*, Energies, 2020, CC BY 4.0)

Fig. 7.12: SM with damper winding

Damper winding (cont.)

- ▶ The damper winding is a short-circuited winding in the rotor slots of the SM.
- ▶ The damper winding is used to dampen the rotor oscillations during transients.
- ▶ This is important for synchronous generators in power systems, where the rotor oscillations can lead to instabilities.

Damper winding model

The SM damper winding can be interpreted as the IM squirrel cage, i.e., the rotor model can be extended accordingly (superposition).

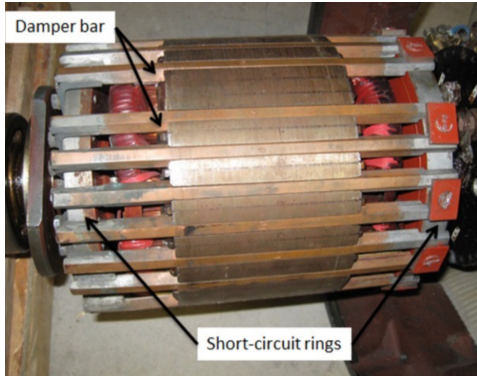


Fig. 7.13: SM rotor with solid damper bars (source: J. Cros et al., *Simulation Methods for the Transient Analysis of Synchronous Alternators*, Renewable Energy, 2016, CC BY 3.0)

SM model with damper winding

From the IM model in dq-coordinates (compare Fig. 6.11) we introduce the short-circuited damper winding voltage equation:

$$0 = \mathbf{R}_{r,DQ} \mathbf{i}_{r,DQ}(t) + \frac{d}{dt} \boldsymbol{\psi}_{r,DQ}(t) = \begin{bmatrix} R_{r,D} & 0 \\ 0 & R_{r,Q} \end{bmatrix} \begin{bmatrix} i_{r,D}(t) \\ i_{r,Q}(t) \end{bmatrix} + \frac{d}{dt} \begin{bmatrix} \psi_{r,D}(t) \\ \psi_{r,Q}(t) \end{bmatrix}. \quad (7.19)$$

Here, the following applies:

- ▶ Capital indices represent the damper winding.
- ▶ $i_{r,DQ}(t)$ and $\psi_{r,DQ}(t)$ are the current as well as flux linkage in the damper winding.
- ▶ $\mathbf{R}_{r,DQ}$ represents the resistance matrix: Since the damper winding eventually does not cover the entire rotor circumference, $R_{r,D} \neq R_{r,Q}$ can apply (compare Fig. 7.12).

The stator and field winding voltage equations remain unchanged:

$$\mathbf{u}_{s,dq}(t) = R_s \mathbf{i}_{s,dq}(t) + \omega_{r,el}(t) \mathbf{J} \boldsymbol{\psi}_{s,dq}(t) + \frac{d}{dt} \boldsymbol{\psi}_{s,dq}(t), \quad u_f(t) = R_f i_f(t) + \frac{d}{dt} \psi_f(t).$$

SM model with damper winding (cont.)

The flux linkage equations become

$$\begin{aligned}\psi_{s,dq}(t) &= \mathbf{L}_{s,dq} \mathbf{i}_{s,dq}(t) + \mathbf{M}_{fs} i_f(t) + \mathbf{M}_{rs} \mathbf{i}_{r,DQ}(t) \\ &= \begin{bmatrix} L'_{s,d} & 0 \\ 0 & L'_{s,q} \end{bmatrix} \begin{bmatrix} i_{s,d}(t) \\ i_{s,q}(t) \end{bmatrix} + M_{fs} \begin{bmatrix} 1 \\ 0 \end{bmatrix} i_f(t) + \begin{bmatrix} M_{dD} & 0 \\ 0 & M_{qQ} \end{bmatrix} \begin{bmatrix} i_{r,D}(t) \\ i_{r,Q}(t) \end{bmatrix}, \\ \psi_f(t) &= L_f i_f(t) + \mathbf{M}_{fs}^T \mathbf{i}_{s,dq}(t) + \mathbf{M}_{fr}^T \mathbf{i}_{r,DQ}(t) \\ &= L_f i_f(t) + M_{fs} \begin{bmatrix} 1 & 0 \end{bmatrix} \begin{bmatrix} i_{s,d}(t) \\ i_{s,q}(t) \end{bmatrix} + M_{fr} \begin{bmatrix} 1 & 0 \end{bmatrix} \begin{bmatrix} i_{r,D}(t) \\ i_{r,Q}(t) \end{bmatrix}, \\ \psi_{r,DQ}(t) &= \mathbf{L}_{r,DQ} \mathbf{i}_{r,DQ}(t) + \mathbf{M}_{rs} \mathbf{i}_{s,dq}(t) + \mathbf{M}_{fr} i_f(t) \\ &= \begin{bmatrix} L_D & 0 \\ 0 & L_Q \end{bmatrix} \begin{bmatrix} i_{r,D}(t) \\ i_{r,Q}(t) \end{bmatrix} + \begin{bmatrix} M_{dD} & 0 \\ 0 & M_{qQ} \end{bmatrix} \begin{bmatrix} i_{s,d}(t) \\ i_{s,q}(t) \end{bmatrix} + M_{fr} \begin{bmatrix} 1 \\ 0 \end{bmatrix} i_f(t).\end{aligned}\tag{7.20}$$

SM model with damper winding (cont.)

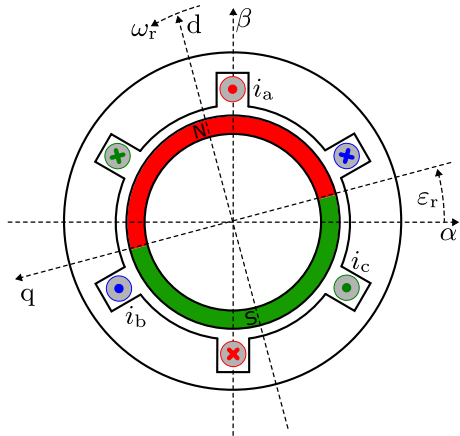
The torque equation results in

$$\begin{aligned} T(t) &= \frac{3}{2} p (\mathbf{i}_{s,dq})^\top \mathbf{J} \boldsymbol{\psi}_{s,dq} \\ &= \frac{3}{2} p [M_{fs} i_f i_{s,q} + (L'_{s,d} - L'_{s,q}) i_{s,d} i_{s,q} + M_{dD} i_{s,q} i_{r,D} - M_{qQ} i_{s,d} i_{r,Q}] . \end{aligned} \quad (7.21)$$

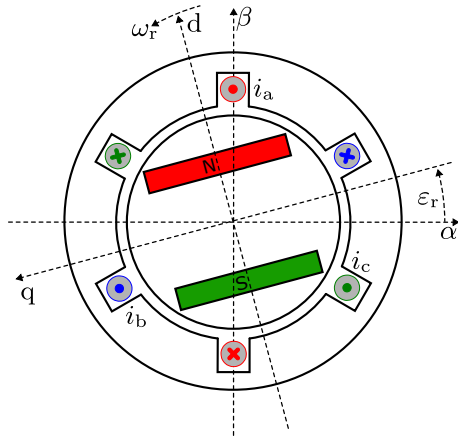
Here, the last two terms represent the torque contribution of the damper winding:

- ▶ In steady state, that is, the stator field rotates synchronously with the rotor, the damper winding current is zero, cf. (7.19). Consequently, the damper torque is zero.
- ▶ Only during transients, when a changing flux linkage induces a voltage within the damper winding, non-zero damper currents occur.
- ▶ The resulting damper torque will oppose the transient and, e.g., dampen mechanical rotor oscillations in generator applications.

Permanent magnet synchronous machine (PMSM)



(a) Surface-mounted PMSM (SPMSM)



(b) Interior PMSM (IPMSM)

Fig. 7.14: SM with permanent magnet excitation

PMSM characteristics

- ▶ Field winding is replaced by permanent magnets (PMs) in the rotor.
- ▶ Typically increases efficiency and power density, since no field winding losses occur.
- ▶ However, PMs are often more expensive than field windings and the machine is less flexible in terms of field weakening.

PMSM applications

Due to weight and size advantages, PMSMs are often used in automotive applications (e.g., electric vehicles) and in highly dynamic industrial applications (e.g., servo drives).

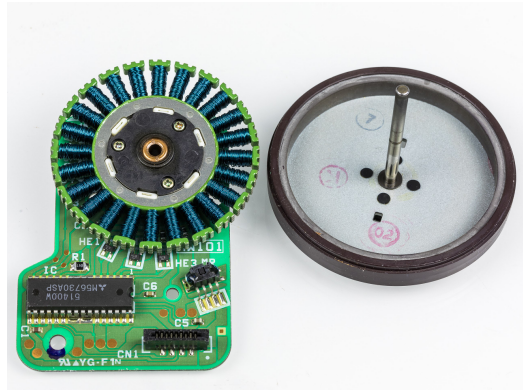


Fig. 7.15: PMSM with external rotor (source: [Wikimedia Commons](#), R. Spekking, CC BY-SA 4.0)

PMSM model

Due to the absence of a field winding, the PMSM model simplifies: The general stator voltage equation in the dq coordinate system remains identical to the SM model

$$\mathbf{u}_{s,dq}(t) = R_s \mathbf{i}_{s,dq}(t) + \omega_{r,el}(t) \mathbf{J} \boldsymbol{\psi}_{s,dq}(t) + \frac{d}{dt} \boldsymbol{\psi}_{s,dq}(t)$$

while the field winding voltage equation is omitted. The stator flux linkage model becomes

$$\boldsymbol{\psi}_{s,dq}(t) = \mathbf{L}_{s,dq} \mathbf{i}_{s,dq}(t) + \boldsymbol{\psi}_{pm} = \begin{bmatrix} L'_{s,d} & 0 \\ 0 & L'_{s,q} \end{bmatrix} \begin{bmatrix} i_{s,d}(t) \\ i_{s,q}(t) \end{bmatrix} + \begin{bmatrix} \boldsymbol{\psi}_{pm} \\ 0 \end{bmatrix}. \quad (7.22)$$

Here, $\boldsymbol{\psi}_{pm}$ represents the (constant) permanent magnet flux linkage. By definition of the dq coordinate system, the permanent magnet flux linkage is directed exclusively along the d-axis (cf. Fig. 7.14). The rotor flux linkage model is omitted, since no field winding is present. Also, a damper winding is very uncommon for PMSMs. Hence, torque equation results in

$$T(t) = \frac{3}{2} p (\mathbf{i}_{s,dq})^T \mathbf{J} \boldsymbol{\psi}_{s,dq} = \frac{3}{2} p i_{s,q} [\boldsymbol{\psi}_{pm} + (L'_{s,d} - L'_{s,q}) i_{s,d}]. \quad (7.23)$$

Isotropic vs. anisotropic PMSM

From (2.23) we know that the relative permeability of the PM material is nearly as that of air, i.e.,

$$\mu_{r,PM} \approx 1$$

applies. Consequently, the PM flux path can be considered as an (additional) air gap. Against this background, the two types for PMSM rotors as in Fig. 7.14 show different characteristics:

- ▶ SPMSM: The PMs are distributed over the entire rotor circumference.
 - ▶ The PM flux path is isotropic, i.e., the same in all directions.
 - ▶ Consequently, the reluctance paths in the d and q axis are identical.
 - ▶ $L'_{s,d} = L'_{s,q} = L'_s$ applies.
- ▶ IPMSM: The PMs are concentrated inside the rotor core.
 - ▶ The PM flux path is anisotropic, i.e., different in the d and q axis.
 - ▶ Consequently, the effective reluctance along the d axis is much higher than along the q axis.
 - ▶ $L'_{s,d} < L'_{s,q}$ applies.

Synchronous reluctance machine (SynRM)

- ▶ SynRM: utilizes only the reluctance torque.
- ▶ No field winding or PMs are present.
- ▶ The rotor is designed such that the reluctance difference in the d and q axis is maximized.
- ▶ PMSM model equations can be used, but the PM flux linkage is zero.

$$\psi_{s,dq}(t) = \mathbf{L}_{s,dq} \mathbf{i}_{s,dq}(t),$$

$$T(t) = \frac{3}{2} p (\mathbf{i}_{s,dq})^T \mathbf{J} \psi_{s,dq} \quad (7.24)$$

$$= \frac{3}{2} p i_{s,q} (L'_{s,d} - L'_{s,q}) i_{s,d}.$$

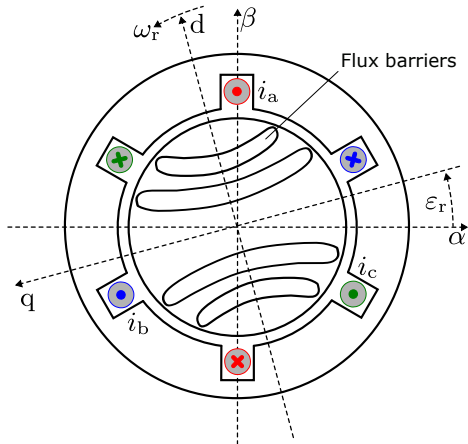


Fig. 7.16: Example of a SynRM with rotor flux barriers (no PMs or field winding present)

Steady-state behavior

We limit the following discussion to the isotropic case

$$L'_{\text{s,d}} = L'_{\text{s,q}} = L'_s$$

which covers the SPMSM and the cylindrical SM. In steady state ($\frac{dx}{dt} = 0$), the flux linked with possibly present damper windings is constant, i.e., no voltage is induced within the damper windings and

$$I_{r,\text{DQ}} = 0$$

applies. Hence, the damper winding can be neglected in steady state. Furthermore, in steady state the field winding current is constant:

$$I_f = \frac{U_f}{R_f} = \text{const.}$$

Consequently, the stator flux linkage share resulting from the field winding $M_{fs}I_f$ is constant and can be interpreted as an equivalent permanent magnet flux linkage. Hence, we will focus on the steady-state behavior of the cylindrical SM in the following, which implicitly covers the SPMSM case as well. The steady-state characteristics of the other SM types are not covered.

Steady-state behavior (cont.)

In steady state, the flux linkage equation remains

$$\boldsymbol{\psi}_{\text{s},\text{dq}} = L'_{\text{s}} \mathbf{I}_{\text{s},\text{dq}} + M_{\text{fs}} I_{\text{f}} \Leftrightarrow \begin{bmatrix} \psi_{\text{s},\text{d}} \\ \psi_{\text{s},\text{q}} \end{bmatrix} = \left(L_{\text{s}} + \frac{M_{\text{s}}}{2} \right) \begin{bmatrix} I_{\text{s},\text{d}} \\ I_{\text{s},\text{q}} \end{bmatrix} + M_{\text{fs}} \begin{bmatrix} I_{\text{f}} \\ 0 \end{bmatrix}.$$

With the decomposition of L_{s} into its leakage part $L_{\sigma,\text{s}}$ and the mutual part M_{s} ,

$$L_{\text{s}} = L_{\sigma,\text{s}} + M_{\text{s}}, \quad (7.25)$$

we obtain

$$\begin{bmatrix} \psi_{\text{s},\text{d}} \\ \psi_{\text{s},\text{q}} \end{bmatrix} = \left(L_{\sigma,\text{s}} + \frac{3}{2} M_{\text{s}} \right) \begin{bmatrix} I_{\text{s},\text{d}} \\ I_{\text{s},\text{q}} \end{bmatrix} + M_{\text{fs}} \begin{bmatrix} I_{\text{f}} \\ 0 \end{bmatrix}. \quad (7.26)$$

In the context of simplified modeling, the assumption is (often) made that the (scaled) mutual inductances are equal, i.e.,

$$M_{\text{fs}} = 3/2 M_{\text{s}} = M$$

leading to

$$\psi_{\text{s},\text{d}} = (L_{\sigma,\text{s}} + M) I_{\text{s},\text{d}} + M I_{\text{f}}, \quad \psi_{\text{s},\text{q}} = (L_{\sigma,\text{s}} + M) I_{\text{s},\text{q}}. \quad (7.27)$$

Steady-state behavior (cont.)

The steady-state voltage equation is

$$\underline{U}_{s,dq} = R_s \underline{I}_{s,dq} + \omega_{r,el} \mathbf{J} \underline{\psi}_{s,dq} \Leftrightarrow \begin{bmatrix} U_{s,d} \\ U_{s,q} \end{bmatrix} = R_s \begin{bmatrix} I_{s,d} \\ I_{s,q} \end{bmatrix} + \omega_{r,el} \begin{bmatrix} -\psi_{s,q} \\ \psi_{s,d} \end{bmatrix}. \quad (7.28)$$

Inserting the (simplified) flux linkage equation (7.27) yields

$$\begin{bmatrix} U_{s,d} \\ U_{s,q} \end{bmatrix} = R_s \begin{bmatrix} I_{s,d} \\ I_{s,q} \end{bmatrix} + \omega_{r,el} \begin{bmatrix} -(L_{\sigma,s} + M) I_{s,q} \\ (L_{\sigma,s} + M) I_{s,d} + M I_f \end{bmatrix}. \quad (7.29)$$

Rewriting the vectorial quantities as complex phasors $\underline{X}_{dq} = X e^{j\phi} = X_d + j X_q$ rotating with the angular frequency $\omega_{r,el} \rightarrow \omega_s$, we obtain

$$\underline{U}_s = R_s \underline{I}_s + j \omega_s [(L_{\sigma,s} + M) \underline{I}_s + M \underline{I}_f] = R_s \underline{I}_s + j \underbrace{\omega_s (L_{\sigma,s} + M)}_{X_s} \underline{I}_s + j \underbrace{\omega_s M \underline{I}_f}_{\underline{U}_i} \quad (7.30)$$

with \underline{U}_i being the internal voltage, i.e., the induced voltage due to the field winding excitation and X_s being the synchronous reactance (which can be empirically identified using open-circuit and short-circuit tests, cf. after next slide).

Steady-state behavior (cont.)

The ECD of the cylindrical SM is shown in Fig. 7.17. Here, the following can be noted:

- ▶ The internal voltage \underline{U}_i is purely imaginary as the field winding current is a DC current and defined as real (convention).
- ▶ If \underline{U}_s is fixed, e.g., by a stiff grid voltage, the stator current \underline{I}_s is determined by the voltage difference $\Delta \underline{U} = \underline{U}_s - \underline{U}_i$.
- ▶ Hence, in grid operation the field winding current I_f is adjusted to reach a certain operation point, that is, the field excitation is controlled.

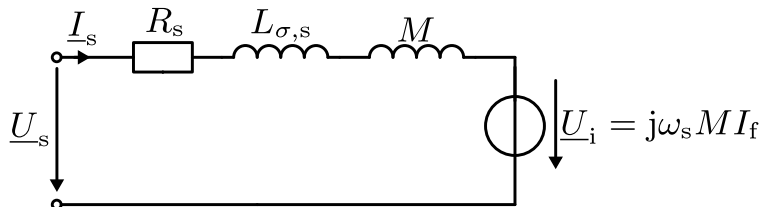


Fig. 7.17: ECD of a (simplified) cylindrical SM in steady state represented by complex phasors

Short-circuit and open-circuit tests

From Fig. 7.17 the open-circuit voltage is

$$\underline{U}_{s,oc} = \underline{U}_i = j\omega_s M I_f. \quad (7.31)$$

Here, the stator current is zero. On the other hand, the short-circuit current is given by

$$\underline{I}_{s,sc} = -\frac{\underline{U}_i}{jX_s} = -\frac{\omega_s M I_f}{j\omega_s (L_{\sigma,s} + M)} = \frac{jM}{(L_{\sigma,s} + M)} I_f. \quad (7.32)$$

Here, the stator voltage is zero and one can observe that the short-circuit current $\underline{I}_{s,sc}$ can be interpreted as the excitation current I_f converted via the inductance ratio. Finally, the synchronous reactance can be calculated by the ratio of the open-circuit voltage and the short-circuit current:

$$X_s = \frac{\underline{U}_{s,oc}}{\underline{I}_{s,sc}}. \quad (7.33)$$

Steady-state torque

The steady-state torque of the cylindrical SM is given by

$$T = \frac{3}{2}p\sqrt{2}I_{s,q}MI_f = \frac{3}{\sqrt{2}}pI_{s,q}MI_f.$$

Here, the factor $\sqrt{2}$ results from the RMS value representation of the AC stator current in the complex phasor component $I_{s,q}$. Note that I_f is a DC quantity, i.e., its RMS value is equal to the DC value in the time domain. From (7.30) we obtain the stator current as

$$\underline{I}_s = \frac{\underline{U}_s - \underline{U}_i}{R_s + j\omega_s(L_{\sigma,s} + M)}. \quad (7.34)$$

Assuming that the ohmic voltage drop is negligible ($R_s \approx 0$), which typically applies to high power machines, the stator current simplifies to

$$\underline{I}_s = j\frac{\underline{U}_i - \underline{U}_s}{\omega_s(L_{\sigma,s} + M)}. \quad (7.35)$$

Steady-state torque (cont.)

The q part from $\underline{I}_s = I_{s,d} + jI_{s,q}$ is

$$I_{s,q} = \frac{|\underline{U}_i - \underline{U}_s|}{\omega_s (L_{\sigma,s} + M)}. \quad (7.36)$$

From Fig. 7.18 we identify

$$\sin(\theta) = \frac{|\underline{U}_i - \underline{U}_s|}{|\underline{U}_s|}$$

and can rewrite $I_{s,q}$ as

$$I_{s,q} = \frac{|\underline{U}_s|}{\omega_s (L_{\sigma,s} + M)} \sin(\theta). \quad (7.37)$$

Here, θ is the load angle counted from \underline{U}_i to \underline{U}_s .

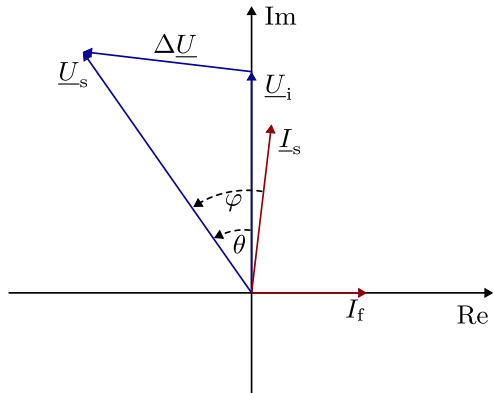


Fig. 7.18: Exemplary phasor diagram of the cylindrical SM

Steady-state torque (cont.)

Moreover, from (7.30) we can express the field winding current (amplitude, DC quantity) as

$$I_f = \sqrt{2} \frac{|\underline{U}_i|}{\omega_s M}. \quad (7.38)$$

Inserting the expressions for $I_{s,q}$ and I_f into the torque equation yields

$$T = 3p \frac{|\underline{U}_s| |\underline{U}_i|}{\omega_s^2 (L_{\sigma,s} + M)} \sin(\theta) = 3p \frac{U_s U_i}{\omega_s^2 (L_{\sigma,s} + M)} \sin(\theta). \quad (7.39)$$

Hence, the load angle θ determines the torque of the cylindrical SM:

- ▶ For $\theta < 0^\circ$, the torque is negative (generator mode, if $\omega_r > 0$).
- ▶ For $\theta = 0^\circ$, the torque is zero.
- ▶ For $\theta > 0^\circ$, the torque is positive (motor mode, if $\omega_r > 0$).
- ▶ For $\theta = \pm 90^\circ$, the absolute torque is maximal.

Stable steady-state operation (with fixed stator excitation)

- ▶ From (7.39) we see that the torque depends on $\sin(\theta)$.
- ▶ Beyond $\theta = \pm 90^\circ$, the absolute torque decreases again.
- ▶ If the SM is operated with a fixed stator excitation, e.g., by a stiff grid voltage, the load angle θ is determined by the mechanical load.
- ▶ If the absolute mechanical load is increased such that $|\theta| > 90^\circ$ applies, the SM will lose synchronicity and stall.
- ▶ Hence, the stable operation range is limited to $|\theta| \leq 90^\circ$ (while in practice an additional safety margin is considered).

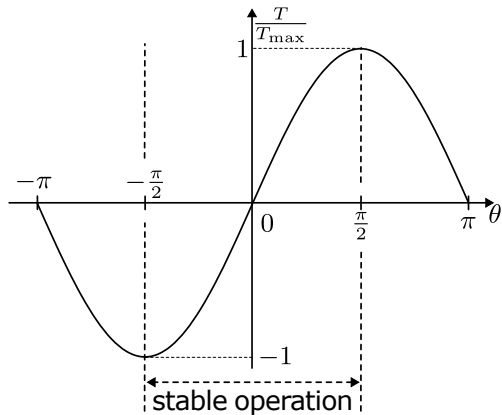


Fig. 7.19: Torque vs. load angle for the cylindrical SM

Power balance

The SM's complex power is given by

$$\underline{S} = 3\underline{U}_s \bar{\underline{I}}_s = 3(P + jQ) = 3Se^{j\varphi} \quad (7.40)$$

with $\bar{\underline{X}}$ being the complex conjugate and the factor 3 results from the representation of the three-phase machine in an orthogonal coordinate system (cf. Clarke transf.) plus the RMS phasor representation of currents and voltages. Above, S is the apparent power, P and Q are the active and reactive power, respectively. The active power is

$$P = 3\text{Re} \{ \underline{U}_s \bar{\underline{I}}_s \} = 3U_s I_s \cos(\varphi) \quad (7.41)$$

and the reactive power is

$$Q = 3\text{Im} \{ \underline{U}_s \bar{\underline{I}}_s \} = 3U_s I_s \sin(\varphi). \quad (7.42)$$

Here, φ is the power factor angle, that is, the phase change between stator voltage and current (compare Fig. 7.18).

Power balance (cont.)

From (7.39) we receive the active power as

$$P = T\omega_r = T \frac{\omega_s}{p} = 3 \frac{U_s U_i}{\omega_s (L_{\sigma,s} + M)} \sin(\theta). \quad (7.43)$$

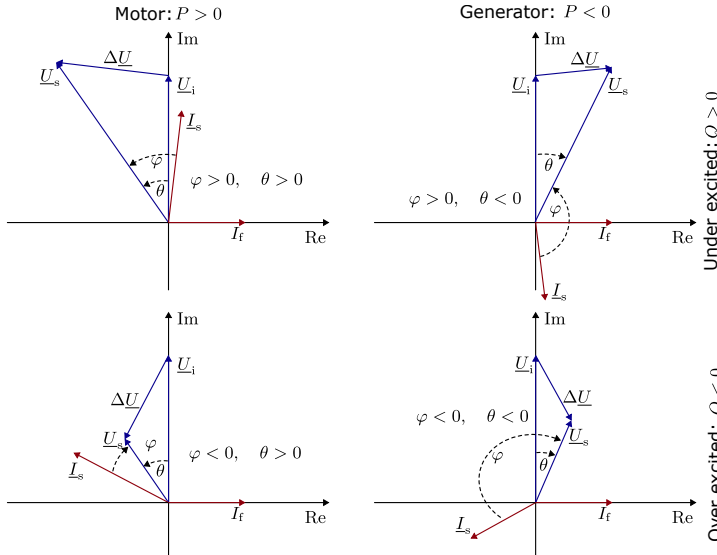
For the reactive power we insert (7.35) in (7.42) and obtain (after some rewriting)

$$Q = 3 \frac{U_s}{\omega_s (L_{\sigma,s} + M)} (U_s - U_i \cos(\theta)). \quad (7.44)$$

Four quadrant operation

Due to a combination of θ and U_i , which are adjustable via the field winding current I_f , the (cylindrical) SM can cover all four quadrants of operation (i.e., combine positive / negative signs of both the active and reactive power). This is why the externally-excited SM is often used in generator / power plant applications.

Phasor diagrams for the cylindrical SM in all four quadrants



English-German dictionary

Oliver Wallscheid



English-German dictionary I

AC machine	Wechselstrommaschine
acceleration	Beschleunigung
active power	Wirkleistung
air gap	Luftspalt
angle	Winkel
apparent power	Scheinleistung
armature	Anker / Läufer
autotransformer	Spartransformator
braking	bremsend
brush	Bürste
brushless	bürstenlos

English-German dictionary II

capacitance	Kapazität [Größe]
capacitor	Kondensator [Bauelement]
circuit	Schaltkreis
commutation	Kommutierung
compensation winding	Kompensationswicklung
conductance	Leitwert
conductivity	Leitfähigkeit
control	Regelung
copper	Kupfer
current	Strom
damper winding	Dämpferwicklung
DC machine	Gleichstrommaschine

English-German dictionary III

differential equation	Differentialgleichung
displacement	Verschiebung
displacement current	Verschiebestrom
displacement field	Elektrische Flussdichte
drive	Antrieb
driving	antreibend
eddy currents	Wirbelströme
efficiency	Wirkungsgrad
energy	Energie
equivalent circuit diagram	Ersatzschaltbild
excitation	Erregung
fan	Lüfter

English-German dictionary IV

fed-in winding	Träufelwicklung
field	Feld
field weakening	Feldschwächung
field winding	Erreger(-wicklung)
flux	Fluss
flux linkage	Flussverkettung
force	Kraft
form-wound winding	Formspulenwicklung
frequency	Frequenz
friction	Reibung
fundamental wave	Grundwelle
heat	Wärme

English-German dictionary V

inductance	Induktivität [Größe]
induction machine	Asynchronmaschine
inductor	Spule [Bauelement]
innere voltage	Polradspannung
interpoles	Wendepolwicklung
inverter	Wechselrichter
iron	Eisen
jerk	Ruck
lap winding	Schleifenwicklung
leakage	Streuung
load	Last / Belastung
losses	Verluste

English-German dictionary VI

machine	.	Maschine
magnetic domain	.	Weiss-Bezirk
magnetomotive force	.	magnetische Spannung
mass	.	Masse
momentum	.	Impuls
nameplate	.	Typenschild
oscillation [quantity depending on time]	.	Schwingung [Größe in Zeit]
permanent magnet	.	Permanentmagnet
permeance	.	Permeanz
phasor	.	Zeitunabh. komplexer Zeiger
power	.	Leistung
power electronics	.	Leistungselektronik

English-German dictionary VII

power factor	Leistungsfaktor
reactive power	Blindleistung
rectifier	Gleichrichter
reluctance	Reluktanz
resistance	Widerstand [Größe]
resistor	Widerstand [Bauelement]
root mean square	Effektivwert
rotor	Rotor
salient pole rotor	Schenkelpolläufer
saturation	Sättigung
separately excited DC machine	Fremderregte Gleichstrommaschine
series DC machine	Reihenschlussmaschine

English-German dictionary VIII

shaft	Welle
shut DC machine	Nebenschlussmaschine
slip	Schlupf
slip ring	Schleifring
slot	Nut
slot wedge	Nutkeil
speed	Geschwindigkeit
squirrel cage	Käfigläufer
starting torque	Anlaufdrehmoment
stator	Stator
steady state	Stationärer Zustand
steel	Stahl

English-German dictionary IX

synchronous machine	.	Synchronmaschine
tap	.	Anzapfung
terminal	.	Anschlussfeld
three phase machine	.	Drehstrommaschine
torque	.	Drehmoment
transformer	.	Transformator
transient	.	Transienter Zustand
turn	.	Windung
unit	.	Maßeinheit
velocity	.	Geschwindigkeit
voltage	.	Spannung
wave [quantity depending on time and space]	.	Welle [Größe in Zeit und Raum]

English-German dictionary X

wave winding	Wellenwicklung
windage	Luftwiderstand
work	Arbeit
yoke	Joch